Multi-functional Biomolecule-embedded Nanomaterial Interfaces via Layer-by-layer Assembly

by

Yuanyuan Zhang

A dissertation submitted to the Graduate Faculty of
Auburn University
in partial fulfillment of the
requirements for the Degree of
Doctor of Philosophy

Auburn, AL
August 6, 2016

Keywords: Layer-by-layer assembly, Multi-walled carbon nanotubes, Multi-enzyme, Discriminative detection, Enzyme cascade Sucrose/O_2 biofuel cell, Drug delivery

Approved by

Aleksandr Simonian, Chair, Professor of Materials Engineering
Jeffrey Fergus, Professor of Materials Engineering
Dong-Joo Kim, Professor of Materials Engineering
Curtis Shannon, Professor of Chemistry and Biochemistry

Abstract

Preparation of functional interfaces on different substrates has drawn extensive research efforts for various purposes. Biointerfaces featuring an integration of a wide variety of biomaterials on electrode surfaces has been a hot topic since it is the most critical aspect in creation of biosensor, biofuel cell, and other bioelectronics devices. Recent research progress addresses the demand for hybrid bioelectrocatalytic systems, combining one or more biocatalysts and nanomaterials, like nanoparticles, carbon nanotubes (CNTs) in the biointerfaces. Here in the dissertation, we move forward towards the design of hybrid multienzyme-CNTs layered thin-film biointerfaces for advanced biosensor, biofuel cells development. Understanding of the interactions between biomolecules-nanomaterials interfaces, structural organization of layer-by-layer (LbL) self-assembled multilayers, electron transfer functions of the biointerfaces on the electrode as well as renewability of the biofunctionalized CNT interfaces were studied.

In the first section, LbL biointerfaces consisted of alternating cushion layers of oppositely charged CNT-polyethyleneimine (CNT-PEI) and CNT-DNA, and a functional interface consisting of alternating layers of CNT-PEI and negatively charged CNT-acetylcholine esterase (CNT-AChE, pH 7.4) were fabricated under real-time monitoring. Comprehensive interfacial properties were investigated using different

characterization tools. A partial desorption of the top enzymatic layer in the LbL structure was observed with a desorption strategy employing alkaline treatment, while further assembly of functional layers regained the functionality of biointerfaces. In the second section, a novel multienzyme-CNTs biosensing interfaces for biosensing application via LbL assembly of MWCNT-organophosphate Hydrolase (MWCNT-OPH) and MWCNT-AChE along with the same set of CNT-DNA and CNT-PEI cushioning bilayers on GCE were investigated. Design of the nanoarchitecture, including total number of layers, relative position of biocatalysts, and concentration of CNTs were explored. Successful discriminative detection of OP and non-OP pesticides was achieved with the biosensor. In the third section, we further employed the versatile LbL assembly technique to modify GCEs and screen printed electrodes (SPEs) utilizing MWCNTs/polyelectrolyte binary composites and an enzyme cascade (MWCNT-Invertase and MWCNT-GDH) to facilitate efficient electron transfer in sucrose/O_2 biofuel cell. The LbL architecture showed advantages for sequential enzymatic reaction that favored the electron transfer and efficient penetration of substrate and products in a cascade system and therefore an enhancement of current density.

Acknowledgments

First of all, I would like to express my deepest appreciation to my committee chair, my advisor Prof. Aleksandr L. Simonian. Without his generous guidance and persistent support, I couldn't realize the achievements in my PhD program at Auburn University. He is not only my advisor in academic researches, but also a mentor in my life. I'm honored being his student. I will cherish all advices and experiences he shared to me for the rest of my life. Also, I would like express my gratitude to my committee members, Prof. Jeffrey Fergus, Prof. Dong-Joo Kim and Prof. Curtis Shannon for the suggestions provided on my research with their profundity of knowledge in Chemistry and Materials science. My sincere gratitude to Prof. Christopher Easley for being an external reader.

I am also grateful to Dr. Mary Arugula who led my way in my projects and generously gave me instruction throughout the years. Thank Dr. Xiaoyun Yang and Jeffrey Kirsch, who shared with me their knowledge and trained me skills I needed to initiate my projects. Thank Fuling Yang and Lang Zhou for being great labmates and friends of mine. Thank my undergraduate Shannon Williams, who provided me help in my research and corrections in English speaking and writing. I appreciate the help from Mr. Steven Moore for technical support, making my work easier. Thanks for the chances to use SEM provided by Dr. Prorok, AFM by Prof. Robert Ashurst and his

student Jie Zhong, Raman by Prof. Curtis Shannon, polymer synthesis support from Porf. Gisela Buschle-Diller group. Thanks Dr. Majid Beidaghi, Dr. Dong-Joo Kim and Dr. Jeffrey Fergus for supporting me in application of Outstanding Doctoral Students Award, which is a big encouragement to me.

I would like to express my great gratitude to Rhonda Cattley and Dr. Russ Cattley for warming my heart as my “American Parents” in Auburn. They help and care my whole family from all aspects since the first day we knew, making our life in Auburn easier, happier and full of love. Thank all MATL fellows for colleagueship and friendship, Dr. Zhizhi Sheng, Dr. Honglong Wang, Dr. Jing Dai, Dr. Lin Zhang, Dr. Yating Chai, Dr. MariAnne Sullivan, Dr. Naveed, Anqi Zhang, Yan Chen, Liangxi Li, Yang Tong, Songtao Du, Wenya Du, Xingxing Zhang, Zhan Xu, Jiahui Xu, Alina Chanysehva, Yoonsung Chung, Eunji Lee, Dr. Hyejin Park, Hossein Talebinezhad, Armin Vahid Mohammadi and so on. You made my study and life in Auburn valuable.

Finally, I would like to dedicate this work to my dear parents and husband, who always value and support me unconditionally, and my three-month-old son who gave me great happiness since the first day he was born. God bless all of you.

Table of Contents

List of Tables

List of Figures

List of Abbreviations

PSS	poly(styrenesulfonate)
PVS	poly(vinyl sulfate)
PDAI	poly(diethylmethy(4-vinylbenzyl)ammonium iodide)
PAH	poly(allylamine hydrochloride)
PEI	poly(ethyleneimine)
PDDA	poly(diallyldimethylammonium chloride)
PSS	poly(sodium styrenesulfonate)
PAA	poly(acrylic acid)
PPV	poly(ρ-phenylenevinylene)
PAMAM	poly(amidoamine)dendrimer
PVK	poly(N-vinyl-carbazole)
PVPON	poly(N-vinylpyrrolidone)
PMA	poly(methacrylic acid)
PLGA	poly(lactide-co-glycolide)
HA	hyaluronic acid
CNTs	carbon nanotube
MWCNTs	multi-walled carbon nanotubes
SWCNTs	single-walled carbon nanotubes
LDHs	layered double hydroxides
FRET	fluorescence resonance energy transfer
PB-*b*-PDMAEMA	polybutadiene-*block*-poly(2-(dimethylamino)ethyl

methacrylate)	
GO	graphene oxide
rGO	reduced graphene oxide
PNIPAM	poly(N-isopropylacrylamide)
NH_2-PNIPAM	amine-terminated poly(N-isopropylacrylamide)
LCST	lower critical solution temperature

1. Introduction

1.1 Bioelectrocatalysis

Bioelectrocatalysis is an electrochemical catalysis process playing an important role in development of biosensor, biofuel cell and other wide range of bioelectronic devices. This process features direct/indirect electron transfer between biological catalysts and electrodes[1]. When considering electron transfer process, the biointerfacial properties is of central importance, where the interactions between the biocatalysts and electrodes make the most critical part of it.

1.2 Functional biointerfaces

Many types of natural biocatalysts-substrates were extensively studied to develop improved bioelectrocatalytic interfaces. Inspired by biomimetic techniques, emerging progress has been achieved on utilizing artificial biomaterial e.g. synthetic polymer, engineered protein for creation of unique-functioning biointerfaces with high specificity, long stability and dynamic molecular recognition to biological function[2]. Recently research interests has been attracted in applying of such smart biointerface in novel biosensor, biofuel cells and controlled drug delivery development. However, this is out of the scope of my study in this dissertation. Among different bioelectrocatalysts including microbes, organelles, nucleic acids and so on, enzymes catalyzing specific types of biological reaction were considered possessing the unique specificity, selectivity and efficiencies on electrode surfaces, and in this study, the enzyme-based functional biointerfaces for bioelectrocatalysis studies will be emphasized.

1.3 Biointerfaces design

As mentioned above, interactions between biomolecules and electrode surfaces are crucial in order to improve the functionality of biocatalytic interfaces. For enzymes involving electron transfer, a close contact between the enzyme and electrode surfaces is desired. The process can be enhanced due to reduced distance for direct electron transfer mechanism. Allocation of enzymes onto electrode surface also increase the localized enzyme concentration, and therefore improve the electrochemical performance. However, random distribution of enzymes on the electrode surface usually results in low enzyme activity due to a small portion of unfavorable enzyme orientation. Moreover, in a remarkable number of enzymatic system, electron transfer ultimately happens via mediated electron transfer process where a small redox-active mediator is usually involved to shuttle the electrons between the enzyme and electrode surfaces. Therefore, to achieve an optimal efficiency in more complexed system, the importance of a rational design of an appropriate biointerface on the molecular level should not be underestimated.

Polymers/hydrogels plays vital role in developing tailored biointerfaces on electrode surfaces. Electrode surfaces modified with polymers/hydrogels yields larger surface area and increases the loading of enzyme. Polymers grafted with active redox compounds provides scaffold by cross-link enzymes onto its 3D architecture, meanwhile enables free motion of electrons across its immobilized network to electrode surfaces. Metal nanoparticles, naonowires, carbon nanotubes as emerging nanomaterial category, features excellent electrical, optical properties as well as catalytic properties. They were extensively explored to immobilize enzymes via covalent bonding between

functional groups and were successfully demonstrated to allow for better enzyme orientations and enhanced electron transfer. Another type of bioeletrode modification was realized by utilizing compound with useful functional groups, e.g. Pyrene[3]. Pyrene bonds a graphitic basal plane of carbon electrode via pi-pi stacking, and the functional group at the other end links with enzymes by forming an amide group.

1.4 Multifunctional biointerfaces

Dramatic research efforts has been devoted into functional biointerfaces for bioelectrocatalytic system development[4,5]. As we move forward, new challenges has raised in demand of advanced biosensor and biofuel cells with novel and non-traditional biointerfaces. Examples include biosensors with multiple recognition elements working together, e.g. two or more enzymes; biofuel cells with cascade enzymes and electrocatalysts for deeper oxidation; hybrid nanocomposites system combining biopolymer, biocatalysts and metal nanoparticles/carbon nanotubes, and so on. In those complexed system, the biointerfaces nanoarchitecture should be tailored to realize better interactions and desired properties. The arrangement should favor the functioning of two or more different biocatalysts with minimal interference, since it is challenging to ensure different catalysts work synergistically or independently in identical conditions. The system should enhance stability of the biocatalysts with the utilization of proper scaffolding structure to realize long lifetime system. More important, a spatial organization allows for more efficient motion of electrons and moieties is needed for improved bioelectrocatalytic performance.

In this dissertation, we've been endeavored for creation of hybrid enzyme-carbon nanotube

multilayered thin film biointerfaces on electrode surface for development of multifunctional bioelectrocatalytic system. A versatile self-assembly technique called layer-by-layer assembly were extensively investigated for this purpose. The following chapter will be first dedicated for introduction of this technique.

1.5 Layer-by-layer (LbL) assembly

1.5.1 Introduction of LbL assembly

Thin film preparation on a variety of substrate surfaces have been a hot subject. While conventional strategies for ultrathin film preparation include Langmuir-Blodgett (LB) technique and self-assembled monolayer (SAM), the main drawback for LB method is it requires materials to be amphiphilic and SAM is not practical in multi-layer films construction. In response to challenges on fabrication of multi-layer films, LbL assembly offers a simple, inexpensive and versatile way for different types of materials and multi-layer structure formation.

With several suggestive research reported by Iler and Kirkland[6,7] in 1965-1966, and Fromherz et al and Golander et al[8,9] during the 80's, the first research that fully characterizes and explains the buildup of LbL films composed of positively and negatively bolaform molecules was published by Decher and Hong in 1991[10]. Later, deeper understanding was achieved via more available characterization techniques with efforts from different research groups. In 1992, Decher and his co-workers first featured polyelectrolytes (PSS and PVS as polyanions and PDAI and PAH as polycations) for buildup of LbL films via electrostatic interaction and observed the linear increase

of film thickness versus number of deposition layers. One year later, a complete characterization of oppositely charged PVS and PAH alternate thin-film systems was conducted by Lvov et al,[11] and an advanced demonstration of stratification of LbL films was observed with neutron reflectivity by Schmitt et al, which showed great potential for establishing thin films with precise thickness and desired architecture via LBL assembly. Furthermore, the mechanism behind LbL assembly was lit up by Bernt et al.[12] through a surface force measurement i.e. charge neutralization, saturation and reversal. Later on, techniques such as quartz crystal microbalance (QCM) measurement,[13,14] surface ζ-potential measurements[15,16,17] and so on were further used in *in situ* evaluation of LbL assembly processing and monitor of charge inversions.

With gradual comprehensive understanding of the process, LbL assembly was increasingly realized and employed for more and more multi-layered thin-film studies. Various types of physiochemical molecular interactions have been investigated in LbL assembly, including electrostatic interactions,[15] hydrogen-binding, [18]charge transfer bonding,[19] coordination bonding,[20] molecular recognition,[21] hydrophobic interactions,[22] stereo-complex formation,[23] covalent bonding,[24] or a combination of these. While wide range of molecular interaction mechanisms involves wide variety of systems and techniques, consensus was achieved among the studies that LbL assembly technique showed great simplicity and low cost, great freedom in materials variability and precise control over thin film architecture.

Electrostatic interaction, for example, is currently the most dominant approach for LbL assembly in chemical, biochemical and biomedical applications. One of its most prominent advantages is simple and low cost. The process involves alternative deposition of oppositely

charged layers with deposition of each layer followed by washing away the unbounded groups. The process is simple and low cost without any sophisticated procedures (Figure 1).

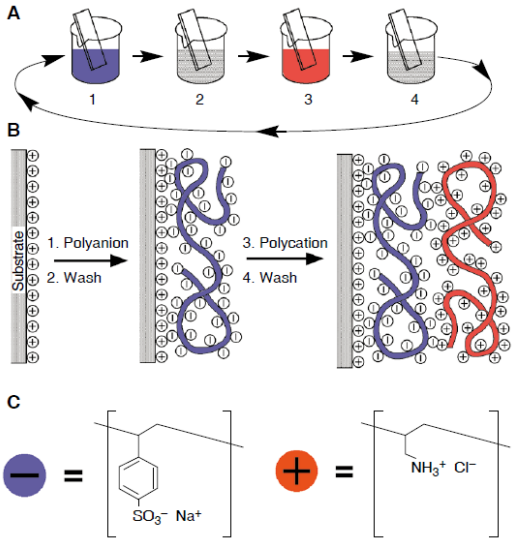

Figure 1. Fabrication of nanostructured multilayer films via electrostatic interaction[15]

Since LbL assembly has become the prime choice for fabrication of multilayer films, a wide variety of materials were incorporated and employed. In addition to conventional series of polyelectrolytes/functional polyelectrolytes[25,26,27] such as PEI, PAH, PDDA, PSS, PVS, PAA, PPV and PAMAM, the category extended to biomaterials including protein/various enzymes,[28] DNA,[29] polysaccharides,[30,31] even charged virus[32] and further expanded to in-organic materials, such as carbon nanotubes,[33,34,35] nanoparticles,[36] quantum dots,[37,38] nanocrystals[39,40] etc. Such wide variety of materials were all demonstrated and reported as layer elements in LbL assembly for proper applications.

Another prominent advantage of this “bottom-up” approach is its versatility for design and fabrication of tailored nano-architectures with functional components. The majority of current

reported nanostructures involve assembly of functional building blocks into ultrathin films anchored on supporting substrates/core with desired sequence, organization, controlled thickness and molecular structure. Its non-selective characteristics to the substrate adapts it to a wide variety of substrate surfaces ranging from SiO_2 slide, glassy carbon electrode, screen printed electrode, gold electrode, gold particles and other solid substrate surfaces. Free standing nanostructures via LbL assembly featuring multidimensional interactions, changeable shape, air/fluid permeability and smart interfaces responsive to certain external stimuli[41] were also reported. Such structures can be obtained by using sacrificial substrates (planar, spherical, or cylindrical) for shaping. LbL assembly followed by removal/decomposition of substrates, freestanding LbL structures can be obtained.

1.5.2 Applications of LbL assembly

Owing to various advantages of LbL assembly, many kinds of applications based on this methodology have been reported continuously. Majority of applications were proposed in chemical, biochemical and biomedical fields, which involve diverse applications including sensing/biosensing, drug storage and controlled release, surface modification, regulated permeation, etc.

Ji et al[42] reported LbL films of rGO and ionic liquids for highly selective gas sensing. The GO was reduced in the presence of various ionic liquids so that the rGO nanosheets were decorated with charges, followed by alternative LbL assembly with PSS on the surface of a QCM sensor. The QCM sensors showed decrease in frequency upon gas adsorption and both quantitative and

qualitative determination between benzene vapor, cyclohexane vapor and their mixture. Li et al[43] prepared LbL films of LDH nanosheets/PVK via hydrogen-bonding and perylene/PVK via π-π interaction for fluorescence sensing for volatile organic compounds based on 2D FRET. Blue luminescence of perylene occurs from PVK to perylene molecules within LDH nanosheets and suppresses when it exposes to volatile organic compounds. The response was fast and reversible, making it a good potential for luminescent sensor applications. Moraes et al[44] studied LbL immobilization of antigenic peptide with silk fibroin. The peptide NS5A-1 derived from hepatitis C virus NS5A protein was immobilized into LbL silk fibroin films onto carbon screen printed electrode. A high response in amperometry was observed in the presence of anti-hepatitis C virus. Such LbL films provided a new architecture for novel immunosensors development. Chung et al[45] initially studied and compared the sensitivity of LbL assembled GO and rGO thin films on Au films for development of SPR-based sensors. Different layers of GO and rGO on Au films were obtained by alternative dipping of Au substrate in positively and negatively charged GO solutions and the resulted multilayer sensors were successfully used in biomolecular sensing.

LbL assembly for development of enzyme/polyelectrolyte based biosensors were extensively demonstrated for detection of chemical and biochemical. [36,39,40,46,47,48,49] Current advances in utilizing of the versatile LbL assembly were extended to multi-enzyme, enzyme cascade assembly for improved performance in novel design and applications. Xiang et al[50] achieved dual amplified ultrasensitive electronic detection of cancer biomarkers utilizing LbL assembly of multienzyme/polyelectrolyte. The target protein, carcinoembryonic antigen (CEA), is sandwiched between an electrode surface-confined capture anti-CEA antibody and the secondary signal anti-

CEA/enzyme-LBL/SWCNT-COOH bioconjugate. The biocatalytic signal amplification for trace CEA monitoring with ultrahigh sensitivity is achieved through both the numerous enzymes loaded on the CNTs via LbL assembly and redox-recycling of the enzymatic products in the presence of the secondary enzyme and the corresponding substrate. Cai et al[51] fabricated a bienzyme biosensor for the detection of cholesterol based on functionalized CNTs and bienzyme/polyelectrolyte fabricated through LbL assembly. Being wrapped with cationic PAH, the nanocomposite MWCNTs mixed with gold nanoparticles (GNPs) was water soluble and positively charged. Based on electrostatic interaction, bienzyme biosensor was fabricated by LBL assembly of the positively charged nanocomposite and the negatively charged enzymes, horseradish peroxidase (HRP) and cholesterol oxidase (ChOx) with good sensitivity, stability, and controllability for the detection of cholesterol. Begum et al[52] presented a novel compartmentalization of multi-enzyme systems via LbL assembly in nanoscale silica layer for rapid conversion of polysaccharides to useful products. Three-step enzyme cascade, including cellulose, ADP-dependent glucokinase and a glucose-6-phosphate dehydrogenase were utilized for catalyzing the conversion of cellobiose to 6-phosphogluconolactone via the intermediates glucose and glucose-6-phosphate. It was demonstrated that the relative position of first-step enzyme and rate-limiting enzyme can affect the overall rate of cascade reactions. More importantly, compartmentalization of the cascade enzymes presented improved performance over enzymes distributed into the same silica layer, showing strong evidence of great advantage of LbL architecture over sequential cascade reactions.

The nature of LbL assembly in wide selection of responsive components with desired properties led to development of drug storage and controlled release system. Ochs et al[53] prepared

biodegradable, covalently stabilized capsules via LbL assembly with tunable degradable properties. PGA modified with alkyne moieties and PVPON was alternately assembled on silica particles via hydrogen-bonding. The films were cross linked with bis-zaide linker followed by removal of the sacrificial template and PVPON at physiological pH through hydrogen bond disruption, yielding one-component PGA_{ALK} capsules, which was inherently enzymatically degradable. Moreover, a stratified hybrid capsule with similar aforementioned system was also investigated, which was promising for the design of tailored drug-delivery vehicles. Demuth et al[54] developed an enhanced transcutaneous vaccine delivery using microneedles coated with LbL stabilized lipid nanocapsules. The system composed PLGA microneedle arrays coated with LbL assembled biodegradable cationic PBAE and anionic ICMV, which loaded with a protein antigen and the molecular adjuvant monophosphoryl lipid A. Application of the microneedle arrays on mice skin for 5 mins resulted in rapid transferal of LbL films from microneedle surfaces into the tissue. It was found microneedle-mediated transcutaneous vaccination with ICMV-carrying multilayers promoted robust antigen-specific humoral immune responses with a balanced generation of multiple IgG isotypes, showing as a promising platform for noninvasive vaccine delivery system. Chen et al[55] succeeded in incorporation of single charged all-trans retinoic acid, as a negatively charged moiety, into layered polyelectrolyte films on surfaces by LbL assembly. The release of the retinoic acid from the films was regulated by the capping layers. The system was verified to release over 5 days in buffer solution. The controlled release of RA from multilayer films can serve as a model system to study the influence of small molecules on cell growth. More recently, improved and targeted drug deliveries were reported with LbL assembled microcapsules assisted by nanoparticles.[56,57,58]

Huang et al[56] report a novel drug delivery system composed of LbL milk protein casein (CN) coated iron oxide nanoparticles. Doxorubicin (DOX) and indocyanine green (ICG) were two drugs incorporated into the inner polymeric layer, and subsequently coated with casein. The resulting casein coated iron oxide nanoparticles (CN-DOX/ICG-IO) were stable in the acidic gastric condition with the presence of gastric protease while released when the casein outer layer was gradually degraded by the intestinal protease in the simulated intestine condition. Such unique properties enable maintenance of the bioactivity of the drugs and thus enhance the drug delivery efficiency without significant degradation. In addition, the magnetic iron oxide nanoparticle core offered an MRI contrast enhancing capability for *in vivo* imaging guided targeted drug delivery.

LbL assembly of high versatility was also intensively applied in surface modification upon diverse surfaces, e.g. solid substrate, medical devices, even cells for desired purpose. Shukla et al[59] proposed a method for hemostatic LbL multilayer coatings utilizing all FDA approved bio originated materials, such as tannic acid and bovine thrombin upon clinically-used gelatin sponge and showed rapid hemostasis efficiency in porcine spleen injury model. Holmes and Tabrizian[60] embedded lipoplexes containing plasmid DNA within polyelectrolyte multilayers composed of glycolchitosan (Glyc-CHI) and HA to produce a film system that enables localized, surface-based transfection. Lipoplex containing Glyc-CHI/HA films were found to successfully transfect NIH3T3 fibroblasts and HEK293 kidney cells in vitro. This film system is promising in serving as coating for implantable devices, such as stents, orthopedic implants and other tissue engineering scaffolds. LbL assembly was also demonstrated for surface modification on cell surfaces. Kozlovskaya et al[61] reported cell surface modification through LbL assembly of hydrogen bonded

multilayers incorporation of tannic acid and PVPON, which leads to high viability of the coated cells over long term compared with cell encapsulation using ironically paired coatings. The highly permeable LbL shell favoring an easy access of nutrients and inducer molecules to the cell's interiors contributed to the high cytocompatibility. LbL assembly of nonionic components could be very important to living cell surface engineering in biomedical applications. Gentile et al[62] achieved a functionalized and resorbable surface to contact soft tissues to improve the antibacterial behaviour during the first week after its implantation in the treatment of periodontal and bone infections. Solvent-cast PLGA films were aminolysed and modified via LbL to obtain a nano-layered coating using PSS and PAH as polyelectrolytes. Antibiotic metronidazole was also incorporated in the layers. The biocompatibility was evaluated in vitro with L929 mouse fibroblasts and the antibacterial properties were demonstrated successfully against the keystone periodontal bacteria Porphyromonas gingivalis, which has an influence on implant failure, without compromising in vitro biocompatibility. This study further demonstrated LbL as a coating technology for the manufacture of medical devices with advanced functional properties.

The wide selection of materials/components and architecture endows LbL films desired properties, which showed potential in regulated permeation for desired target molecules. Broderick et al[63] utilizing LbL multilayers of particular combination of polymers achieved water permeable and water-impermeable properties. Water permeability was achieved by covalent LbL assembly between PEI and an amine-reactive polymer containing azolactone functionality in polar aprotic. While water impermeability can be achieved upon the same films by functionalization with hydrophobic small-molecule amine, *n*-decyl-amine, leading to prolonged dissolution and release

of underlying watersoluble substrate. The highly tunable property is highly desired for penetration/prevention of water molecules. Gas barrier and selectivity was also achieved via LbL assembled graphene and polyelectrolyte films, reported by Yang et al.[64] Number of GO layers and alternately assembled PEI changes the supertortuosity and diffusion lengths for gas molecules and thus controls the permeation of certain gas molecules, demonstrated with O_2 and CO_2.

Other fabrication techniques, such as spin-coating, spraying and photolithography also have been extensively employed into LbL assembly. Such micro-, nano-structures were mainly investigated for functional physical systems development such as photovoltaic devices,[65] field effect transistors (FET),[66,67] electrochemical capacitors/supercapacitors,[68,69] solar cells anodes,[70,71] advanced materials/nanomaterials, etc.

1.6 Bio-functionalized nano-materials application in LbL assembly

More recently much attention has been paid on incorporation of nanomaterials in tailored architectures via LbL assembly for improved biochemical systems development. Nanomaterials were involved in signal transduction, scaffolding, or recognition events to indicate the detection of analyte.[72] Ideally, nanomaterials that allows for retention of biological activity, nanomaterial properties, simplicity and control of the film architecture is desired. Nanomaterials, including carbon nanotubes, nanoparticles, quantum dots and other nanoengineered/structured materials have been successfully demonstrated to be promising for the design of functional thin films, which impart new properties and applications.

1.6.1 Carbon nanotubes and graphene

CNTs have attracted considerable attention due to their high electrical conductivity, large surface area, superior chemical and stability and potential biocompatibility. These features are highly suitable as biochemical sensors and in bioanalytical field settings. While raw CNTs has limitations in the processibility in solution due to CNTs precipitate via strong van der Waals interactions between each other. Various surface modifications upon CNTs were managed to overcome this barrier. For example, several biocompatible and versatile polymers, such as nafion, chitosan, PEI, DNA and PAA, using non-covalent bonding via **π-π** stacking interactions or electrostatic interactions, are quite popular for solubilizing CNTs without damaging their intrinsic properties. In a similar way, biofunctionalized CNTs, involving chemical functionalization of CNTs using strong acids, provide an excellent scaffolding structure for the immobilization of enzymes without sacrificing bioactivity of enzymes. Upon modification, CNTs-biopolymer conjugates therefore can be successfully adapted in LbL assembly. Other carbon based materials, such as graphene and GO have recently been frequently utilized in LbL assembly for controlled morphology and structure.[45,47] The two-dimensional sheet structure makes it great candidate in LbL assembly, while the large surface area further enhances the feasibility for surface modification and selective binding with biomolecules, such as antibodies, ssDNA and so on.

1.6.2 Nanoparticles (NPs) and Quantum dots

Metal NPs were employed as promising nanomaterials for their large surface area, optical properties, and electro catalytic effects. Some of metal NPs show selective and strong affinity to

specific functional group,[73,74,75] for example, Au for –SH group, ZrO_2 NPs and TiO_2 NPs for phosphoric group. Magnetic Fe_3O_4 NPs,[38,76] Au NPs and nanoparticle composites can be further functionalized for in site target extraction, separation and enrichment in a system which can allow interaction of conjugates for thin film in LbL structure. Quantum dots are crystalline nanoparticles of semiconductor materials ranging from 2-50 nm in diameter with their emission color and absorption spectrum highly tunable as size changes. Due to this intrinsic and unique optical features, quantum dots have been researched serving as signal tags, labels for fluorescent readout.[77,78] Quantum dots linked with targeted biomolecules can be well integrated in LbL thin films with uniform morphology and controllable thickness in nanoscale films.[79]

1.6.3 Nano-engineered/structured materials

Apart from nanomaterials, nanostructures, such as anisotropic nanoparticulates, such as nanorods,[80] nanocubes,[40] nanowires,[81] mesoporous nanosheets[82] and combinations of all these have also been encapsulated into LbL films structures.

2 Dissertation organization

2.1 Previous work

2.1.1 Single enzyme based biosensing interfaces using LbL assembly

In 2008, our group firstly reported a LbL-assembled SWCNT lysozyme (LSZ) coatings precisely controlled for thickness and alignment to maintain high antimicrobial activity [83]. We have demonstrated by measuring the rate of lysis of Gram-positive bacteria by LSZ, an antimicrobial enzyme found in human tears and chicken egg whites. DNA-SWCNT and LSZ-SWCNT dispersions were prepared and the strong coulombic interactions between DNA and LSZ were exploited in the LbL assembly. Due to the anionic nature of SWCNT-DNA and cationic nature of SWCNT-LSZ, they were able to be used in the LbL process to assemble antimicrobial thin-films. An exposed SWCNT-LSZ layer exhibits antimicrobial activity over the long-term, which is advantageous over a controlled release coating (Figure 2).

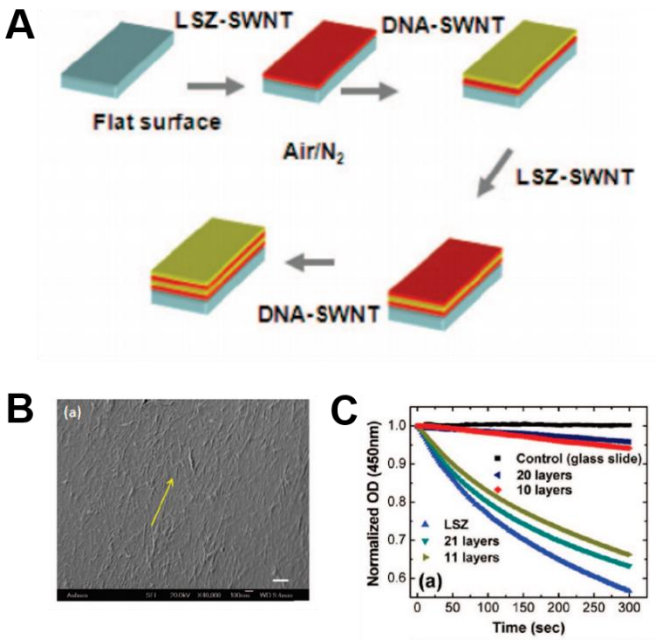

Figure 2. (A) Schematic diagram of LbL assembly of LSZ-SWNT and DNA-SWNT. (B) SEM images of LbL assembly of LSZ-SWNT/DNA-SWNT of the 8th layer. (C) Effect of different layers of LBL coating against *M. lysodeikticus* in turbidimetric assay.

In 2010, we further reported an advanced LbL catalytic interfaces utilizing organophosphorus hydrolase (OPH) through direct hydrolysis reaction for detecting paraoxon (organophosphorus (OP) neurotoxic compounds). The LbL system was based on the interaction of oppositely charged MWCNT-PEI and MWCNT-DNA as strong support for immobilization of MWCNT-OPH. And the catalytic performance for biosensing paraoxon was demonstrated using UV-Vis spectroscopic and amperometric techniques (Figure 3) [84].

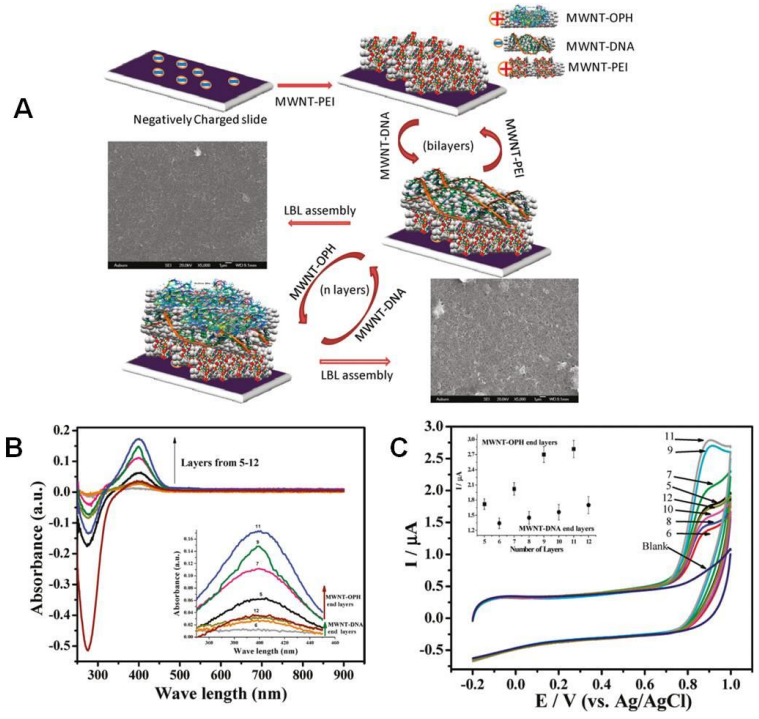

Figure 3. (A) LbL interface design: The initial layers of MWCNT-PEI and MWCNT-DNA (four bilayers as shown in SEM) provide support for subsequent layers of MWCNT-OPH and MWCNT-DNA (nine bilayers are shown in SEM). (B) UV-vis absorption spectra of LbL assembly for different number of layers by exposing the surface to 0.1 mM Paraoxon for 10 min. Odd layers are ending with MWCNT-OPH. (C) CV response using LbL assembly for different number of layers (odds ending with MWCNT-OPH and evens ended with MWCNT-DNA). Inset: Correlation of current at 0.90 V vs number of layers (maximum peak current corresponding to PNP oxidation potential).

Since the majority of reported biosensors used for neurotoxin detection are still inhibition enzyme based, using Acetylcholinesterase, AChE. Usually the inhibition level corresponds to the concentration of neurotoxins present. We also investigated single inhibition enzyme AChE based

biosensing interfaces using LbL for detecting of neurotoxin.

2.2 Research objectives

Over the past decade considerable attention has been drawn towards architectures of two dimensional and three dimensional nanostructures with excellent functions that are attractive for practical applications. There are large amount of research paper on application of LbL assembly since it creates new insights and concepts for development of novel technologies, e.g. new nanostructure, new nanomaterials. However, the LbL assembly in our system are to be more sophisticated involving both nanomaterials MWCNT and immobilized biomolecules/biopolymers (e.g. DNA, PEI, enzyme) in a layer. And to the best of our knowledge the properties of the biofunctionalized MWCNT interfaces as well as the interactions between the biofunctionalized MWCNT interfaces in an LbL assembled system were not specified and emphasized yet.

Therefore we began our research by investigating the properties of MWCNT immobilized biomolecule interfaces. The study was conducted upon MWCNT-AChE inhibition based biosensing interfaces via LbL assembly. Real-time visualization of the LbL assembly, desorption, and regeneration of MWCNT-biomolecule interfaces on gold and GC electrode were realized using surface plasmon resonance (SPR) followed by validation with electrochemistry characterization. Meanwhile, the surface property after LbL modification, e.g. effective surface area, roughness, electrochemical property were obtained with SEM, AFM and impedance analyses. The other aspects is to understand the interactions between biomolecule-MWCNT layers, such as structure-

affinity, structure-stability, and structure function relationships. This includes understanding how the enzyme layers can be structured, how the presence of each next layer can influence the catalytic activity of the previous layer, how deep might the substrate penetrate through multiple layers, and how the composition of layers might influence on the overall interfacial properties, which will in turn lead to development of the principles of interface design. Furthermore, with advent of developing neurotoxin inhibition based AChE or other enzyme biosensors, developing a simple, reliable, and cost-effective method of renewing an inhibited biocatalyst (e.g., enzymatic interfaces) is needed to advance multiuse, reusable sensor applications. We also explored the feasibility of simple renewal of the inhibited MWCNT-AChE interfaces using pH treatment.

Followed by understanding of fundamental properties and interactions, we are able to better design biointerface architecture as well as control its function for desired applications. We extended the versatile LbL assembly technique for constructing novel multi-enzyme based sensor and energy-conversion system. Therefore, in rest of my research projects, we employ the versatile LbL assembly towards several novel applications, e.g. MWCNT/multi-enzyme based biosensor for discrimination system, MWCNT/cascade enzyme based biofuel cell system etc. Critical factors affecting the performance of biosensor and biofuel cell performance, such as density, sequence or organizations of layers and diffusion coefficient of molecules through LbL structures etc were emphasized. More details concerning the importance of each investigations will be elaborated in related section in this dissertation.

Overall, the investigations in this dissertation contribute to a better scientific understanding of LbL assembly of biofunctionalizd MWCNT interfaces and create new insight in extension of the

versatile LbL assembly technique in development of novel sensor and energy technologies, meanwhile also serve as guidance for researches in seeking improvement on performance of related bioelectrocatalytic systems.

3 Layer-by-Layer Assembled Carbon Nanotube-Acetylcholinesterase/Biopolymer Renewable Interfaces: SPR and Electrochemical Characterization

3.1 Introduction

The Layer-by-Layer (LbL) self-assembly technique is a prime, low-cost choice for fabricating nanostructured multilayer films due to its simplicity, wide selection of materials, multiple applications and precision film composition control. First demonstrated by Decher et al.,[15] the adsorption process involves fabricating multilayers with a tailored architecture by applying consecutive electrostatic interactions of cationic and anionic polyelectrolytes using a variety of organic and inorganic materials including carbon nanotubes (CNTs),[85] nanocrystals,[86] nanoparticles,[87] DNA/protein,[29,88] a variety of enzymes,[28] e.g. glucose oxidase,[89,90] catalase,[90,91] peroxidase,[92] lysozyme,[83] organophosphorus hydrolase (OPH),[84] acetylchlolineasterase (AChE),[93] and other biological components. Importantly, CNTs have attracted considerable attention due to their strong electrical conductivity, absorptive properties, good mechanical strength, and potential biocompatibility. These features provide extremely powerful platforms for wide range of CNT applications in physical devices, and are highly suitable as bio/chemical sensors and in bioanalytical field settings.[94,95,96,97] While raw CNTs are impractical to use directly, several biocompatible and versatile polymers, such as nafion, chitosan, polyethylenimine (PEI), and polyacrylic acid (PAA), using non-covalent bonding via **π-π** interactions or electrostatic interactions, are quite popular for solubilizing CNTs without damaging their intrinsic properties.

In a similar way, biofunctionalized CNTs, e.g. CNTs combined with biopolymers, can enhance direct electron transfer and provide an excellent scaffolding structure for the immobilization of enzymes without sacrificing bioactivity of enzymes in development of biosensors.[83,84,98,99]

Previously, our group reported on LbL-assembled CNT lysozyme coatings precisely controlled for thickness and alignment to maintain high antimicrobial activity.[83] Advanced LbL catalytic interfaces for detecting paraoxon (organophosphorus (OP) neurotoxic compounds) through hydrolysis reaction, based on the interaction of oppositely charged MWCNTs-PEI and MWCNTs-DNA as strong support for immobilization of MWCNTs-OPH, have also been reported[84] using UV-Vis spectroscopic and amperometric techniques. However, the direct "visualization" of a stepwise signal increase during the LbL multilayer fabrication, indicating successive formation of biofunctionalized CNT enzyme/polyelectrolyte interfaces, has not been reported until now. Here, we utilized surface plasmon resonance (SPR) for real-time, optical monitoring of LbL-assembled, nanostructured, PEI/DNA/PEI/AChE layers to construct a multilayered, AChE biosensor. SPR monitoring relies on a change in the refractive index of the media due to presence of different molecules at the interfacial region on gold surface. Furthermore, we used SPR to explore regeneration of the sensor surface through absorption and desorption of polyelectrolytes (PEI and DNA) and AChE dispersed with and without CNTs.

A large number of reports have described AChE biosensors possessing good speed and sensitivity, high selectivity, and miniaturization.[96,100,101,102] However, regeneration of biofunctional interfaces is not well documented, and most reports of inhibition-based detection neglect the restoration of enzyme activity; although usually a correlation between activity loss (inhibition) and

analyte concentration can be found.[100,101,102] Another important reason such a regenerative system has not been realized is the lack of simple, reliable and cost-effective regeneration methods. Commercial re-activators have been widely applied in AChE recovery using traditional approaches, but these are plagued by unstable recovery percentages affected by many different factors, e.g. concentration of inhibitors, different types of neurotoxins etc.[103,104] Therefore, it is important to explore practical, simple, and reliable approaches that allow regeneration of inhibition-based enzymatic biosensing systems in multiple analytical applications.

It is well known that the net charge of polypeptides is dependent on pH and acid or alkaline treatment of a polypeptide can change its net charge. This could result in the electrostatic repulsion between protein layers and consequently leading to desorption of protein layers.[105,106] Therefore, we chose pH treatment for our investigation of desorption behavior of enzymatic layers in LbL self-assembled interfaces (schematic Illustration shown in Figure 4). This could serve as a basis for investigating the alternative approach for regeneration of biofunctional interfaces for multiple uses. In this study, the renewal of AChE enzymatic layers at LbL self-assembled biosensor interfaces was explored by SPR and verified by amperometry. Surface characterizations using Scanning Electron Microscope (SEM) and Atomic Force Microscope (AFM) were performed to validate the LbL self-assembly fabrication.

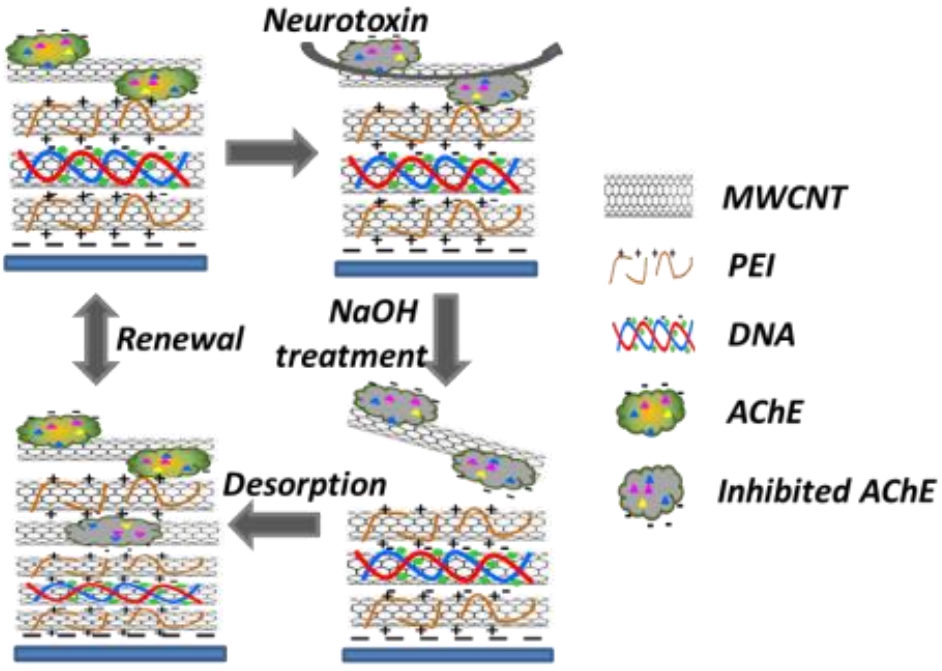

Figure 4. Schematic illustration of the process for renewal of the enzymatic layer in Layer-by-layer (LbL) self-assembled biosensor interfaces

3.2 Materials and methods

3.2.1 Materials

Paraoxon was obtained from ChemService, Inc. (West Chester, PA). Multi-walled carbon nanotubes (purity 95%, length 1-5 μm, diameter 30 ± 10 nm), acetylcholine esterase (AChE) from electrophorus electricus eel (E.C 3:1:1:7, 518 units/mg solids), acetyl thiocholine (ATCh), lyophilized salmon sperm DNA salt, N-hydroxysulphosuccinimide (NHS), N-ethyl-N-(3-dimethylaminopropyl) carbodiimide hydrochloride (EDC), polyethyleneimine (PEI, Mw~750,000, branched), 2-(N-morpholino) ethanesulfonic acid (MES), N-cyclohexyl-2-aminoethanesulfonic

acid (CHES), phosphate buffered saline (PBS), tris(hydroxymethyl)aminomethane (TRIS), sodium hydroxide (NaOH), pralidoxime (PAM) were all obtained from Sigma-Aldrich (St. Louis, MO). Ultrapure DI water obtained from Millipore Direct-Q Water system (resistivity, 18.2 MΩ cm^{-2}) was used for all the sample preparations.

3.2.2 Instruments

SPR experiments were performed using SPREETA^{TM} SPR system from Texas Instruments (Dallas, TX, USA). The device consists of a portable SPR sensor, integrated multichannel flow cell, and 12-bit interface box connected to the computer with the MultiSPR software package. The portable Spreeta sensor is a fully integrated sensing chip containing a gold SPR surface, light emitting diode (LED) light source, a reflecting mirror to direct polarized light to a photodiode array and a temperature sensor. All electrochemical measurements were recorded with a CHI 660 (CH Instruments, Austin, TX) potentiostat connected to a computer utilizing the chi990b software package. The flow injection analysis system for amperometric measurement contains a multichannel syring pump (KdScientific Legato 200 Series), injection valve, 150 uL sample injection loop as well as BASi flowcell apparatus with integrated auxiliary electrode, a glassy carbon (GC) working electrode (6 mm diameter) and a reference electrodes Ag/AgCl (3 M KCl) (Figure 5). Scanning Electron Microscope (JSM-7000F field emission SEM, JEOL Ltd, Japan) and Atomic Force Microscope (Nano-R^{TM} AFM, Pacific Nanotechnology. Inc.) were used to characterize the electrostatically self-assembled interfaces on GC electrode.

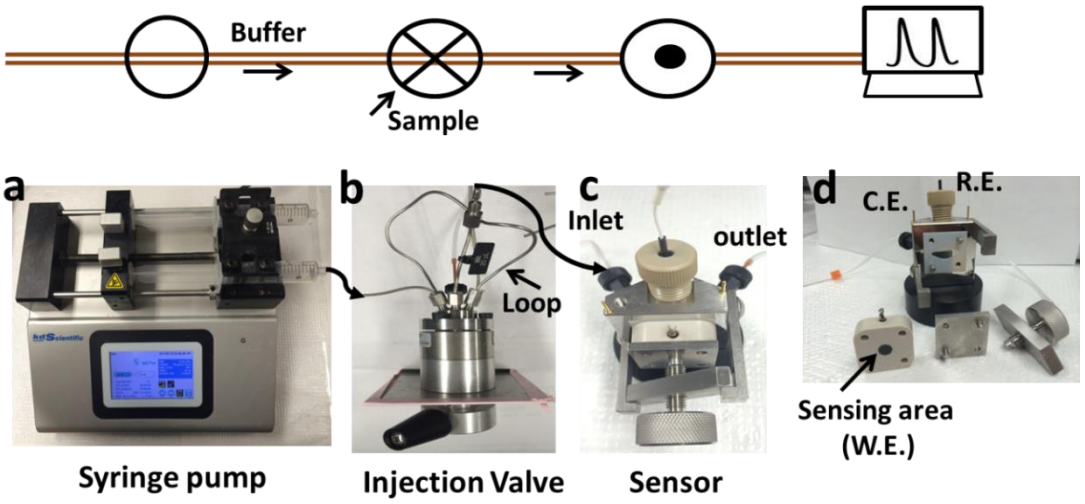

Figure 5. Flow injection analysis system comprised of four major elements, (a) a multichannel syringe pump (KdScientific Legato 200 Series), (b) injection valve and 150 uL sample injection loop, (c) the BASi flowcell apparatus with integrated auxiliary electrode, a glassy carbon (GC) working electrode (6 mm diameter) and a reference electrodes Ag/AgCl (3 M KCl). MWCNT-(PEI/DNA/(PEI/AChE)3) was built onto the surface of the GC working electrode and inserted in the flow cell along with 0.002" (51 μm) thick gasket and (d) different parts of the BASi flowcell.

3.2.3 Preparation of soluble PEI, DNA and AChE

Soluble PEI and DNA solutions of 0.2 mg/mL were prepared in deionized water (pH 6.8) and AChE (400 units/mL) was prepared in TRIS buffer (20 mM, pH 7.5). All the solutions were prepared freshly and stored at 4 °C before use.

3.2.4 Preparation of MWCNTs dispersed PEI, DNA and AChE

Preparation of carboxylated MWCNTs and MWCNTs immobilized with PEI, DNA and AChE

was based on the previously reported protocol[84] with several modifications. Two mg of carboxylated MWCNTs were suspended in 10 mL of 1 mg/mL PEI solution and sonicated in an ultrasonication bath for 1 h in ice bath, followed by centrifugation (4 ℃, 13200 rpm, 30 min) to eliminate the unbounded PEI. The bound MWCNTs-PEI sediment was re-dispersed into 5 mL deionized water (pH 6.8) and stored in 4°C. Similarly, MWCNTs-DNA composite was obtained by sonicating a mixture of 2 mg carboxylated MWCNTs and 10 mL of 1 mg/mL DNA (final concentration of 0.1% w.t.) followed by centrifugation and re-dispersion into 5 mL deionized water (pH 6.8). Finally, 0.4 mg/mL MWCNTs-PEI and MWCNTs-DNA solutions were prepared and stored at 4 °C before use.

Two mg of carboxylated MWCNTs were dispersed into a solution containing 1 mL of MES buffer (50 mM, pH 4.7) and 1 mL of 20 mM NHS. Later 1 mL of 320 mM EDC was added and immediately the mixture was stirred for 30 min. Note that all the buffer, EDC and NHS concentrations were previously optimized. The excess of unbound EDC and NHS was removed by filtering the activated MWCNTs through 0.2 μm polycarbonate membrane (Whatman) and rinsed with MES buffer (50 mM, pH 6.2) under vacuum filtration. The as-prepared MWCNTs-NHS ester conjugate was re-dispersed into 3 mL phosphate buffer (0.1 M, pH 8.3) containing 400 Units/mL AChE for immobilization. The immobilization process was allowed to proceed overnight on a platform shaker at 4 °C. The MWCNTs-AChE precipitate was then centrifuged (13200 rpm at 4 °C for 30 min each at least) three times and rinsed with MES buffer between each to remove unbound enzyme. Finally the MWCNTs-AChE composite was suspended in 1 mL of TRIS buffer (pH 7.5) and stored in refrigerator (4°C) for further fabrication of LbL biosensor.

3.2.5 SPR real-time monitoring of LbL self-assembly, desorption and renewal of enzymatic interfaces

Prior to the experiment the SPR sensor surface was meticulously cleaned with piranha solution (H_2SO_4 and H_2O_2, 3:1; *attention: caution must be taken as the piranha solution readily causes chemical burns and is highly corrosive, particularly with organic materials*) for 3 min and thoroughly rinsed with deionized water followed by 2 min of plasma cleaning. The experimental set-up was then initialized under ambient room conditions and calibrated with DI water (refractive index (RI): 1.33). DI water was pumped into the flow cell of the SPR system through two inlet channels and flowed until the baseline reached a stable value. The LbL self-assembly was initiated by pumping positively charged MWCNTs-PEI dispersion into the flow cell at a constant flow rate (50 µL/min) over the surface of the gold chip until stable response unit (RU, 1 RU = 10^{-6} RI unit) was obtained. Then, negatively charged MWCNTs-DNA dispersion was pumped across the SPR chip to form an anionic/cationic binding layer on gold surface. Once the signal was stabilized, another layer of positively charged MWCNTs-PEI was assembled followed by injecting of TRIS buffer to serve as a background signal. Further, electrostatic binding of negatively charged MWCNTs-AChE layer was subsequently conducted. Desorption of the enzymatic layer was carried out by flowing 6 M NaOH through the gold surface followed by rinsing with deionized water. The whole treated surface was then subjected to another set of electrostatic self-assembly of polyelectrolyte/enzyme nanocomposites deposition and desorption. Variations of SPR signal as a function of real time was monitored for three consecutive cycles for

both soluble and CNTs dispersed PEI/DNA/PEI/AChE assembly. The change in RU and corresponding RI value caused by all the layers was recorded and calculated.

3.2.6 LbL self-assembly of bio-functionalized MWCNTs on GC electrode

Prior to multilayer assembly onto the GC electrodes, the electrodes were cleaned and electrochemically pretreated with 1 M NaOH for 5 minutes at 1.2 V vs Ag/AgCl to induce a negatively charged surface. The electrodes were rinsed with DI water and dried with high purity nitrogen gas for further assembly. Twenty µL of MWCNTs-PEI (positively charged) dispersion was dropped onto the GC electrode for 15 min, rinsed with DI water to remove the unbound MWCNTs-PEI and dried with nitrogen. Then, MWCNTs-DNA (negatively charged) dispersion was dropped upon MWCNTs-PEI for 15 min followed by the same rinsing and drying procedures. The following layers of MWCNTs-PEI and MWCNTs-AChE (negatively charged at pH 7.4) were assembled in a similar way and repeated for three times to stabilize the structure and the final layer of 20 µL MWCNTs-AChE was allowed to dry at 4 °C before use. Finally, an 8-layer bio-nanocomposite of MWCNTs-(PEI/DNA/(PEI/AChE)$_3$) was constructed on the GC electrode.

3.2.7 SEM and AFM characterization of LbL assembly on GC electrode

LbL assembled bio-functionalized MWCNTs interfaces were fabricated by deposition of 3 layers of MWCNTs-PEI/DNA/PEI and 8 layers of MWCNTs-(PEI/DNA/(PEI/AChE)$_3$). The resulting surfaces were characterized by SEM and AFM on the GC electrode.

3.2.8 Electrochemical measurement and determination of enzyme activity

All electrochemical measurements were performed with a GC electrode at room temperature. The amperometric detection of AChE hydrolysis of ATCh is based on detection of the enzymatic reaction product thiocholine (TCh), an electroactive species that has an oxidation peak at 0.61 V vs Ag/AgCl:

$$\mathrm{ATCh + H_2O \xrightarrow{AChE} TCh + Acetic\ Acid} \quad (1)$$

A flow rate of 5 mL/hr was set for amperometric detection in this study. The 500 µM ATCh substrate solutions prepared in 10 mM PBS buffer (pH 7.4) were injected at five consecutive time intervals to monitor the activity of nanostructured AChE biosensor in flowing buffer stream. The biosensor was then incubated with PX (25 µM) for 15 min to obtain 95% inhibition and the activity was again measured with amperometry. After the inhibition test, renewal of the enzymatic layer was performed by treating the electrode with 6 M NaOH for 10 min. Then, new layers of MWCNTs-PEI followed by MWCNTs-AChE were deposited. For comparison, the activity of the renewed sensor was measured. All the measurements were carried out at room temperature. The inhibition percentage as well as recovery percentage was calculated according to the subsequent equations.

$$\text{Inhibition \%} = \frac{C_{initial} - C_{inhibition}}{C_{initial}} \quad (2)$$

$$\text{Recovery \%} = \frac{C_{renewal} - C_{inhibition}}{C_{initial} - C_{inhibition}} \quad (3)$$

3.2.9 Reactivation with commercial oximes

Recovery of MWCNTs-AChE activity using commercially standard re-activator pralidoxime (PAM) was conducted as a referring procedure using the same flow injection analysis system via amperometric analysis with a GC electrode at room temperature. Initial signal of the sensors was collected utilizing 500 μM ATCh. The sensors were then separately incubated in different concentrations of PX solutions (5, 10, and 25 μM), for 15 min and the signals from each were measured. Finally, the sensors were incubated in PAM solution (5 mM, 10 min) and the recovered enzyme activities were measured. Inhibition and recovery percentages of MWCNTs-AChE activity with commercial re-activators was also calculated according to equations (2) and (3).

3.3 Results and discussion

3.3.1 SPR characterization: adsorption and desorption behavior of soluble PEI, DNA and AChE

A SPR sensogram of the LbL self-assembly of soluble components is shown in Figure 6A. After the baseline with water was stabilized, solutions of positively charged PEI, negatively charged DNA, positively charged PEI, and negatively charged AChE were consecutively injected into the system. Each injection was successively introduced only after a signal of previously injected component was stabilized, and the difference between the RU changes were calculated respectively (Figure 6B). A sharp RU increase in a stepwise manner demonstrated the formation of LbL self-assembly between oppositely charged PEI (ΔRU = 1087, ΔRI = 0.0011), DNA (ΔRU = 3936, ΔRI = 0.0039), PEI (ΔRU = 3629, ΔRI = 0.0036) and AChE (ΔRU = 13560, ΔRI = 0.01356)

on gold surface due to electrostatic interactions. PEI and DNA are polycationic and polyanionic, respectively. TRIS buffer (20 mM, pH 7.5) was used to disperse AChE enzyme, setting it apart from its isoelectric point (pH 5.5) and therefore exhibited negative charges during layer deposition. The strong electrostatic interactions between PEI, DNA and PEI served as adhesive or cushion support and provided sufficient charge for strong binding of the following AChE layer. As a background signal, the RU change from TRIS buffer was negligible.

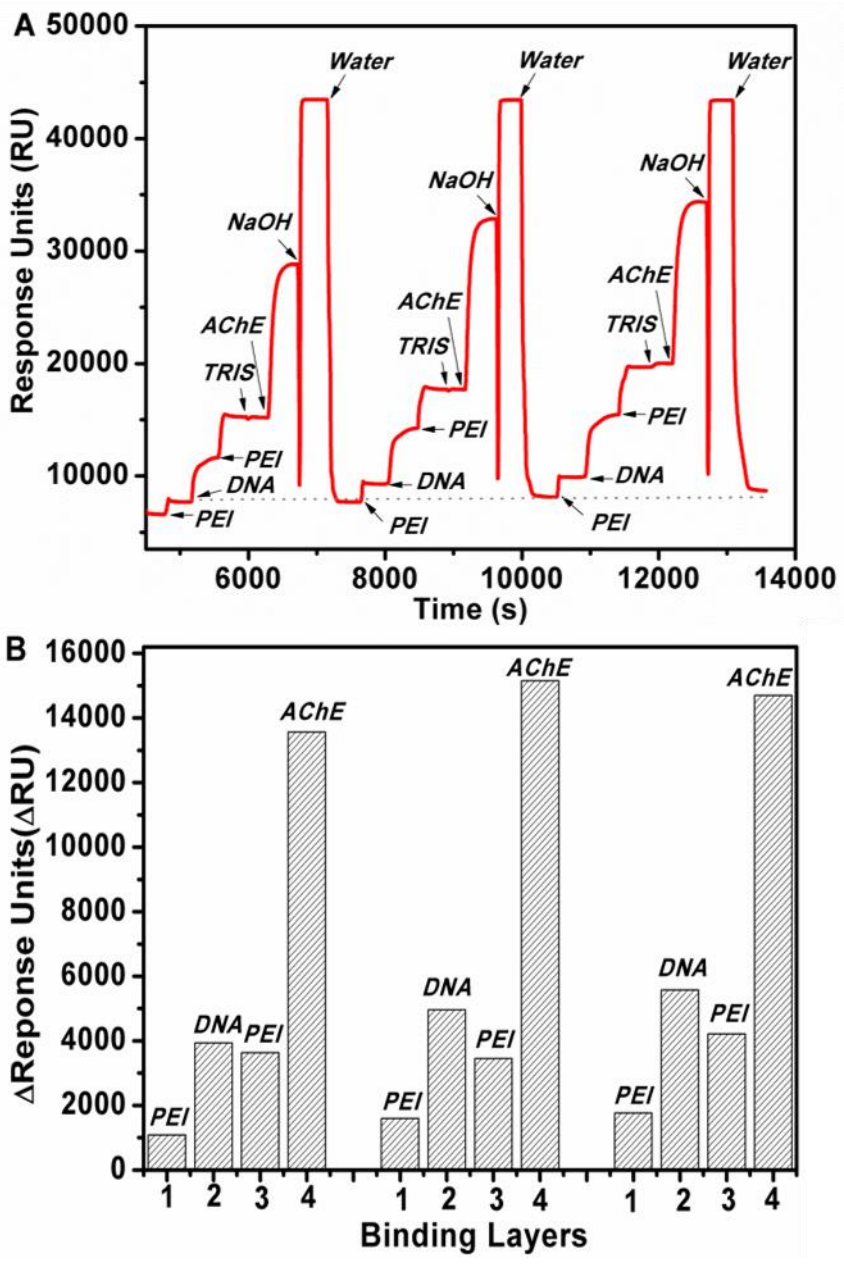

Figure 6. (A) SPR characterization of LbL self-assembly, desorption and renewal of soluble PEI/DNA/PEI/AChE enzymatic interfaces on gold surface, (B) Bar graph showing change of response units of each binding layer in three cycles.

To desorb the active layer of the LbL assembly, 6 M NaOH was injected and a sharp reduction

in RU (ΔRU = 21124) was observed (corresponding ΔRI = 0.02112), indicating a significant desorption of layers on gold surface. An immediate increase in RU signal was observed and should attribute to refractive index of NaOH and the subsequent binding of ions from NaOH on the gold surfaces. The last step of washing with deionized water then further removed the residual molecules on the gold surface and the RU signal decreased down to the PEI layer (RU = 7682, RI = 1.3377), indicating a strong desorption of the layers. The same consecutive LbL self-assembly and desorption process on the gold surface was further repeated for three times. Applying NaOH upon the second and third cycle both exhibited thorough desorption, with the signal dropping down to nearly the starting baseline. The remaining PEI layer after NaOH treatment in initial cycle was attributed to the strong interaction between polycationic PEI and gold surface upon direct binding. This phenomena was further confirmed in a control experiment (Figure 7) by applying NaOH after direct binding of one layer of PEI, two layers of PEI/DNA, three layers of PEI/DNA/PEI on gold surfaces, respectively. Slight desorption was observed for the PEI layer directly bound to the gold surfaces, whereas the stripping behavior of the DNA layers and the PEI layer onto the DNA layer was observed upon NaOH treatment. The bar graph shown in Figure 1B represents the change in RU of the three consecutive cycles. The three cycles displayed similar binding and desorption behaviors with corresponding ΔRU numbers that are very similar on the gold surface, illustrating the feasibility for total regeneration of enzymatic interfaces on gold surfaces for soluble PEI, DNA and AChE.

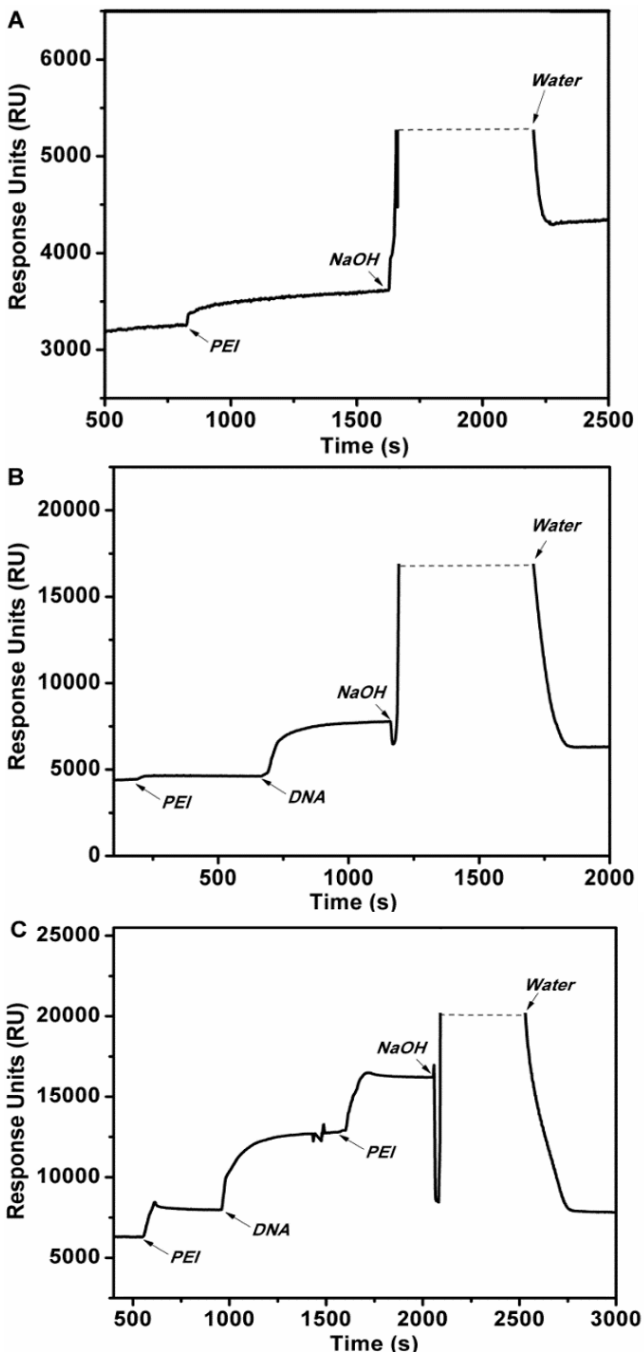

Figure 7. Control experiment showing applying of NaOH after binding of one layer PEI, two layers of PEI/DNA, three layers of PEI/DNA/PEI.

3.3.2 SPR characterization: adsorption and desorption behavior of MWCNTs dispersed -PEI,

DNA and AChE

A SPR sensogram of MWCNTs dispersed PEI, DNA and AChE is shown in Figure 8A. The initial binding of positively charged MWCNTs-PEI (0.4 mg/mL) resulted in a large change in RU (ΔRU = 8197, ΔRI = 0.00819), which is can be attributed to the binding of both the PEI and bulky carbon nanotubes. The following adsorption of oppositely charged MWCNTs-(DNA/PEI/AChE) was further collected with changes in RU of 2788, 899 and 671, respectively. The decreasing fashion in change of RU could be due to the SPR signal attenuated within the given resolution as number of MWCNTs layers increased onto gold surface.

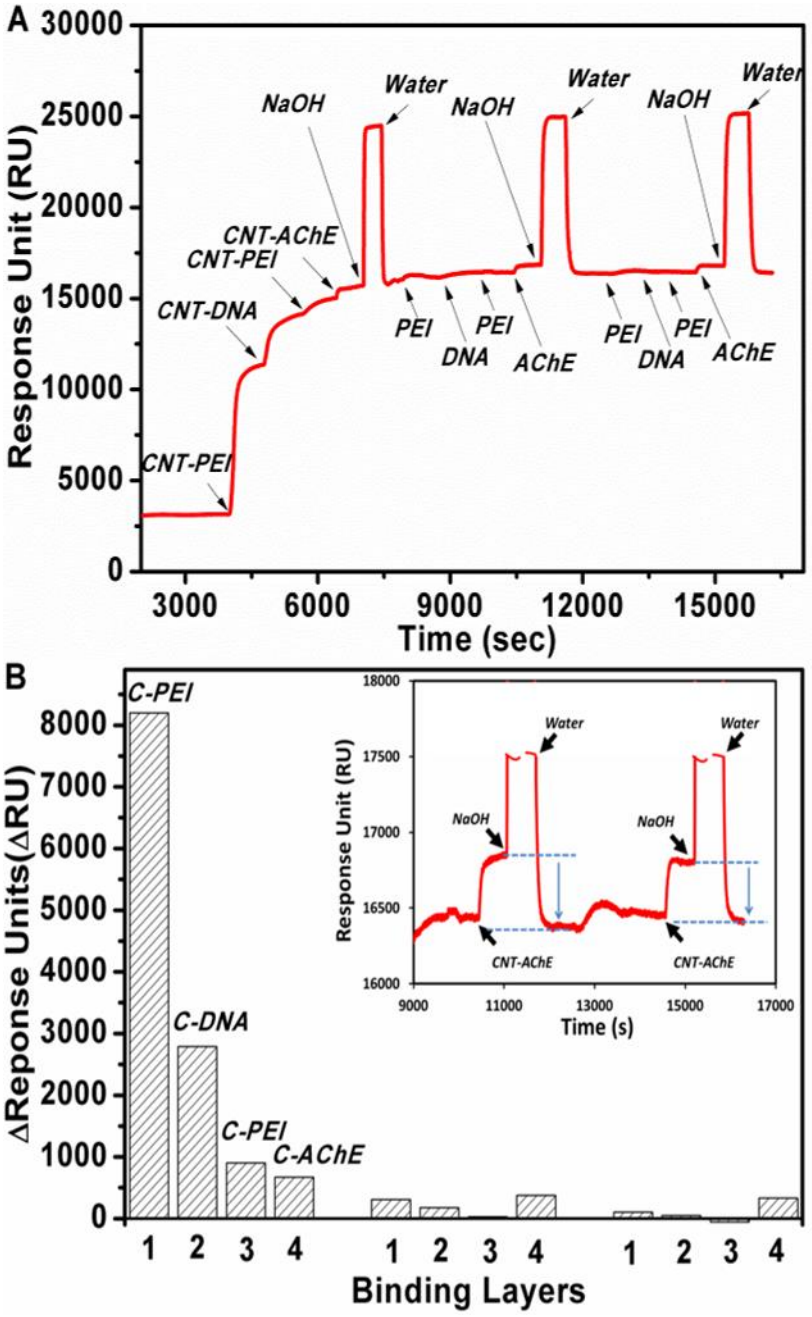

Figure 8. (A) SPR characterization of LbL self-assembly, desorption and renewal of MWCNTs-PEI/DNA/PEI/AChE enzymatic interfaces on gold surface, (B) Bar graph showing change of response units of each binding layer in three cycles;, inset showing enlarged desorption behavior of MWCNTs-AChE layer after NaOH treatment in (A)

Interestingly, as distinguished from that for soluble PEI, DNA and AChE, the 6 M NaOH treatment did not substantially strip off all the MWCNTs-layers. Only a partial desorption upon the topmost layer was observed. The figure inserted in Figure 9B shows the desorption behavior of the MWCNTs-AChE layer after treatment with NaOH. The change of conformation of polymers induced by binding onto MWCNTs and the unique surface chemistry of MWCNTs makes the interaction between layers rather complicated to definitively study. It is possible that the adsorption behavior between MWCNTs-biopolymers is governed not only by electrostatic interactions between polymers, but also by the high binding energy of MWCNTs on gold surface.[107,108] PEI and DNA are both macromolecules with high cationic/anionic charge density and therefore have a strong electrostatic interaction. While wrapped onto MWCNTs, the interactions between MWCNTs and gold surfaces may have further enhanced the binding of MWCNT-biopolymers. Conversely, AChE, with lower charges, was located in the uppermost layer, and potentially had a weaker electrostatic interaction with the assembly.[109,110] Additionally, the interaction between MWCNTs and gold surface may be attenuated as the distance increases between each surface. Therefore it was not surprising that partial desorption of the uppermost MWCNTs-AChE layer was observed by applying 6 M NaOH, while the supporting layers were less affected. Investigation of desorption by applying NaOH after the adsorption of one layer MWCNTs-PEI, two layers of MWCNTs-PEI/DNA, three layers of MWCNTs-PEI/DNA/PEI on gold surfaces, respectively, were conducted. Similar desorption behavior was observed with removal of topmost MWCNTs-AChE layer behavior (Figure 10).

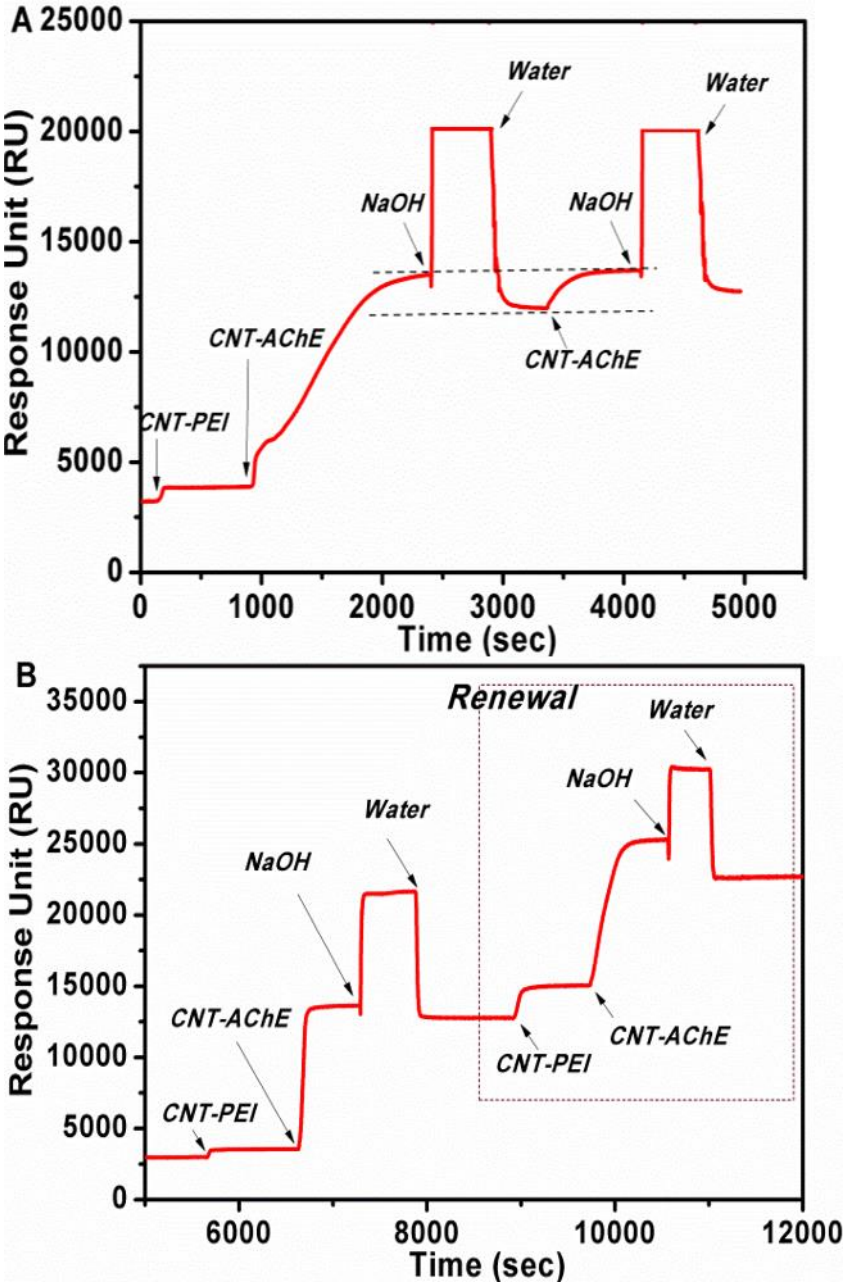

Figure 9. Direct assembly of CNT-AChE (A) versus assembly of CNT-PEI/AchE (B) after NaOH treatment

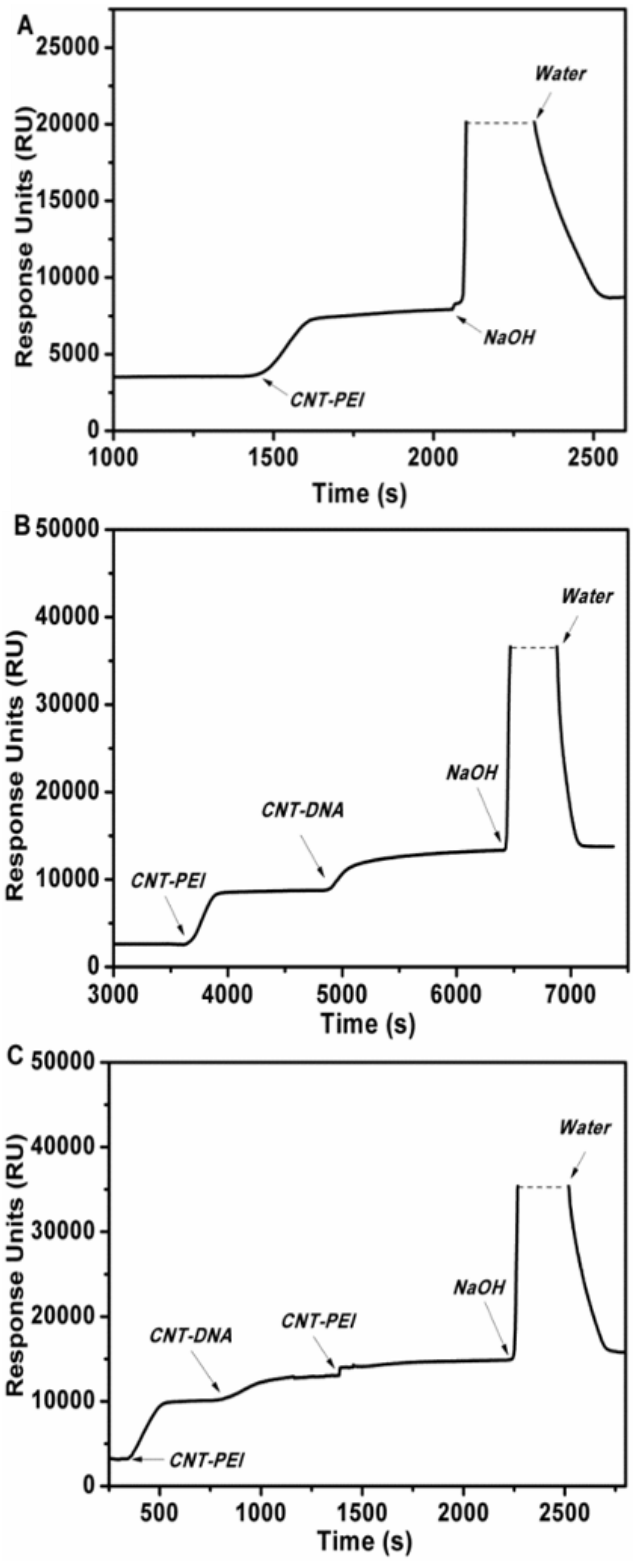

Figure 10. Control experiment showing applying of NaOH after binding of one layer CNT-PEI, two layers of CNT-PEI/DNA, three layers of CNT-PEI/DNA/PEI.

After NaOH treatment, the subsequent binding of MWCNTs-PEI, DNA, PEI and AChE upon the treated interfaces was still observed and ΔRU was shown in Figure 8B. To illustrate the subsequent binding process, comparison experiments were conducted with diluted solutions of MWCNTs-PEI and AChE (0.1 mg/mL). Figure 6A demonstrated the direct assembly of MWCNTs-AChE while Figure 6B showed the assembly of MWCNTs-PEI layer followed by MWCNTs-AChE upon the treated surface. The RU change in direct assembly of MWCNTs-AChE (Figure 9A) was very small (ΔRU = 1674, ΔRI = 0.00169), compensating for the desorbed amount. In comparison, the MWCNTs-PEI binding upon treated interfaces was comparable to the initial MWCNTS-PEI layer. It should also be noted that the RU change of following MWCNTs-AChE layer (ΔRU = 10223, ΔRI = 0.01025) was comparable to that of initial MWCNTs-AChE layer (ΔRU = 10064, ΔRI = 0.01007), completely renewing the enzymatic interfaces. This phenomenon demonstrated the negative charge of surface after NaOH treatment and the feasibility of layer regeneration, providing a novel approach for renewal of enzymatic interfaces in LbL-assembled AChE biosensor.

3.3.3 Surface characterization of MWCNTS thin films on GC electrode

Figure 11 A-B represents the top view SEM images of the LbL assembled thin films with bio-functionalized MWCNTs of 3 layers and 8 layers on GC electrode, respectively. Randomly oriented bio-functionalized MWCNTs can be clearly observed in the thin film, and with the increase of layers, a thicker MWCNTs surface was displayed, further demonstrating the

effectiveness of LbL process. The random orientation and intertwined microstructure was attributed to kinetically electrostatic absorption between oppositely charged species during self-assembly process.[85] Tapping-mode AFM image in Figure 11C-D also showed an interlocked network structure of bio-functionalized MWCNTs, and with the increase of the number of layers, surface roughness increased due to the increased thickness (Figure 11C-D).

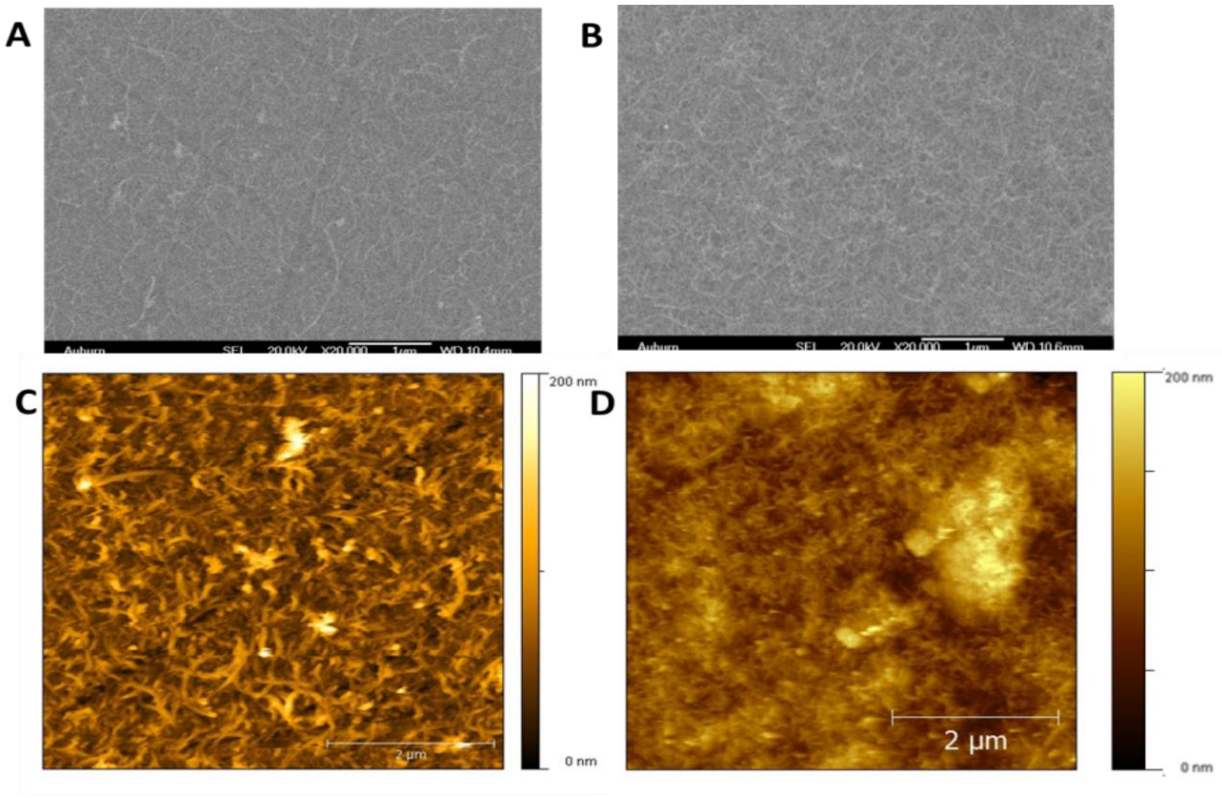

Figure 11. SEM characterization of 3 layers (A) and 8 layers (B) and corresponding AFM characterization of 3 layers (C) and 8 layers (D) bio-functionalized MWCNTs on GC electrode

3.3.4 Amperometric measurement of enzyme activity in renewed biosensor interfaces

As demonstrated previously in equation (1), amperometric measurements of LbL-based

MWCNTs-(PEI/DNA/(PEI/AChE)$_3$) sensors to 500 μM ATCh solution in flow system with five continuous injections were conducted. It was observed that ATCh itself could be oxidized on the bare electrode above 0.3 V versus Ag/AgCl in absence of AChE (Figure 12, pink curve). In the presence of AchE, an obvious oxidation peak was observed. Furthermore, the oxidation peak current on a LbL assembled MWCNTs modified electrode was observed to be much higher than background signal of ATCh itself. We observed in our study that CNTs greatly enhanced the amperometric signal of the enzymatic product when compared with LBL without CNTs and decreased the over-potential of thiocholine oxidation (Figure 13). In addition, five consecutive injections of ATCh showed a high consistency in current signal, indicating good stability of the LbL-based MWCNTs immobilized biomolecules structure on GC electrode. Further amperometric measurements were used to understand the effects of PX exposure and renewal of LbL AChE sensor. When the sensor was subjected to 25 μM PX incubation for 15 min, the peak current greatly decreased (green curve) compared to the absence of PX. However, after renewal of electrode with NaOH treatment followed by assembly of fresh layers of MWCNTs-PEI/AchE, the peak current recovered completely to the initial levels (red curve), indicating the complete regeneration of inhibited AChE biosensor. A high average recovery of 97.1 ± 2.7 % was achieved with good stability. The average percentage of inhibition and recovery with respect to the amperometric current was calculated and shown in Table 1. The baseline for the renewed sensor increased slightly due to the increase in resistance resulting from the increased number of MWCNTs layers on GC electrode surface. From the above electrochemical results, the experiment has demonstrated the successful assembly and renewal of enzymatic interfaces on GC electrode, consistent with the SPR

characterization of LbL self-assembly and renewal of MWCNTs-AchE interfaces on gold surface.

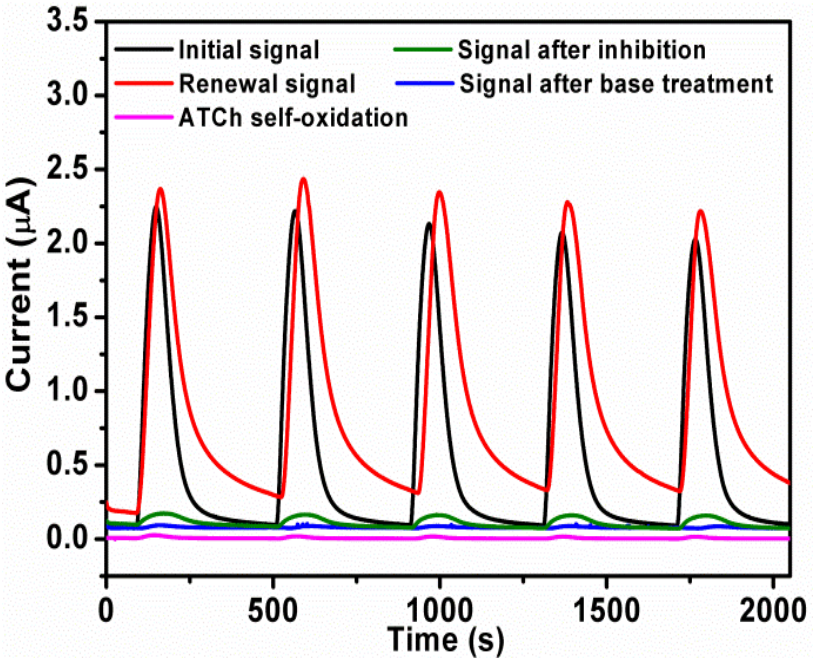

Figure 12. Representative amperometric measurements of 500 μM ATCh with initial, inhibited and renewed enzymatic interfaces on GC electrode (0.61V, at room temperature)

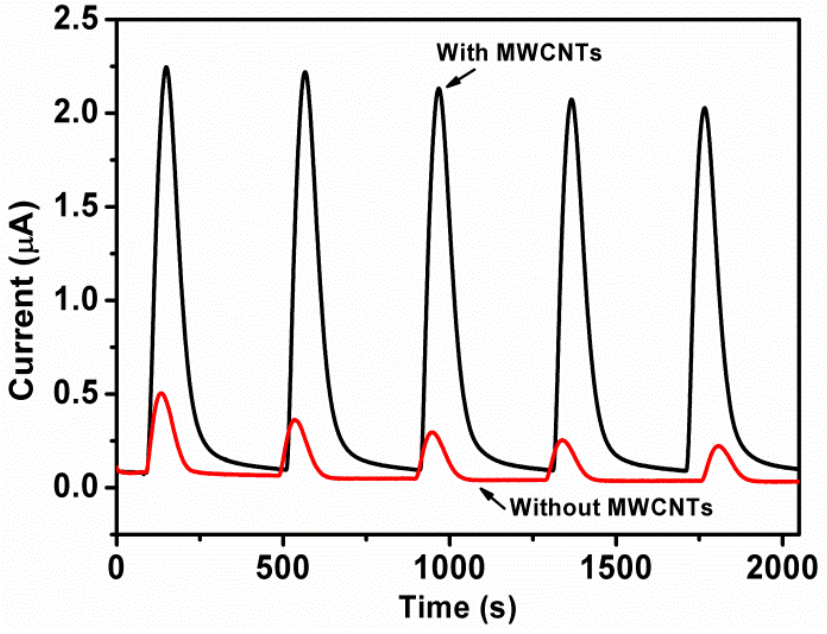

Figure 13. Detection of 500 μM ATCh on LBL with/without MWCNTs

Table 1. Average percentage of inhibition and recovery with respect to the amperometric measurement of 500 µM ATCh with MWCNTs-(PEI/DNA/(PEI/AChE)$_3$) biosensor using Renewal approach.

Amperometric measurement	Initial Current (µA)	Inhibition with 25 µM PX, 15 min	Renewal Current(µA)
Average (n=3)	2.04 ± 0.18	0.065 ± 0.015	1.98 ± 0.22
Inhibition %		96.78 ± 0.6%	
Recovery %		97.1 ± 2.7%	

3.3.5 Comparison of reactivators with renewal approach of enzymatic interfaces

Reactivation of PX-inhibited MWCNTs-AchE with the commercially standard reactivator PAM is shown in Figure 14. The bar graph represents the recovery percentage of the sensors with different inhibition percentages, which correspond to differening concentrations of PX. More than 90% of AChE activity was recovered by 5 mM PAM when the sensor was 85% inhibited by PX. However, when the inhibition was increased to 90% and more than 95%, the recovery efficiency dramatically reduced to 26%, and 6% respectively. While the recovery percentage of reactivators has shown a dependence on the inhibition percentage, the renewal approach presented here has been demonstrated to be advantageous in obtaining a high recovery percentage, while avoiding the uncertainty raised from inhibitors or reactivators. It has also eliminated the use of high concentration reactivators in effective renewal of enzymatic biosensing system. Moreover, once

the enzyme activity from renewed enzymatic interfaces is determined, it can simultaneously serve as its own baseline for the second use or even multiple uses.

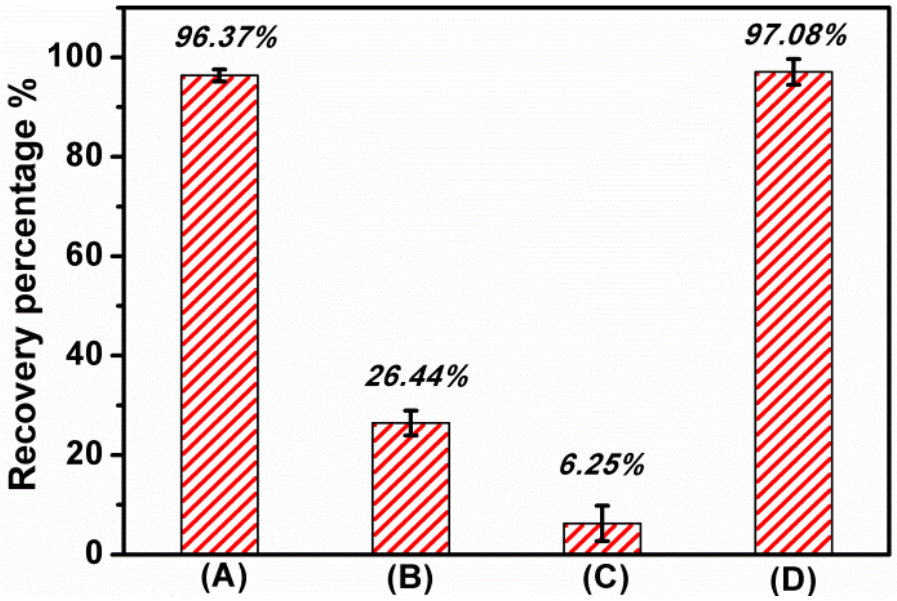

Figure 14. Recovery of inhibited MWCNTs-AChE (A) 85% inhibition, (B) 90% inhibition, (C) more than 95% inhibition with PAM (5 mM, 10 min) and (D) renewal approach via amperometric analyses on GC electrode (0.61V, at room temperature)

3.4 Conclusions

This study demonstrated the feasibility of a renewal approach as an alternative for oximes in conventional reuse of LbL based MWCNTs-AChE biosensors. SPR played a major role in real-time monitoring of cationic and anionic enzyme/polyelectrolyte multi-layer assembly of the film in a step-wise fashion and desorption of the layers via high pH treatment on the gold surface. Different numbers of layers of the LbL assembly were characterized by SEM and AFM.

Amperometric measurements on the CNT interfaced biofunctionalized AChE biosensor showed stable and reproducible peak current signals. The recovery efficiency with conventional reactivators was adversely affected with an increase in inhibition percentages (greater concentrations of inhibitor). However, the renewal approach effectively recovered nearly 100% of AChE activity independent of inhibition. Therefore, our proposed approach proved to be advantageous in regeneration of enzyme activity, combined with excellent properties of nanomaterial. Such a simple, inexpensive approach demonstrates great potential of LbL self-assembled inhibition-based enzymatic interfaces in a biosensing system for long-term usage and multiple uses.

4 Layer-by-layer assembled multi-enzyme/CNT biosensor for discriminative detection between organophosphorus and non-organophosphorus pesticides

4.1 Introduction

Development of highly sensitive and discriminative techniques for detection of toxic analytes has been one of the top research priorities in the past decades. Extensive use of pesticides and release of tremendous amounts of their residues in the environment such as soil, water and food raised serious public concerns regarding health, environment and food safety.[111] Organophosphates (OP) and carbamates (non-OP) are highly neurotoxic compounds, and with much lower doses can cause chronic delayed onset toxicity to nerve cells. Several studies have shown that low level exposure of these pesticides attribute to the inhibition of acetylcholine esterase (AChE) enzyme, which regulates the turnover of neurotransmitter acetylcholine in synaptic transmission. Consequently, acetylcholine accumulation in receptor sites can lead to various clinical complications ultimately leading to death.[112,113] Therefore, their detection in environmental and biological samples using sensitive methods is highly demanded. Chromatography based traditional instrumentation - HPLC, GC-MS and LC-MS are the most important OP and non-OP detection methods. However, these methods require meticulous sample preparation, labor intensive and sophisticated expensive instruments.

Acetylcholine esterase (AChE) inhibition based electrochemical biosensors have received high attention for analyses of pesticide compounds, based on their simplicity, rapidity, high

specificity, and reduced sample preparation.[96,114,115,116] The inhibition mechanism involves high affinity of both OPs and non-OPs towards AChE enzyme where the hydroxyl of the serine residue within the active site is phosphorylated (OPs) or carbamylated (non-OPs). Several other enzymes including butrylcholine esterase,[117] and urease[118,119] have been used in the development of variety of electrochemical biosensors based on inhibition mode in which the signal from electroactive product is inversely proportional to the pesticide concentration. Various other inhibition sensors have been developed on bi-enzyme cascade reactions (AChE and Choline Oxidase (ChOx)) for recognizing acetylcholine/ choline based on amperometric detection of H_2O_2.[120,121,122] Although majority of present biosensors are inhibition/catalytic based, remarkably all of them are based on "one analyte – one biorecognition element" detection pathway which is not specific enough to derive conclusion and thus rendering impossible to discriminate, a series of key pesticide analytes. In contrast, if measured with more than one biorecognition structure/element and target the same analyte, an unambiguous result can be achieved. In this line, multi-enzyme biosensing systems that provide versatility for detection of multi-analytes opens up new possibility for multiplexed assays of different chemical analytes.

Recently, organophosphate hydrolase (OPH) was recognized as an alternative recognition enzyme for direct detection of organophosphate, as the detection signal is directly proportional to the concentration of the OP.[123,124] The enzyme hydrolyzes OP molecule and the products can be measured by spectrophotometric and electrochemical means. In 1996, we offered a new "kinetic" approach for the direct detection of OP neurotoxins based on the enzyme OPH. It has been demonstrated that the enzymes cleaves the P-O, P-F, P-S or P-CN bonds which can result changes

in pH, that can be directly detected by electrochemical[125] and optical technique.[126,127] Flow injection amperometric detection of OP nerve agents based on OPH biosensor was also reported.[128] Simonian et al. further identified a novel multi-enzyme strategy for discrimination between different classes of neurotoxins.[129,130,131]

Recent advances for development of enzyme-based biosensors have been focused on incorporating enzymes with novel nanomaterials of fascinating electronic, mechanical and optical properties, e.g. carbon nanotubes (CNTs),[132] graphene oxide,[133,134] nanoparticles,[76,135] and quantum dots[121] etc. For example, CNT modification enhances direct electron transfer for electrochemical-based biosensors and provides excellent scaffolding structures for enzymes while retaining their bioactivities, resulting in overall performance of biosensors with improved features such as fast response time, signal amplification, higher sensitivity, better selectivity and stability. A key issue in these novel biosensors is the method of enzyme immobilization onto nanomaterials and their integration in biosensor. Ideally, a method that allows for high loading, retention of biological activity, nanomaterial properties, simplicity and control of the film architecture is desired. To overcome these challenges, literature shows a diverse set of CNT immobilization strategies for enzyme immobilization. Physical adsorptions were reported between enzymes and modified/functionalized nanomaterial surfaces through electrostatic interactions.[128,134] Although this method is relatively simple requiring no cross-linking reagents, enzyme leaching is the major problem.[136] Covalent immobilization facilitates strong amide bonding between enzyme and functionalized nanomaterials or covalent linkage of enzyme and nanomaterials via coupling reagents.[137,138] Other methods including electropolymerization,[139] layer-by-layer (LbL) assembled

multilayer interfaces were also reported. LbL assembly due to its simplicity and versatility has emerged as one of the most popular approach for the fabrication of the biofunctionalized multilayers based on the alternating assembly of oppositely charged layers. It has been demonstrated to be an effective approach for the attachment of a variety of enzymes onto CNTs and self-assembly of organized CNT-biopolymer/CNT-enzyme multilayered biosensor.[83,84,99,140] Previously, our group has reported on LbL assembly of CNTs coatings armored with lysozyme with precisely controlled thickness/alignment and LbL self-assembly processes for fabrication of MWCNT-OPH/MWCNT-DNA multilayer biosensor for organophosphate detection.[84]

Here we report, the fabrication of a novel nanotechnology-enabled multianalyte biosensor platform based on intercalation of CNTs covered with oppositely charged biopolymers and enzymes, for the assembly of unique nanointerfcases for discriminative detection of OP and non-OP pesticides. To achieve this goal, LbL assembly of electrostatically interacted enzyme armored MWCNT-OPH and MWCNT-AChE with a set of cushioning bilayers consisting of MWCNT-polyethyleneimine (PEI) and MWCNT -DNA on glassy carbon electrode was fabricated. The key idea is the combination of direct catalytic OPH reaction and inhibition based AChE reaction renders discriminative screening of OP and non-OPs from unknown samples. We report fabrication, optimization and characterization of LbL bio-nanostructure biosensor using surface plasmon resonance technique (SPR), electrochemical impedance spectroscopy (EIS), cyclic voltammetry (CV) and UV-vis spectrophotometry for discriminative detection between paraoxon (model of OP) and carbaryl (model of non-OPs) with high specificity and sensitivity (Schematic illustration shown in Figure 15).

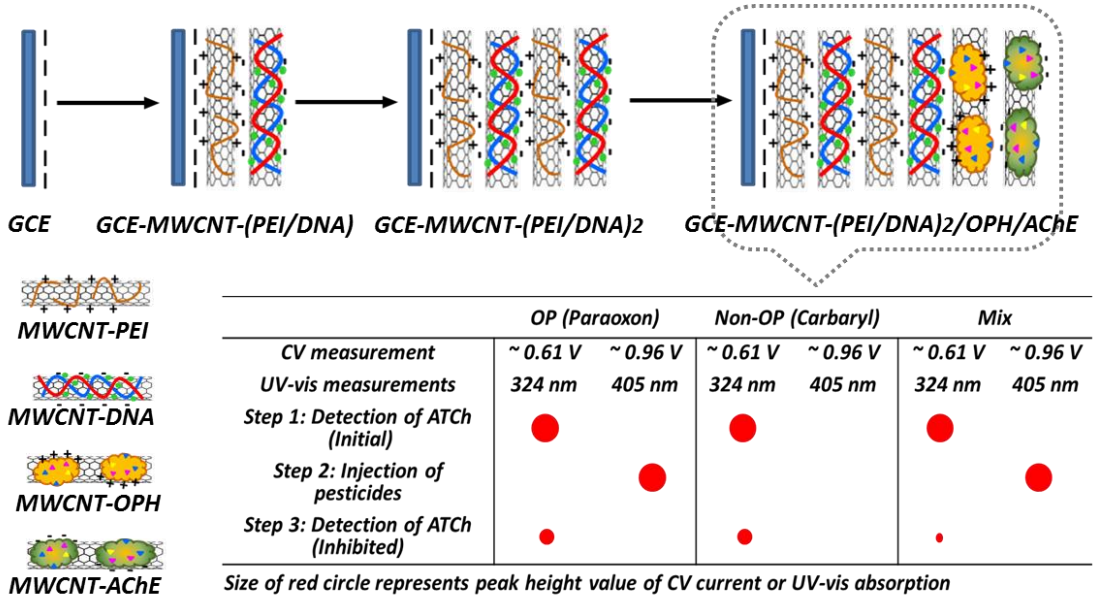

Figure 15. Schematic illustration of LbL assembly and bi-enzymatic layer in biosensor interfaces constructed on the GCE and discriminative detection of OP and non-OP using electrochemical and optical methods.

4.2 Materials and methods

4.2.1 Materials

OPH was isolated from a recombinant *Escherichia coli* strain using published procedures. Paraoxon (PX) was obtained from ChemService, Inc. (West Chester, PA) and dissolved in DI water and stirred at 4 °C for at least 72 hours before use. Carbaryl (1-Naphthyl-N-methylcarbamate, 559814), multi-walled carbon nanotubes (MWCNTS) (purity 95%, length 1-5 μm, diameter 30 ± 10 nm), acetylcholine esterase from electrophorus electricus eel (E.C 3:1:1:7, 518 Units/mg solids), lyophilized salmon sperm DNA salt, N-hydroxysulphosuccinimide (NHS), N-ethyl-N-(3-

dimethylaminopropyl) carbodiimide hydrochloride (EDC), polyethyleneimine (PEI), 4-Aldrithiol (98%), 2-(N-morpholino) ethanesulfonic acid (MES), N-cyclohexyl-2-aminoethanesulfonic acid (CHES), phosphate buffered saline (PBS), tris(hydroxymethyl)aminomethane (TRIS), potassium ferricyanide $K_3Fe(CN)_6$, potassium ferricyanide $K_4Fe(CN)_6$ were all obtained from Sigma-Aldrich (St. Louis, MO). Dimethyl sulphoxide (DMSO) A.C.S grade and Acetonitrile was obtained from Fischer Scientific. Ultrapure DI water obtained from Millipore Direct-Q Water system (resistivity, 18.2 MΩ cm^{-2}) was used for all the sample preparations.

4.2.2 Preparation of enzyme/polymer nanocomposites

The OPH and AChE were immobilized onto carboxylated MWCNTs by NHS/EDC carbodiimide chemistry via two-step process.[141,142] Briefly, 2 mg of carboxylated MWCNT was dispersed into 2 mL of MES buffer (50 mM, pH 4.7) followed by addition of 1 mL of 20 mM NHS and 1 mL of 320 mM EDC. The solution was stirred for 30 min and filtered through 0.2 µm polycarbonate membrane under vacuum filtration with thorough rinsing with MES Buffer (50 mM, pH 6.2) to remove excess unbound NHS and EDC. The as-prepared MWCNT-NHS ester conjugate was re-dispersed into 3 mL phosphate buffer (0.1 M, pH 8.3) and 400U of AChE or 562U of OPH was added into the solution for enzyme immobilization. The immobilization process was allowed to proceed overnight on a platform shaker at 4 °C. The MWCNT-AChE or MWCNT-OPH precipitate was then centrifuged (13200 rpm, 30 min) and rinsed with MES buffer subsequently for three times. After centrifugation purification the MWCNT-AChE and MWCNT-OPH were suspended in 1 mL of TRIS buffer (20 mM, pH 7.5) and 1 mL CHES buffer (20 mM, pH 8.9),

respectively and stored in refrigerator (4°C) for further use.

Preparation of MWCNT-PEI and MWCNT-DNA was based on the previously reported protocol. Two mg carboxylated MWCNT was dispersed in 10 mL of 1 mg/mL PEI solution followed by tip-sonication for 1h in ice bath. After centrifugation purification, the prepared MWCNT-PEI sediment was re-dispersed into 5 mL deionized water. MWCNT-DNA was prepared with similar process described. Stock solutions of 0.4 mg/mL MWCNT-PEI and MWCNT-DNA were obtained as final concentrations which were stored at 4 °C until further use.

4.2.3 *Electrode preparation and modification*

Prior to casting the nanocomposites, GCE electrode is activated through alumina polishing and subsequent amperometric treatment with 1 M NaOH at 1.2V vs Ag/AgCl for 5mins. The negatively charged electrode was rinsed and dried with high purity nitrogen gas. Then 20 µL of positively charged MWCNT-PEI nanocomposite suspension was drop cast onto the GCE and left for 15 mins drying at room temperature to allow sufficient electrostatic interaction. The modified electrode was rinsed with DI water to remove the unbound MWCNT-PEI and dried. Subsequently, 20 µL of negatively charged MWCNT-DNA was deposited followed by 15 min drying-rinsing-and drying. This is followed by deposition of another bilayer of MWCNT-$(PEI/DNA)_2$ to serve as strong cushion layers for further assembly (Figure 15). Twenty µL of MWCNT-OPH/MWCNT-AChE was deposited upon cushion layers, dried- rinsed with PBS buffer. The prepared nanostructured biosensor was stored in 4 °C before use.

4.2.4 LbL interface optimization and evaluation of biosensor

To achieve optimal biosensor configuration analysis of substrate penetration through the layers was conducted. Assembly of AChE nanocomposite within varying inter layers (bottom to top position 2^{nd}, 4^{th} , 6^{th}, 8^{th}) on 8 layered structure, total number of nanostructured layers (2, 4, 6, 8, 10), and different amounts of CNTs were used to optimize the LbL formation by measuring the corresponding amperometric response towards acetylthiocholine (ATCh) at a fixed concentration of 125 μM or 250 μM concentration of paraoxon. Configuration of the resulting multilayered bi-enzyme biosensor, Figure 15 was utilized for further characterization.

4.2.5 SPR monitoring of LbL self-assembly

SPR experiments were performed with SPREETA^{TM} Texas Instruments (Dallas, TX, USA) using the Multi SPR software package. SPR technique was used for the real-time visualization of self-assembly process of MWCNT-$(PEI/DNA)_2$/OPH/AChE on gold surface. Prior to installation, the SPR gold sensor surface was meticulously cleaned with piranha solution (H_2SO_4 and H_2O_2 (3:1); *attention: caution must be taken as the piranha solution readily causes chemical burns and is highly reactive, particularly with organic materials*) for 3 min and thoroughly rinsed with deionized water followed by 2 min plasma cleaning. The experimental set-up was then initialized in the air and calibrated with DI water (refractive index (RI): 1.3333). DI water was pumped into the flow cell on to the SPR gold sensor surface through two inlet channels until the baseline reached a stable value. The LbL self-assembly was initiated by flowing positively charged MWCNT-PEI into the flow cell at a constant flow rate (50 μL/min) over the negatively charged

surface of the gold chip. This was followed by subsequent pumping of negatively charged MWCNT-DNA and two bilayers of MWCNT-PEI/DNA as cushion support. Upon achieving stable value, MWCNT-OPH/AChE were flowed across to form LbL MWCNT-$(PEI/DNA)_2$/OPH/AChE on the gold surface. Before injection of enzyme layers, 20 mM CHES buffer and 20 mM TRIS buffer were injected as background signal.

4.2.6 *Electrochemical and UV-Vis measurements*

Cyclic voltammetric experiments were performed using an electrochemical analyzer CHI 660 (CH Instruments, Austin, TX) potentiostat connected to a computer with chi990b software package. The electrochemical impedance spectroscopy (EIS) data was collected with Gamry instruments Reference 600 potentiostat/galvanostat/ZRA connected to computer with Gamry Echem Analyst software. A conventional three-electrode system consisting of bare or modified glassy carbon electrode (GCE, 3-mm diameter) as a working electrode, Ag/AgCl (3 M KCl) as the reference and platinum wire as counter electrode was used. EIS was performed in 0.4M KCl solution at the formal potential (0.22V) of $[Fe(CN)_6]^{3-/4-}$ with a frequency range from 100 kHz to 0.01 Hz, amplitude of 5 mV in 1mM $K_3Fe(CN)_6/K_4Fe(CN)_6$ solution (1:1) mixture as electroactive probe. Cyclic voltammograms of $[Fe(CN)_6]^{3-/4-}$ were carried out in 0.4mM KCl solution containing 1mM $K_3Fe(CN)_6/K_4Fe(CN)_6$ (1:1) mixture at scan rate of 0.1V/s. Pesticide detection by cyclic voltammogram and UV-vis experiments were conducted using 10mM PBS buffer, pH 7.4. UV-vis spectrophotometer (Amersham Biosciences Ultrospec 2100 pro) with 1 mL PMMA cuvettes was used for collecting UV-Vis absorption spectrum data. All experiments were carried out at room

temperature (25±2˚C).

4.2.7 *Inhibition of AChE with OP and non-OP*

The MWCNT-(PEI/DNA)$_2$/OPH/AChE biosensor was employed for discriminative detection of OP and non-OP using three step process. First, the electrode was tested for initial CV responses in 10 mM PBS buffer pH 7.4 containing 1 mM ATCh (5 min reaction with stirring before test). In second step inhibition assays were performed by incubating the electrode in desired concentrations of pesticides for 15 mins. Finally, the electrode was rinsed and tested again in fresh solution of 1 mM ATCh at similar conditions. The inhibition percentage of AChE was calculated using Eq. 1

$$\frac{I_0 - I_{inhibition}}{I_0} \times 100\% \quad \text{(Eq. 1)}$$

where I_0 and $I_{inhibition}$ are the signals obtained at step 1 and step 3. Inhibition (%) vs concentration of OP and non-OP were plotted to obtain linear calibration graphs.

4.2.8 Real sample detection

Apples were bought from local supermarket in Auburn, Alabama. Prior to sample preparation, apples were washed and cleaned with 5% acetonitrile to eliminate potential contamination of pesticides.[143] 10 mM PBS buffer was first spiked with a known concentration of paraoxon or carbaryl and sprayed onto the apple skin that was peeled and cut into 2 cm × 2 cm pieces. The samples were allowed to stand for 15 min, dissolved with 1 mL 5% acetonitrile, and vortexed to extract the pesticide. The solvent was dried in fume hood, and then the residues were reconstituted with 200 μL of PBS buffer followed by inhibition analyses with MWCNT-

$(PEI/DNA)_2$/OPH/AChE bi-enzymatic biosensor. Paraoxon and carbaryl quantities were calculated using standard curves that were obtained from known concentrations of pesticides.

4.3 Results and discussion

4.3.1 *Optimization of LbL nano structured biosensor*

As shown in Figure 16A, the sequence of position of MWCNT-AChE layer within biopolymer interlayers attributed to the permeability of substrate reaching the enzyme. As more layers covered onto MWCNT-AChE, the amperometric response decreased due to less permeability of substrate to the enzyme. Therefore highest enzyme activity was achieved when MWCNT-AChE layer was placed at the terminal 8^{th} layer. With enzyme layer on top, the effect of thickness of total number of layers on the electrode ranging from 2 to 10 layers increased amperometric response for 2 to 6 layers while decreased for 8-10 layers (Figure 16B). The reason was that the lower number of layers had easy diffusion of substrate molecules and good electron transfer to the electrode surface while increased number of layers led to a thicker surface and high resistance.[120] The optimized concentrations of MWCNTs obtained were 0.1 mg/mL for MWCNT-PEI and MWCNT-DNA and 0.2 mg/mL for MWCNT-AChE and MWCNT-OPH (Figure 16C).

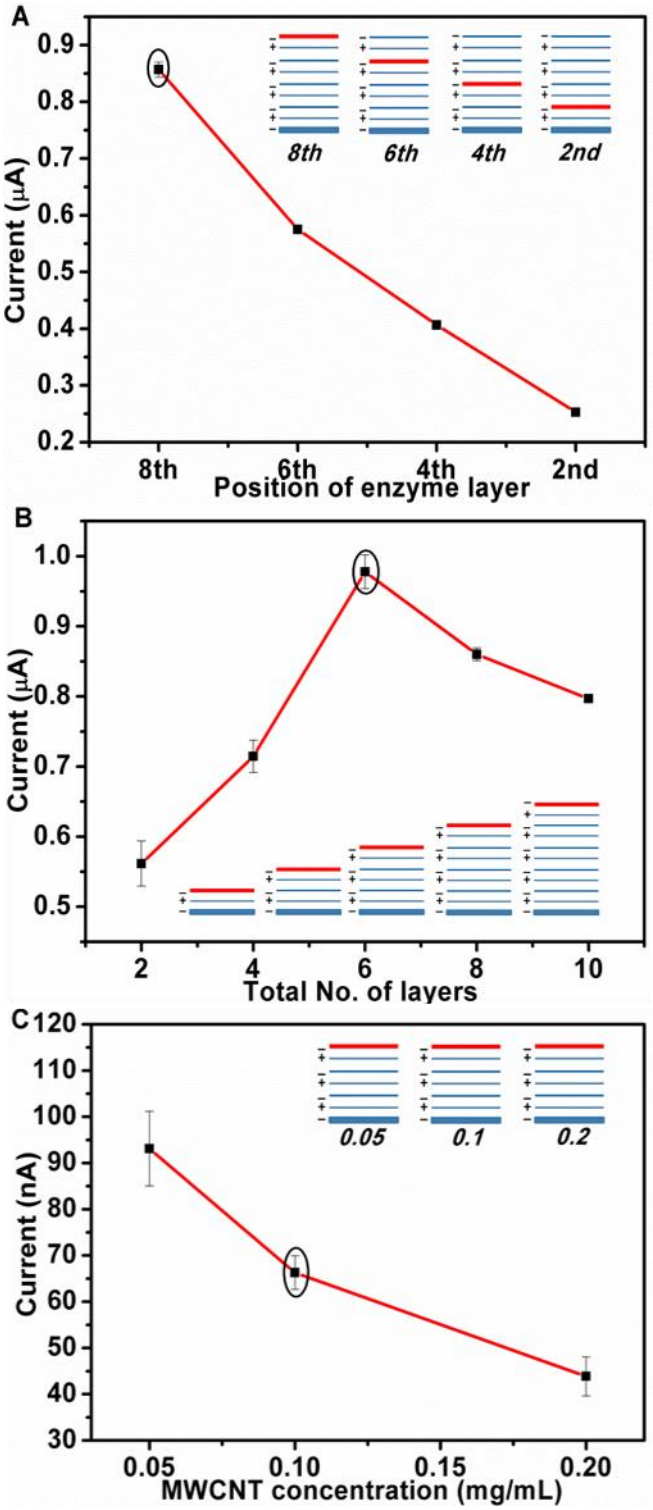

Figure 16. LbL assembly of enzyme nanostructure with various parameter optimizations: (A) position of enzyme layer, (B) total number of layers with enzyme on the top, and (C) MWCNT

concentration. The final optimized parameters were achieved when enzyme layer was at terminal position (A) with total number of 6 layers (B) using 0.1 mg/mL cushion CNT-$(PEI/DNA)_2$ layers (C).

4.3.2 SPR characterization of LbL self-assembly

Figure 17A demonstrates the stepwise formation of LbL self-assembly between MWCNT-PEI ($\Delta RU = 97.38$, $\Delta RI = 0.9834 \times 10^{-4}$) and MWCNT-DNA ($\Delta RU = 1444.05$, $\Delta RI = 1.4246 \times 10^{-3}$) with additional bilayers of MWCNT-PEI ($\Delta RU = 455.72$, $\Delta RI = 4.7611 \times 10^{-4}$) and MWCNT-DNA ($\Delta RU = 1865.39$, $\Delta RI = 1.8429 \times 10^{-3}$). ΔRU (1 RU = 10^{-6} RI unit) values represent the change in response units (RU) between the initial signal and stabilized signal for each layer. The strong electrostatic interactions between bilayers of PEI and DNA served as cushion support for immobilization of cationic OPH and anionic AChE layer. The CHES and TRIS buffers set apart the enzyme nanocomposites from their isoelectric points to exhibit sufficient charges required for LbL formation. Injection of buffers slightly increased the RU signal which were further subtracted as background for MWCNT-OPH ($\Delta RU = 277.14$, $\Delta RI = 2.8574 \times 10^{-4}$) and MWCNT-AChE ($\Delta RU = 573.14$, $\Delta RI = 5.9278 \times 10^{-4}$) binding. SPR study was successfully employed for visualization of formation of six-layered MWCNT-$(PEI/DNA)_2$/OPH/AChE biosensing interfaces on gold surface, indicating the effectiveness of electrostatically interacted LbL self-assembly processes.

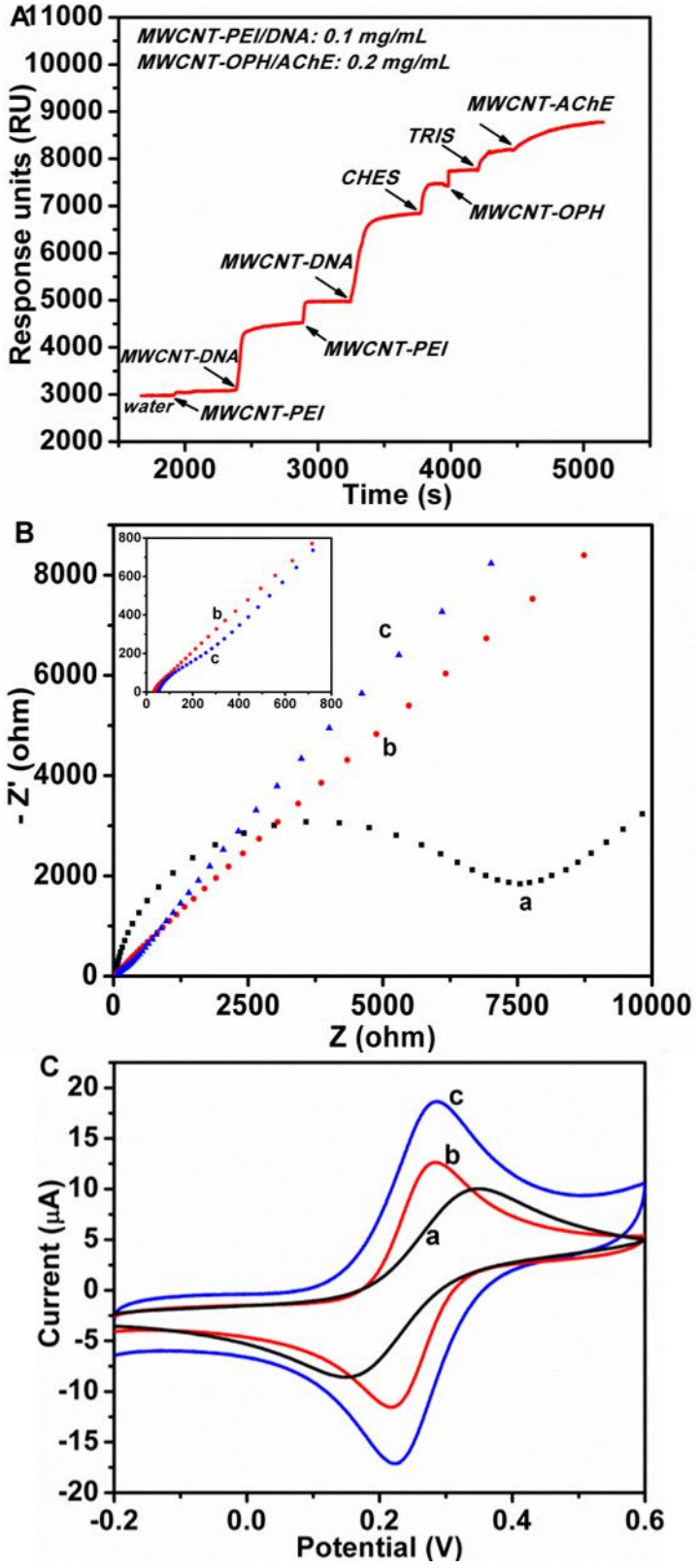

Figure 17. (A) SPR real time monitoring of LbL self-assembly process for desired LbL

nanostructure. (B) EIS and (C) CV of (a) bare GCE , (b) GCE-MWCNT-$(PEI/DNA)_2$, (c) GCE-MWCNT-$(PEI/DNA)_2$/OPH/AChE ; bare and modified electrodes in 0.4 M KCl containing 1 mM $[Fe(CN)_6]^{3-/4-}$(1:1) with a frequency range from 100 kHz to 0.01 Hz with an amplitude of 5 mV.

4.3.3 Electrochemical characterization of modified electrode

The bare and surface modified electrode were investigated using EIS and CV with $[Fe(CN)_6]^{3-/4-}$ as redox probe. Figure 17 B&C illustrates the results of impedance spectroscopy on a) GCE, b) MWCNT-$(PEI/DNA)_2$ and c) MWCNT-$(PEI/DNA)_2$/OPH/AChE. The Z' and $-Z''$ are the real and imaginary variables of impedance, respectively. Typically, the diameter of semicircle observed at higher frequencies of impedance (Nyquist) plot correspond to the charge transfer resistence (Ret) and the linear portion at lower frequency depicts diffusion limited process.[120] It can be observed from Figure 17B, the bare GCE shows Ret value of 8239 Ω (curve a) corresponding to huge charge transfer resistance. With addition of $(MWCNT-PEI/MWCNT-DNA)_2$ on the bare electrode, the Ret value dramatically decreased demonstrating excellent electron transfer between $[Fe(CN)_6]^{3-/4-}$ and electrode surface modified with functionalized-MWCNT layers. It can be observed that EIS (curve b) is almost a straight line suggesting that the electrode is diffusionally controlled. However, Ret slightly increased for MWCNT-$(PEI/DNA)_2$/OPH/AChE immobilized GCE (curve c), compared to MWCNT-$(PEI/DNA)_2$. This might be due to the negatively charged AChE enzyme and the thickness of layers that can impede the electron transfer on electrode surface. The impedance results thus obtained by the change in electron transfer provide evidence for the successful LbL assembly of layers on GCE. The cyclic voltammograms corresponding to EIS

experiments further supported the modification process as shown in Figure 17C. The peak current (i_p) of the redox probe increased and the peak potential separation (ΔEp) decreased in the order of a) GCE, b) MWCNT-$(PEI/DNA)_2$ and c) MWCNT-$(PEI/DNA)_2$/OPH/AChE. In addition to impedance measurements, effective surface area of three electrodes was obtained according to Randles Sevick equation

$$I_{pa} = (2.69x10^5)\, n^{3/2}\, AD^{1/2}\, \upsilon^{1/2}\, C \qquad \text{(Eq. 2)}$$

where n is the number of electrons transferred, I_{pa} is anodic peak current (Amp cm^{-2}), C is the concentration of $K_3 Fe(CN)_6$ (mole cm^{-3}), D is the diffusion coefficient ($cm^2\ s^{-1}$), v is the scan rate (Vs^{-1}) and A is the surface area of the electrode (cm^2). The value of D is considered as 0.65×10^{-5} $cm^2\ s^{-1}$ at 20 °C. CV were conducted in 1mM $K_3Fe(CN)_6$ /1M KCl solution in a potential range of -0.2 to +0.65V at varying scan rates (Figure 18). By performing linear regression for I_{pa} versus $v^{1/2}$ the slope can be obtained (Figure 18), which was further used in Eq.2. for calculating surface area of the electrode. The results indicate that the process is controlled by diffusion. The active surface area for bare GCE, MWCNT-$(PEI/DNA)_2$ and MWCNT-$(PEI/DNA)_2$/OPH/AChE was $0.0596cm^2$, $0.0787cm^2$ and $0.1078cm^2$ respectively. The surface area for bare GCE is in close agreement with values previously reported. The six layered enzyme/polymer nanocomposite was found to have highest surface area.

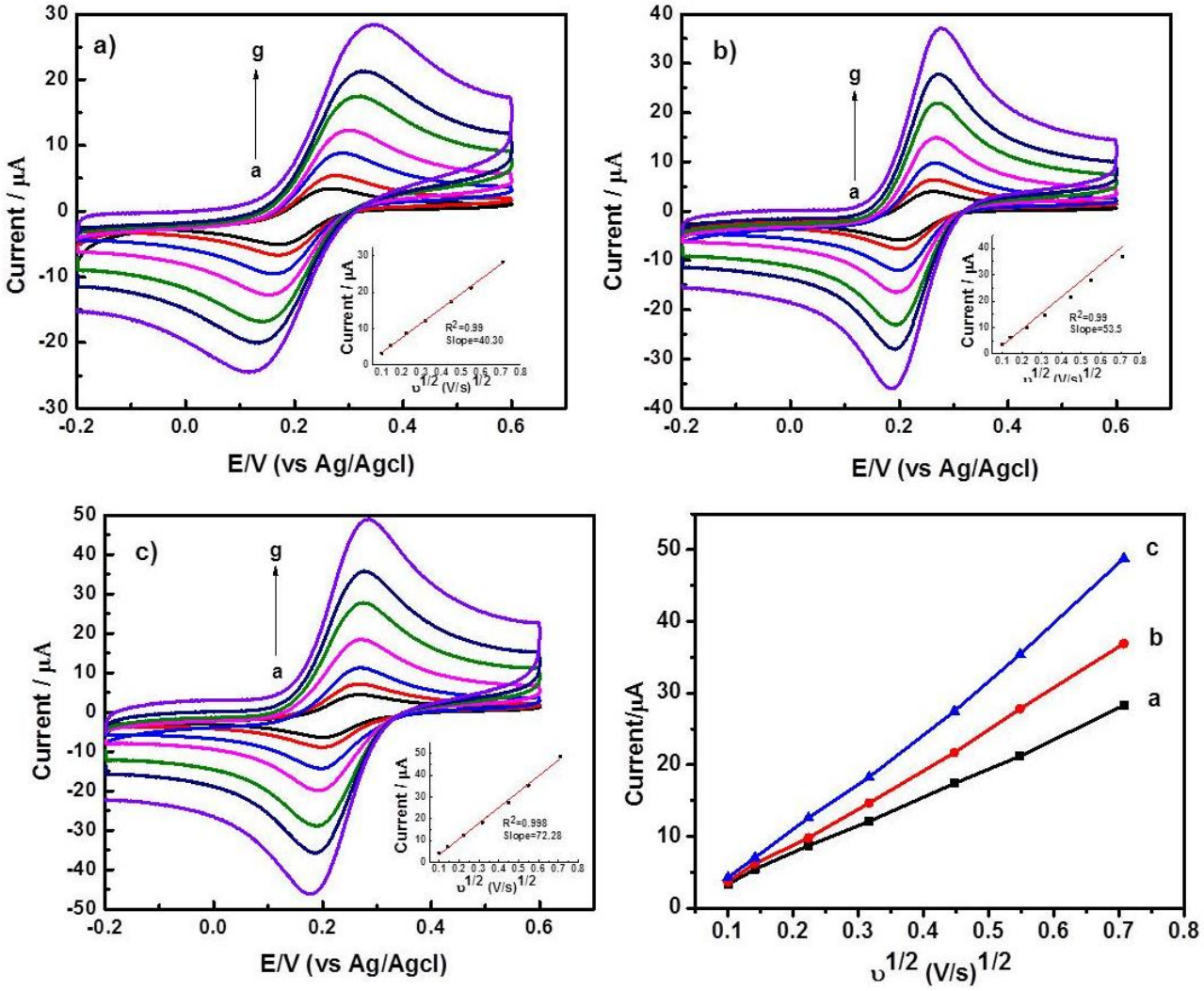

Figure 18. Cyclic voltammograms of (a) GCE (b) GCE/ MWCNT-(PEI/DNA)$_2$ (c) GCE/ MWCNT-(PEI/DNA)$_2$ /OPH/AChE in 1mM $K_3Fe(CN)_6$ with varying scan rates from 0.01 to 0.5V/s. d) Linear relationship between peak current and the square root of the scan rate indicating the process is diffusionally limited.

4.3.4 Discriminative detection of OP and non-OP pesticides

4.3.4.1 Electrochemical approach

Discriminative detection of OP and non-OP pesticides was achieved with GCE -MWCNT-$(PEI/DNA)_2$/OPH/AChE bi-enzymatic biosensor using electrochemical approach. As shown in Figure 19A, cyclic voltammetry responses were examined on modified GCE before and after OP and non-OP inhibition. There was no anodic peak current (green curve) observed with modified GCE when no substrates were added to pH 7.4, 10 mM PBS buffer. However, CV responses showed a peak current (black curve) at 0.61V vs. Ag/AgCl, when 1 mM ATCh was added. This peak was attributed to the oxidation of thiocholine[144], hydrolysis product of ATCh which was considered as the initial response of the biosensor. Detection of OP using 20 µM paraoxon was measured based on AChE partial inhibition at detection potential of 0.61V vs. Ag/AgCl (oxidation of thiocholine). It can be observed from red curve that the peak current decreased and 58.02 ± 3.4% was obtained. This result was further confirmed by direct catalytic hydrolysis of OPH producing ρ-nitrophenol which undergoes oxidation showing significant peak current (blue curve) at detection potential 0.96 V vs. Ag/AgCl. For non-OP detection, carbaryl (40 µM) is not hydrolyzed by OPH showing no peak current at potential 0.96V and therefore, it can only be determined based on AChE inhibition percentage (56.93 ± 4.1%) by measuring thiocholine at 0.61V as shown in Figure 19B. In combination of both OP (20 µM paraoxon) and non-OP (40 µM carbaryl), discriminative detection was achieved by complete inhibition (94.03 ± 2.7%) of AChE enzyme showing no peak current at 0.61V while significant peak current for ρ-nitrophenol at 0.96V was observed from Figure 19C.

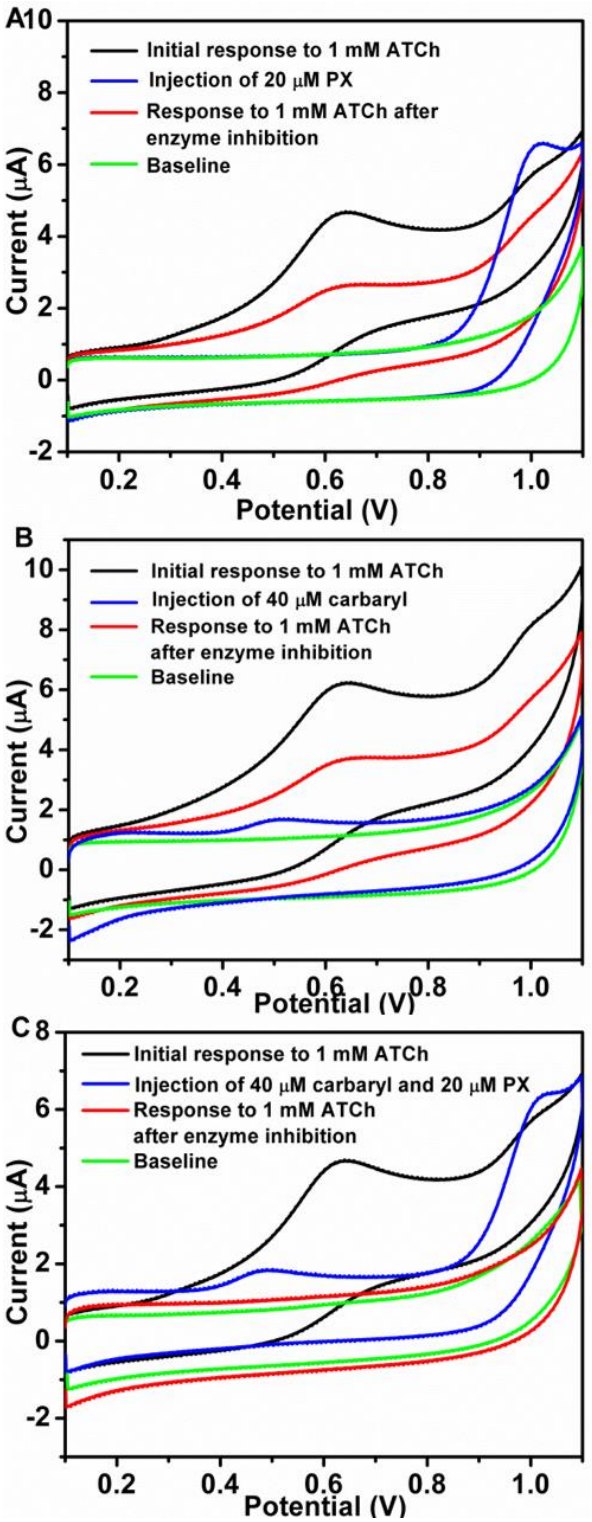

Figure 19. CV response for discriminative detection of (A) OP (20 μM paraoxon), (B) non-OP (40 μM carbaryl) and (C) mix of OP (20 μM paraoxon)and non-OP (40 μM carbaryl).

4.3.4.2 UV-vis approach

The UV-vis measurements of discriminative detection was performed directly on modified screen printed electrode with the same method as fabrication of GCE-MWCNT-$(PEI/DNA)_2$/OPH/AChE. The electrode was initially tested by UV-vis measurements in pH 7.4, 10 mM PBS buffer containing 200 µM ATCh at a wavelength ranging from 300 nm to 600 nm by measuring thiocholine oxidation reaction with 0.1mM 4-Aldrithiol (Stock solution of 12 mM 4-Aldrithiol was prepared in DMSO) producing 4-thiopyridine (WRAIR Assay) which gives observable peak at λ324 nm. Figure 20A black curve displays the optical absorbance at λ324 nm (Absolute peak Abs = 0.16 O.D). Detection of OP (40 µM paraoxon) was based on AChE partial non-competitive inhibition using WRAIR assay. The inhibition level is separated from the initial by ΔAbs = 0.09 O.D. This can be further confirmed by measuring 40 µM paraoxon by OPH hydrolysis producing para-nitrophenol which displays peak (Absolute Abs = 0.19 O.D) at λ405 nm as shown as red curve in Figure 20A. However, in case of non-OP (5 µM carbaryl) which has no absorption band peak can only be detected based on AChE partial non-competitive inhibition, at λ324 nm (ΔAbs = 0.069 O.D) as shown in Figure 20. Discriminative detection of OP (paraoxon) and non-OP (Carbaryl) in combination was achieved based on AChE total non-competitive inhibition at λ324 nm (ΔAbs = 0.12 O.D) with decreased absorbance signal while detecting p-nitrophenol at λ405 nm (Absolute Abs = 0.15 O.D). All absorbance spectra data were collected after 5 mins of enzymatic reactions before (without pesticide) and after inhibition (with 3 min pesticide incubation) Figure 20C. Control experiments were conducted without substrates added

to the buffer electrolyte solution.

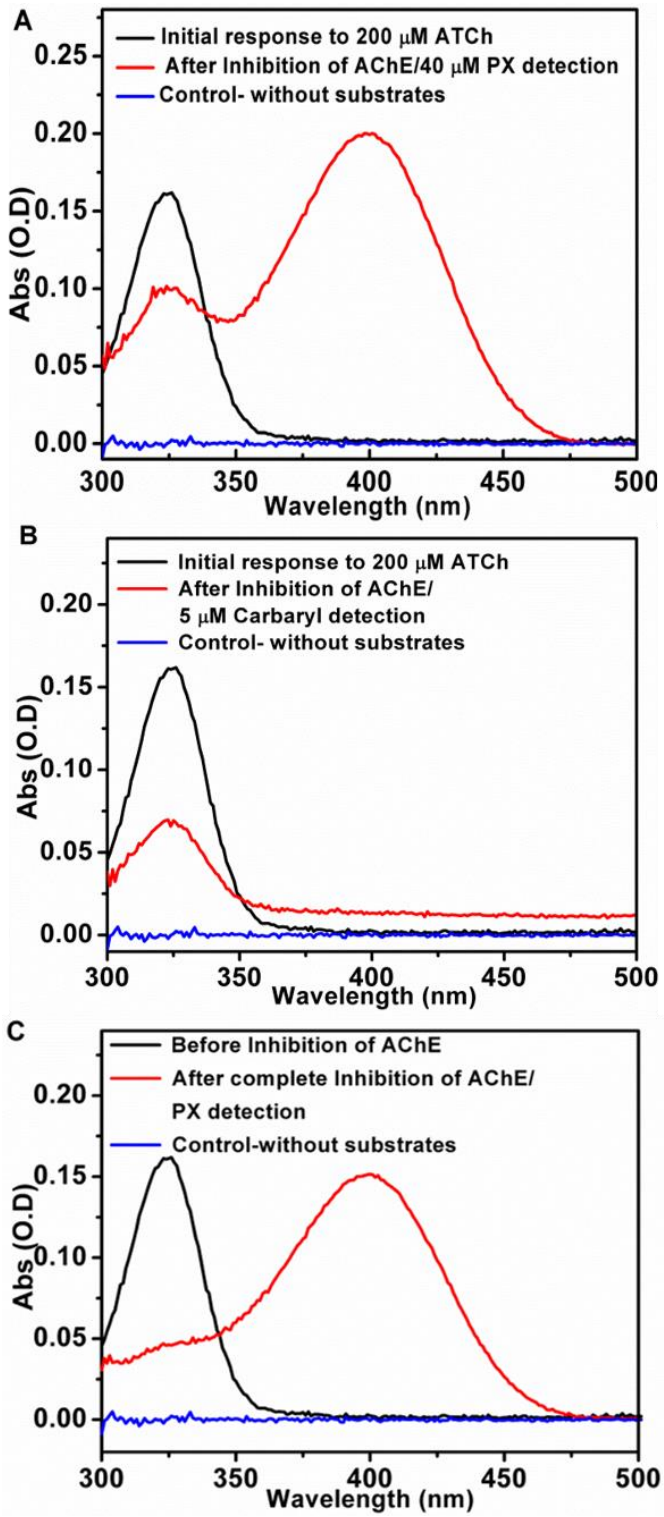

Figure 20. Optical absorbance measurements for discriminative detection of (A) OP (40 μM

paraoxon), (B) non-OP (5 μM carbaryl) and (C) mix of OP (40 μM paraoxon) and non-OP (5 μM carbaryl).

4.3.4.3 Analytical performance

Sensitivity, linearity and dynamic range were investigated for MWCNT-$(PEI/DNA)_2$/OPH/AChE bi-enzymatic biosensor. Paraoxon was determined by both OPH (catalytic) and AChE inhibition based assays, while carbaryl was determined solely by inhibition method. Based on inhibition percentage as shown in Figure 21A&B, the linear response range for paraoxon and carbaryl was 0.5 - 40 μM and 10 - 80 μM with dynamic range 0.5 - 50 μM and 10 - 100 μM respectively. The linear regression equation, $y = 0.021x+0.09135$ with a correlation coefficient (R^2) of 0.970 and $y = 0.00941x+0.11178$ with R^2 of 0.9836 can be established for paraoxon and carbaryl, respectively. The lowest detection concentration obtained for paraoxon and carbaryl detection was 0.5 and 10 μM, respectively. Calibration measurements were conducted in triplicates and good reproducibility was achieved. Similarly, the linear range for direct detection of paraoxon (Figure 21C) obtained was 1 - 64 μM with lowest detectable concentration of 1 μM. The linear regression equation, $y = 0.07303x + 0.1113$ can be established with a correlation coefficient of 0.9842. In order to determine substrate concentration dependence, the biosensor was further analyzed by varying concentrations of ATCh (40 – 640 μM) without pesticide (initial), with 20 μM paraoxon and both 20 μM paraoxon and 40 μM carbaryl. The anodic peak current at 0.61 V vs Ag/AgCl was measured. It can be clearly observed from Figure 21D, due to high catalytic activity of the enzyme the peak current increased with increasing concentration of ATCh showing

linear dependence. However with inhibitors there is decrease in peak current already at 100 µM ATCh and tend to be saturated with higher concentrations. For real samples, the inhibition percentage calculated from the blank sample was found to be 37.06% for paraoxon and 61.2% for carbaryl. The concentrations were further determined to be about 13.3 µM and 53 µM, respectively.

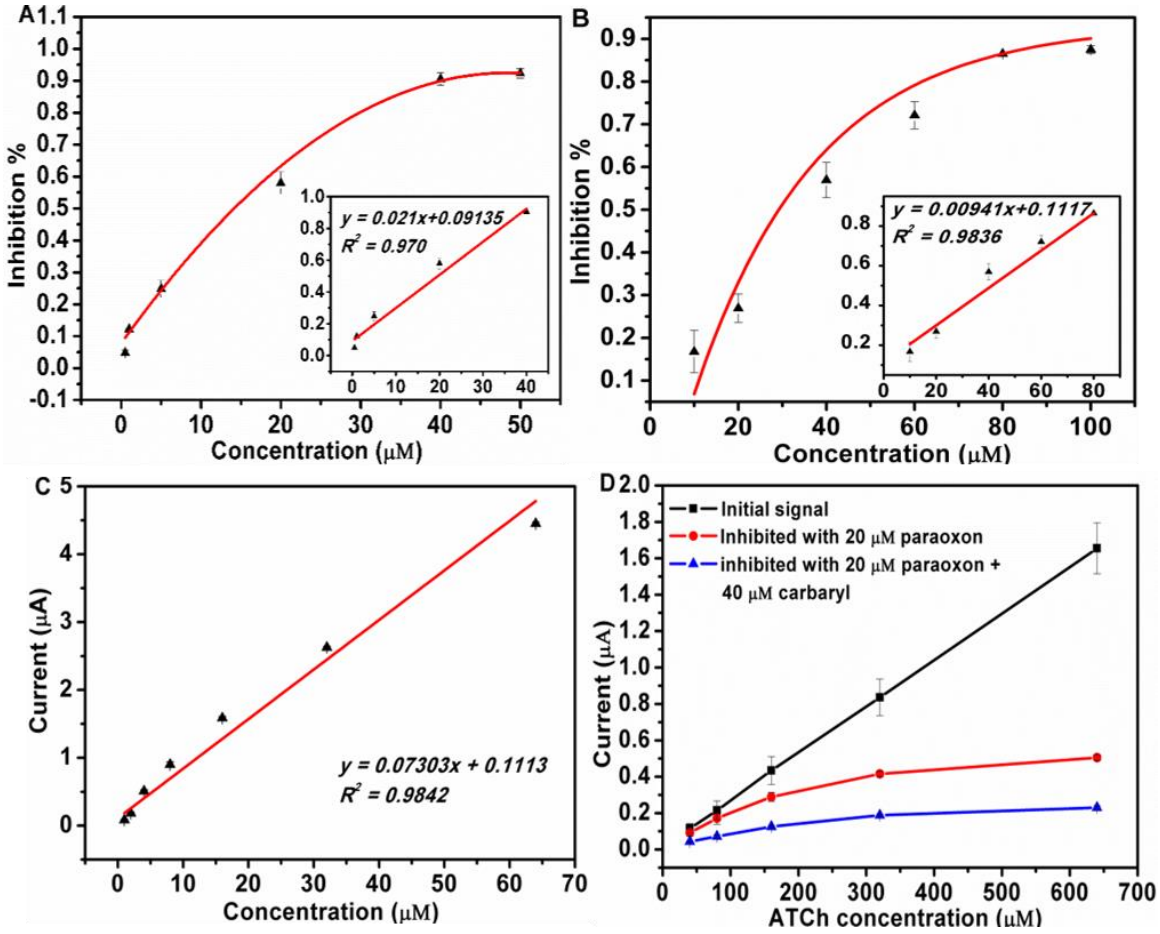

Figure 21. Calibration curve for (A) paraoxon and (B) carbaryl on the bi-enzymatic biosensor through inhibition assay; (C) paraoxon through direct detection assay; (D) calibration curve for ATCh on a) initial bi-enzymatic biosensor, b) 20 µM paraoxon inhibited bi-enzymatic biosensor and c) mix of 20 µM paraoxon and 40 µM carbaryl inhibited bi-enzymatic biosensor

With this study, the MWCNT-$(PEI/DNA)_2$/OPH/AChE bi-enzymatic biosensor showed an acceptable sensitivity and good linearity in nM - μM range of detection for paraoxon and carbaryl, demonstrating the proof of concept of the proposed bi-enzymatic biosensor for analyses of OP, non-OP and both.

4.4 Conclusions

In this study, LbL self-assembly was successfully employed in development of MWCNT-$(PEI/DNA)_2$/OPH/AChE bi-enzymatic biosensor in discriminating between paraoxon and carbaryl pesticides by electrochemical and optical methods. The results demonstrated for the first time the potential for applying bi-enzymatic biosensing system in screening and discriminating two major class of pesticides, OP and non-OP. The cyclic voltammetric results provided good sensitivity, stability and reproducibility. In addition, the biosensor was able to detect pesticides extracted from real samples. In future, we anticipate that this versatile LbL self-assembly approach can be extended to a variety of enzyme to develop multi-enzyme biosensing strategy showing great advantages in multi-analyte discriminative monitoring on single platform for novel biosensing applications.

5 Layer-by-layer assembly of carbon nanotubes modified with invertase/glucose dehydrogenase cascade for sucrose/O_2 biofuel cell

5.1 Introduction

Biofuel cells convert the chemical energy of biofuels into electric energy via the enzymatically catalyzed oxidation and reduction reactions. One of the most important factors affecting the performance of fuel cell is the fabrication of bioanode which has great influence in generation of electrical power outputs. Therefore developing effective bioanodes remains critical. Till date, several reports have been published on various approaches to assemble enzymes on the anodes in BFCs utilizing carbon based materials.[145,146,147,148] Amongst those layer-by-layer (LbL) assembly technique via electrostatic interactions of oppositely charged species has emerged as a very attractive way to construct multilayer films of polyelectrolytes, biomolecules,[149] and organic materials[150,151,152] offering advantages in various fields, such as surface functionalization,[153,154] drug delivery,[56,155] and biosensing.[28,84,156] Its application was considered plausible in the development of amperometric biosensors initiating vast research activities on biosensors comprised of LbL organized multilayers. LbL nanostructures decorated with multi-enzymes were proven to be one of the successful strategies to establish high electrical performance, long-term stability and long lifetime in bioelectronics devices.[28,157,158,159] For example, LbL structures consisting of Au nanoparticles (AuNPs), thiol-functionalized polyaniline and glucose oxidase (GOx) were fabricated for glucose biosensing by Komathi et al.[160] Similarly, Wu et.al and Cui et.al

used LbL assembly of carbon nanotubes (CNTs), AuNPs and an insulating polymer to fabricate a glucose sensor.[161,162] Our group has reported extensively on LbL based single and bi-enzyme biosensing systems incorporating multi-walled carbon nanotubes (MWCNTs) immobilized with organophosphorus hydrolase (OPH) and acetylcholinesterase (AChE), for discriminative detection between organophosphorus and non-organophosphorus pesticides.[84,163]

In these organized LbL nanostructures, a homogenous and stable CNT-based assembly of multi-enzyme interfaces with desired architecture provides control over the position of the polyelectrolyte and the enzyme molecules compared to random hydrogels.[163,164] Furthermore, spatially organized multilayers with close proximity could be very advantageous for sequential enzymatic reactions with single and bi-enzymatic cascade systems that favors efficient substrate/product penetration, molecular recognition, redox mediation and efficient electron transfer.[165,166] To the best of our knowledge, no study on the fabrication of bioanode utilizing an enzyme cascade by layer by layer assembly method and investigation corresponding to its biofuel cell performance has been explored.

On the other hand, the most extensively investigated biofuel resources include saccharides such as glucose and alcohols.[167,168,169] Since the current challenges for biofuel cell development lie in deeper oxidation and improved energy density,[170] recent reports have been mainly focused on disaccharides or polysaccharide based biofuel cells.[171,172] Hickey et al.[173] reported an enzyme cascade system employing invertase, fructose dehydrogenase and glucose oxidase immobilized in ferrocene-modified linear poly(ethyleneimine) (Fc-C_6-LPEI) hydrogel, which was then drop casted onto carbon electrode for catalyzing sucrose oxidation in a biofuel cell. This generated

42±15 μW/cm^2 in 100 mmol/L sucrose. Several other reports include trehalose,[174] cellobiose,[175] and starch[176] based fuel cells obtaining maximum current density of 0.1 mA/cm^2, 1.9 μW/cm^3 and 8.15 μW/cm^3, respectively. Handa et al.[177] fabricated a carbon-felt based invertase, fructose dehydrogenase and glucose oxidase immobilized bioanode mediated by tetrathiafulvalene and bilirubin oxidase immobilized biocathode with ABTS as mediator for sucrose biofuel cell. A maximum power density of 2.9 mW/cm^2 was obtained in 50 mmol/L sucrose. It should be noted that the enzyme cascades so far reported for disaccharides and polysaccharides are based on randomly built hydrogels immobilized on the electrode surfaces.

Herein, we demonstrate a simple strategy via LbL assembly method by alternately assembling oppositely charged CNT-PEI (positive charge) and CNT-DNA (negative charge) for cushion structure for further binding CNT-enzymes invertase (INV) and glucose dehydrogenase (GDH). The aim of this work is to investigate whether the LbL based bionanostructures via layer by layer assembly utilizing small surface area conventional electrodes immobilized with enzyme cascade system is an effective approach to promote electricity generation. A schematic illustration showing the construction of the LbL assembled bioanode is presented in Figure 22.

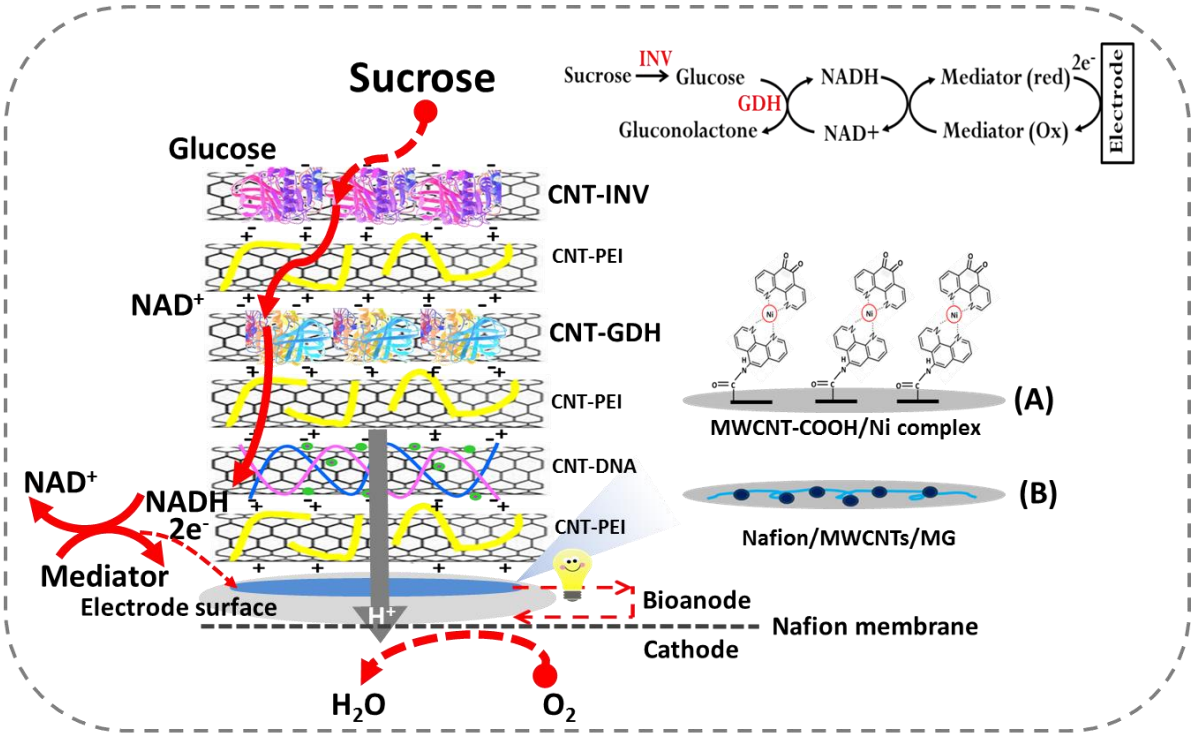

Figure 22. Schematic illustration of LbL assembled bioanode for catalyzing oxidation of sucrose in a biofuel cell. Two types of mediator (A) MWCNT-COOH/[Ni(phendion)(phen)$_2$]Cl$_2$ or (B) Nafion/MWCNTs/MG were modified on electrode surface.

5.2 Materials and methods

5.2.1 Materials and chemicals

Glassy carbon electrodes (GCE, 3 mm in diameter) and screen printed electrodes (SPE, 4*5 mm) were obtained from CH Instruments (Austin, Texas) and Pine Instrument (Grove city, PA), respectively, and used as anode electrodes. Carboxylated multiwalled carbon nanotubes (purity 95%, length 1-5 μm, diameter 30 ± 10 nm) were obtained from Nanolab Technologies (Milpitas, CA). Invertase from baker's yeast (INV, EC 3:2:1:26, 200-300 U/mg solids), glucose

dehydrogenase from Pseudomonas sp. (GDH, EC 1.1.1.47, ≥200 U/mg), dihydronicotinamide adenine dinucleotide (NADH), nicotinamide adenine dinucleotide (NAD^+), methylene green (MG), 5-amino -1,10-phenanthrolin (phen), sucrose, D-glucose, lyophilized salmon sperm DNA salt, polyethyleneimine (PEI), N-hydroxysulphosuccinimide (NHS), N-ethyl-N-(3-dimethylaminopropyl) carbodiimide hydrochloride (EDC), glutaraldehyde, and Nafion were all obtained from Sigma-Aldrich (St. Louis, MO). 1, 10-phenanthroline-5,6-dione (phendion) and $NiCl_2*6H_2O$ were from Acros Organics. Mutarotase (1800 U/mg solids) was obtained from CALZYME laboratories (San Luis Obispo, CA). Synthesis for [Ni(phendion)Cl_2] complex was followed using the procedures reported by Korani et al[178] Ultrapure DI water was used for all the buffer preparations.

5.2.2 Preparation of CNT-biomolecules

Preparation of MWCNT-PEI and MWCNT-DNA was reported in our previous article.[84] INV was immobilized onto carboxylated MWCNTs via the NHS/EDC crosslinking process and the protocol was used as previously described with minor modifications.[163,165] For enzyme immobilization, 2.5 mg of INV was dissolved in phosphate/nitrate buffer (100 mM, pH 7.0) dispersed with EDC/NHS activated MWCNTs and was allowed to incubate overnight at 4°C. Approximately 1.25 mg of GDH enzyme was weighed and dissolved in 70 µL phosphate/nitrate buffer (100 mM, pH 7.0) followed by the addition of 20 µL carboxylated MWCNTs (10 mg/mL) solution and 10 µL glutaraldehyde (0.5%v/v). The mixture was sonicated for 30 s followed by vortex for 1 hr and further 30s sonication. The final mixture was stored in the refrigerator at 4 °C

for further use.

5.2.3 Fabrication of LbL assembled MWCNT-biopolymer/enzyme anode

5.2.3.1 MWCNT-COOH/[Ni(phendion)(phen)$_2$]Cl$_2$ bioanode

Covalent attachment of the [Ni(phendion)Cl_2] complex to carboxylated MWCNT modified GCE/SPE electrode was prepared according to procedures reported by Korani et al.[178] with slight modification. Briefly, 5 μL of carboxylated MWCNTs (1 mg/mL in ethanol) was drop cast onto the electrode surface followed by 5 μL of 5-amino -1,10-phenanthrolin (phen) (10 mM in ethanol) and 5 μL of EDC (30 mM in ethanol). The electrode was kept at 4 °C for 24 hrs for covalent attachment of phen onto the electrode surface. The carboxylated MWCNT/phen modified electrode was further incubated in a 10 mM [Ni(phendion)Cl_2] complex at 45°C for 24 hrs. Since [Ni(phendion)$(phen)_2$]Cl_2 creates a positive charge on the electrode surface,[178] post drying, 20 μL of negatively charged MWCNT-DNA solution was first deposited and subjected to further drying-rinsing-drying to remove the unbound MWCNT-DNA. Using similar procedures another layer of MWCNT-PEI/DNA/PEI was further deposited to serve as a strong support. Twenty μL of negatively charged MWCNT-GDH and negatively charged MWCNT-INV with an interlayer of positively charged MWCN-PEI were deposited, dried and stored in 4 °C before use. The schematic of preparation of CNTs-polymer/enzyme anode assembled in LbL fashion was shown in Figure 22.

5.2.3.2 Nafion/MWCNTs/MG bioanode

MWCNTs (1 mg/mL) were prepared in 10 mL ethanol and Nafion (final concentration 0.1%) and sonicated for 1 hr to obtain homogeneous suspension. Later, 500 μL of MWCNTs solution was transferred into a micro-centrifuge tube and diluted with 500 μL DI water followed by addition of 3.5 μL MG (100 mM). This mixture was vortexed immediately for 5 s and sonicated for 30 s. Subsequently, 20 μL of Nafion/MWCNTs/MG suspension was drop cast onto electrode surface and stored in the refrigerator at 4 °C overnight. Nafion is negatively charged,[179] therefore, 20 μL of positively charged MWCNT-PEI solution was deposited followed by 15 min drying-rinsing and drying process described above. Following bilayers of MWCNT-DNA/PEI, and MWCNT-GDH, MWCNT-PEI and negatively charged MWCNT-INV layers were consecutively constructed on the electrode surfaces.

5.2.4 UV-Vis/Electrochemical characterization of LbL assembled bioanode

All optical measurements were carried out using a UV-Vis spectrophotometer (Amersham Biosciences Ultrospec 2100 pro) with 1 mL PMMA cuvettes. An electrochemical analyzer CHI 760E (CH Instruments, Austin, TX) potentiostat connected to a computer with the CHI 760E software package was used for all electrochemical measurements. A conventional three-electrode system with 3 M Ag/AgCl reference electrode and platinum counter electrode were employed for all measurements. Cyclic voltammetric experiments at various scan rates (0.005, 0.01, 0.05, 0.1 V/s) were carried out on mediator modified electrode surfaces for surface characterization. Phosphate/nitrate buffer (100 mM, pH 7.0) and phosphate/sodium chloride buffer (100 mM, pH 7.0) were used for GCE and SPE, respectively. All experiments were performed at room

temperature (25 ± 2 °C).

5.2.5 Sucrose/O_2 biofuel cell assembly and characterization

The biofuel cell consists of an "I shape" glass chamber separated by the carbon cloth cathode coated with Nafion polymer electrolyte membrane (Figure 22). The fuel solution was added to the upper glass chamber, and the bottom chamber was left open for air breathing allowing O_2 to reach the cathode. The cathode was prepared by hot pressing Pt/C cloth onto Nafion membrane. The Nafion side of the cathode was soaked in concentrated sulfuric acid overnight before use. For the GCE anode, the fuel solution consisted of 200 mM sucrose, 10 mM NAD^+, and 60 μL mutarotase (2000 U/300 μL) with a total volume of 6 mL in phosphate/nitrate buffer (100 mM, pH 7.0), while phosphate/sodium chloride buffer (100 mM, pH 7.0) was used for SPE anode.

5.3 Results and discussion

5.3.1 Sucrose cascade determination

We investigated the activities of the MWCNT-INV/GDH layers by a spectrophotometric method based on the reduction of the cofactor NAD^+ to NADH which can be observed at 340 nm. The increase in absorbance resulting due to catalytic reaction of INV and GDH was found to be slow initially (> 5hrs) as shown in Figure 23. This might be due to the delayed utilization of α-D-glucose by the GDH, which is produced as a product of sucrose hydrolysis. To fasten the NADH production, the substrate and cofactor were increased which reduced the time to 2 hrs. Mutarotase

that can convert α-D-glucose to β-D-glucose was incorporated into the enzyme cascade. In our strategy, optimization of conditions, such as sucrose concentration, amount of enzyme/cofactor NAD^+, and addition of mutarotase were investigated to expedite the enzymatic cascade reaction (Figure 23). The results indicate that the DNA, PEI coated surfaces had electrostatically interacted with GDH and PEI and facilitated in binding of INV. The increase in NADH absorbance indicated that the cascade system worked with high efficiency and reached saturation within 1.5 hr proving the efficient conversion of the substrate and the cofactor. To further reduce the delay time from conversion of anomeric forms of glucose, addition of mutarotase demonstrated steeper slope. Therefore, the overall rate of the cascade can most likely be due to the time required for sucrose hydrolysis and the mutarotation of two anomeric forms of glucose.[173,177] It should be observed that not always higher protein loading density is necessary for higher activity, our results show that with optimal number of layered structures can lead to enhanced enzyme activity and increased NADH production. Also, in our observation, upon interchanging the positions of the enzymes in the cascade such as GDH as the top layer, we observed lower absorbance signals due to inefficient performance of the cascade (Figure 23). These results clearly indicate the importance of the LbL structure for the fabrication of enzyme cascade interfaces.

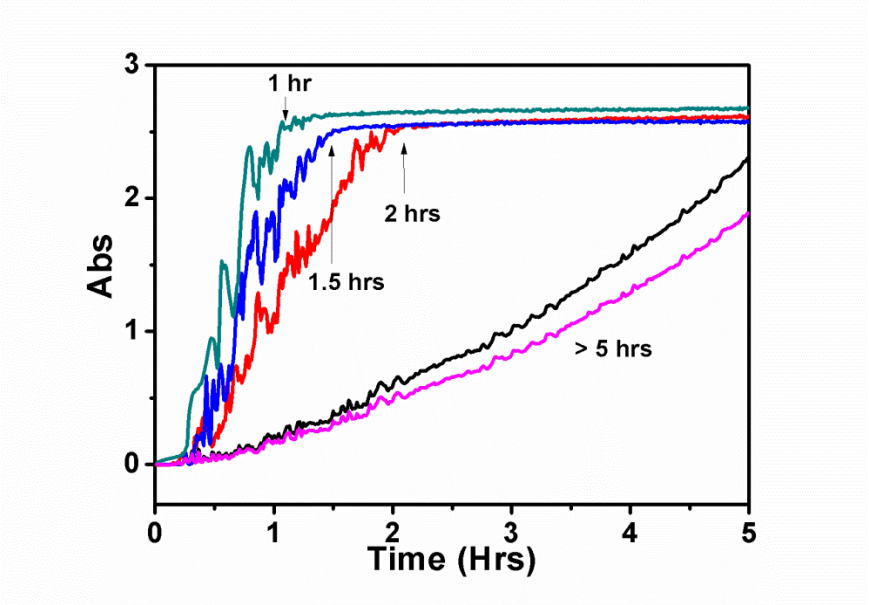

Figure 23. UV absorbance at 340 nm for 5-hour incubation of enzyme cascade bioanode in: 100 mM sucrose and 3 mM NAD^+ (pink line, GDH on the top); 100 mM sucrose and 3 mM NAD^+ (black line, INV on the top), 200 mM sucrose and 10 mM NAD^+ (red line, INV on the top); addition of 10 μL mutarotase, ~ 50 units (blue line, INV on the top); temperature raised to 45 ℃ (green line, INV on the top).

5.3.2 Characterization of electrode

The characteristic of immobilized mediator redox process were investigate. Figure 24 shows the results of the measurements demonstrating the redox peak currents linearly increased with square root of scan rate for modified GCE and SPE. This shows diffusional-limited process for immobilized redox couple on SPE and GCE. The difference in peak potentials ($\Delta E_p = E_{pc} - E_{pa}$) at 100 mV/s scan rate were 102 and 162 mV for Ni complex on GCE and SPE, respectively; 352 and 348 mV for MG on GCE and SPE, respectively. The cathodic and anodic peaks shifted non-

symmetrically, suggesting that the ΔE_p corresponds to quasi reversible diffusional reaction. The average peak potential E_{pc} and E_{pa} for Ni complex on GCE and SPE were -0.018 and -0.093 V vs Ag/AgCl, respectively; -0.139 and -0.348 V vs/Ag/AgCl for MG on GCE and SPE, respectively. The potential values obtained as formal potentials were found to be very close to the MG and Ni complex peaks as shown in previous literature,[178,180] proving that the enzymes in cascade maintained their activities even when wrapped with CNTs or intermingled with biopolymers. Previously, we have successfully demonstrated the increase of LbL assembly process between MWCNT dispersed PEI/DNA and enzymes via electrostatic interactions using surface plasmon resonance (SPR) real time monitoring and electrochemical characterization. Meanwhile optimization of the LbL nanostructure in terms of layer density, number of layers, and position of enzyme layers was also investigated.[163,165] The charged CNT-PEI (positive charge) and CNT-DNA (negative charge) with sufficient opposite charges were demonstrated to serve as a strong cushion for firmly binding of above CNT-enzyme layers.

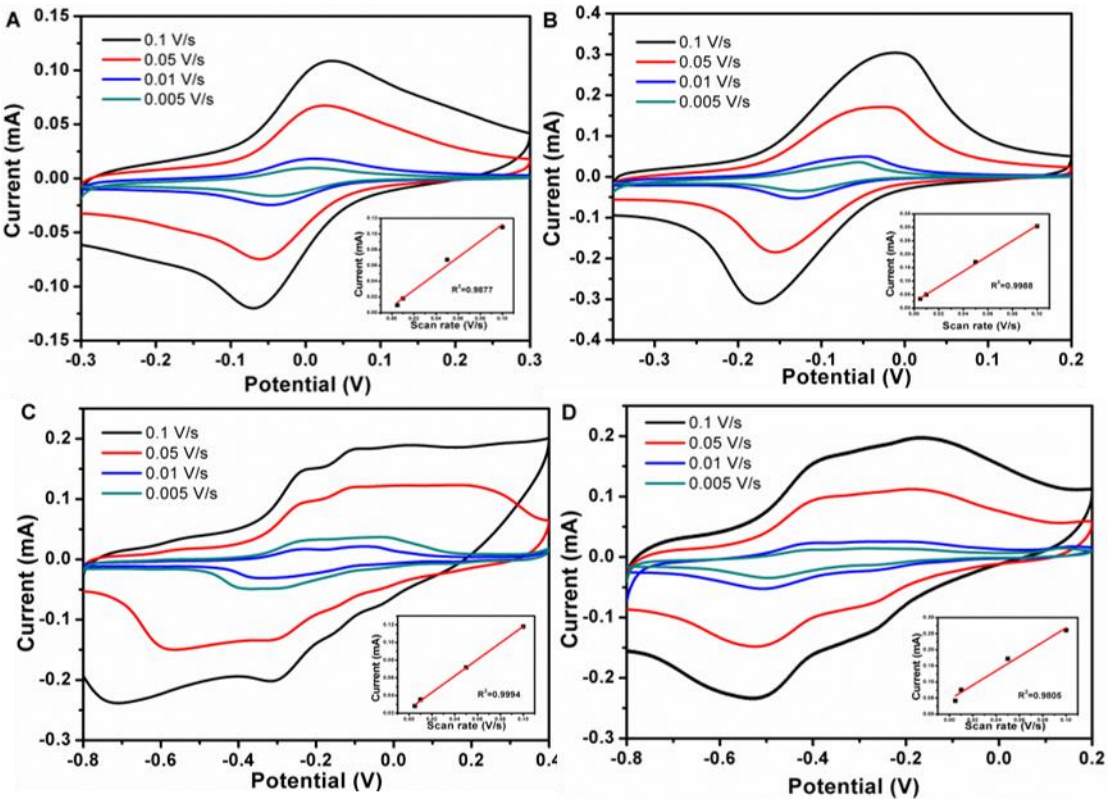

Figure 24. Cyclic voltammetric responses of Ni complex modified GCE (A) and SPE (B); MG/Nafion/MWCNTs modified GCE (C) and SPE (D) at different scan rates. Phosphate/nitrate buffer (100 mM, pH 7.0) and phosphate/sodium chloride (100 mM, pH 7.0) were used for GCE and SPE characterization, respectively.

5.3.3 NADH electrocatalysis with mediator modified electrode

Various electrocatalysts have been reported as efficient electron-transfer mediators for NADH oxidation.[180,181,182] Characteristic voltammograms for 1 mM NADH mediation on GCEs and SPEs were shown in Figure 25. The presence of NADH demonstrated increase in the oxidation peak and a decrease in reduction peak with both mediators on SPE and GCE. The recorded onset potentials for NADH oxidation were -0.17 V and -0.34 V with MG on GCE and SPE, respectively and with

carboxylated MWCNT/[Ni(phendion)(phen)$_2$]Cl$_2$ were -0.20 V and lower than -0.30 V, respectively. The increase of oxidation peak and a decrease in reduction peak on SPE was slightly higher when compared to GCE due to a relatively larger working area of SPE. We found that the modified SPE electrodes redox peak currents with and without NADH showed higher change than the GCE. With GCE the change in peak currents in the presence and absence of NADH, was ~10 µA and SPE ~13 µA. Upon comparison of mediators, the NADH oxidation potentials at the [Ni(phendion)(phen)$_2$]Cl$_2$ modified electrodes were more negative than the MG modified electrode, demonstrating [Ni(phendion)(phen)$_2$]Cl$_2$ has a better mediation potential toward the oxidation of NADH compared with MG.

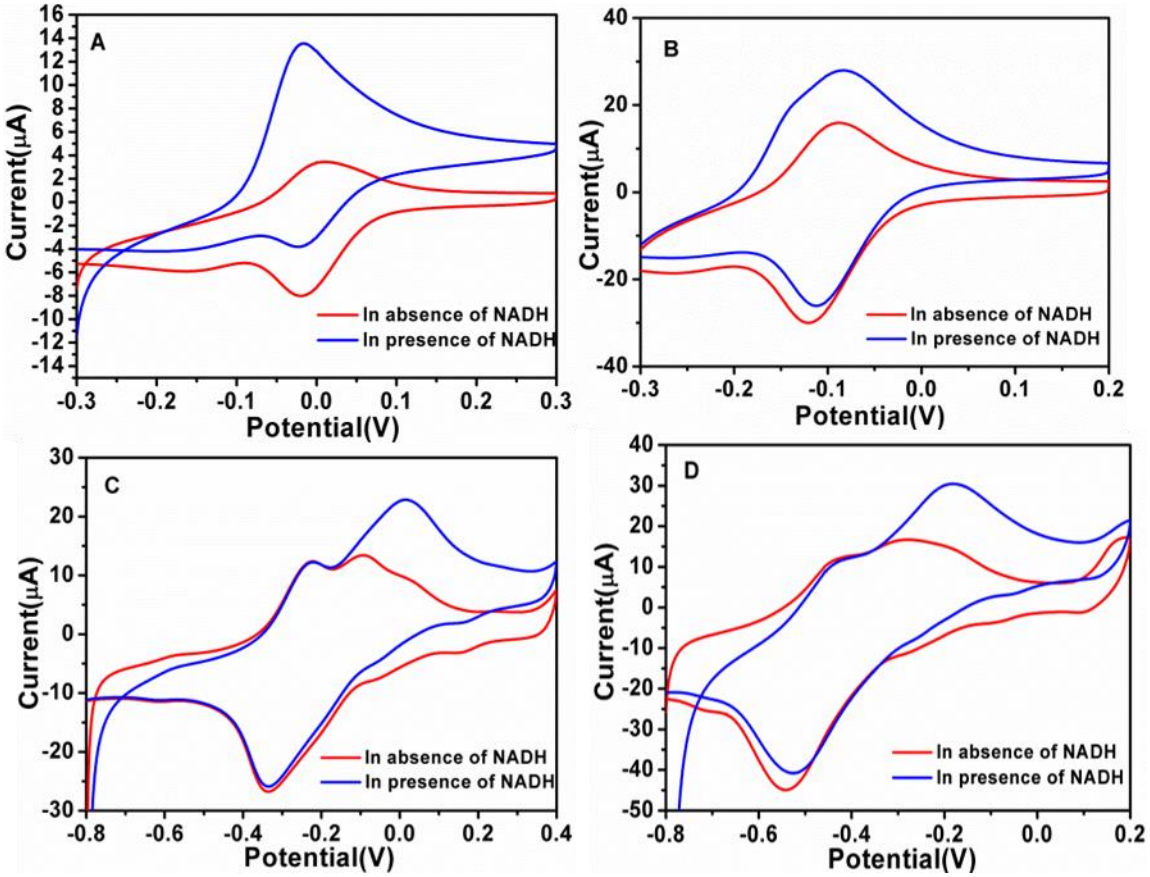

Figure 25. NADH Electrocatalysis with Ni complex on GCE (A) and SPE (B),

MG/Nafion/MWCNTs on GCE (C) and SPE electrode (D), 1 mM NADH, scan rate 5 mV/s

5.3.4 Performance of LbL assembled bioanode

To verify the performance of the LbL assembled bioanode, the nanostructure complex of CNT-enzymes with CNT-cushion layers were first assembled on carboxylated MWCNT/[Ni(phendion)$(phen)_2$]Cl_2 and Nafion/MWCNTs/MG modified electrodes. The cascade involves the hydrolysis of sucrose by INV to glucose and GDH further converting glucose to gluocolactone by reduction of NAD^+ to NADH (Eq. 1-3). The LbL architecture with close proximity in molecular scale within enzyme layers favors the efficient penetration of substrate and products, showing great advantage for the cascade reaction. The bioanode was immersed into 6 mL of PB buffer containing 200 mM sucrose, 3 mM NAD^+ and 60 µL mutarotase. After 3 hrs incubation, cyclic voltammetry was performed to monitor the NADH oxidation. Figure 26 shows the electrocatalytic oxidation of enzymatically produced NADH. The NADH oxidation commenced at -250 and -300 mV at MG modified GCE and SPE, respectively, while the oxidation started at -300 and -350 mV on carboxylated MWCNT/[Ni(phendion)$(phen)_2$]Cl_2 modified GCE and SPE. The change in peak currents at oxidative potentials was ~200 µA and ~220 µA for Ni complex modified GCE and SPE, respectively (Figure 26A&B); ~300 µA and ~350 µA for MG/Nafion/MWCNTs modified GCE and SPE, respectively (Figure 26C&D). To verify whether the current was due to the enzymatic reduction of NADH, a control experiment in the absence of CNT-enzyme layers were carried out under the same condition which resulted in reduced electrocatalytic activitiy (partial data shown in Figure 27). Therefore, the results implied that all

the elements in LbL assembled enzyme cascade bioanode are indispensable for full electrocatalytic oxidation of sucrose, showing great potential for application of the proposed bioanode for biofuel cell development.

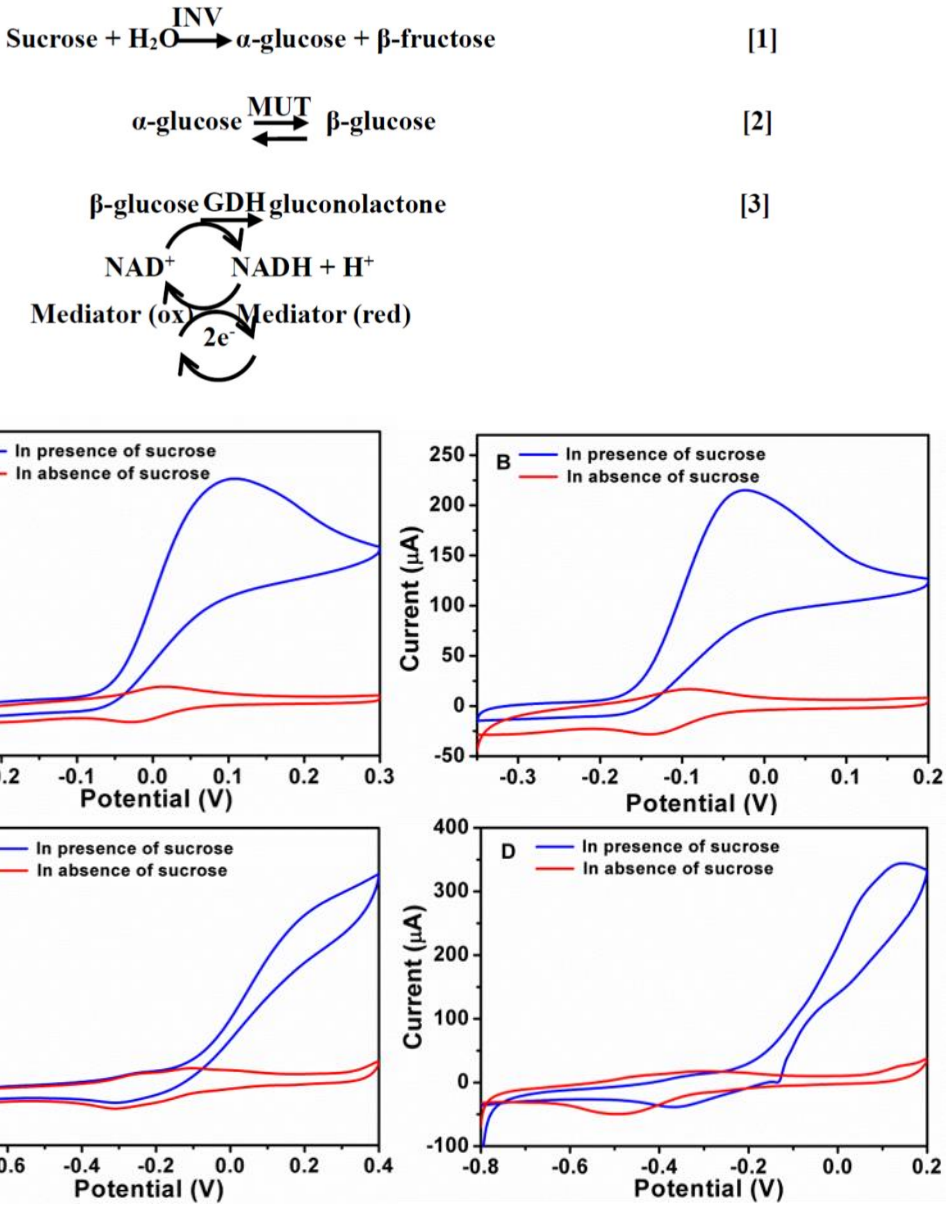

Figure 26. Electrocatalytic effect of Ni complex on enzymatically produced NADH with GCE (A) and SPE (B), MG/Nafion/MWCNTs on GCE (C) and SPE electrode (D), 200 mM sucrose, 3 mM NAD^+, scan rate 5 mV/s

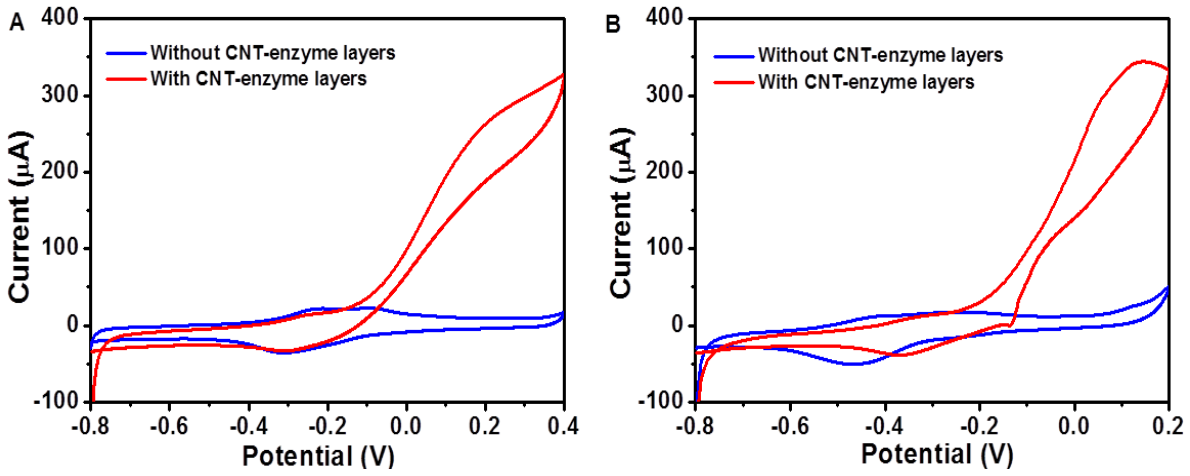

Figure 27. Cyclic voltammetric responses of LbL assembled bioanode without CNT-enzyme layers and with CNT-enzyme cascade on MG/Nafion/MWCNTs modified GCE (A) and SPE (B), 200 mM sucrose, 3 mM NAD^+, scan rate 5 mV/s

5.3.5 Sucrose/O_2 biofuel cell operation

The open circuit potential (OCP) was measured and allowed to reach steady state. Linear sweep voltammetry (LSV) from just above the measured OCP potential to 0 mV was subsequently employed to obtain polarization and power curves at 1 mV/s and the data is presented as current and power densities. Control experiments were performed by substituting the top MWCNT-INV enzyme layer with a MWCNT-DNA layer. To examine the performance of LbL assembled sucrose bioanodes, the "I-shape" sucrose/O_2 enzymatic biofuel cell was assembled with an air breathing Pt membrane serving as cathode, as shown in schematic illustration (Figure 22). The biofuel cells with different mediators were characterized using LSV sweeping from their corresponding OCP to 0 V. The representative polarization curves as well as calculated power curves were displayed

in Figure 28. A summary of the biofuel cells performances showing OCP, maximum power density, maximum current density were concluded in Table 2.

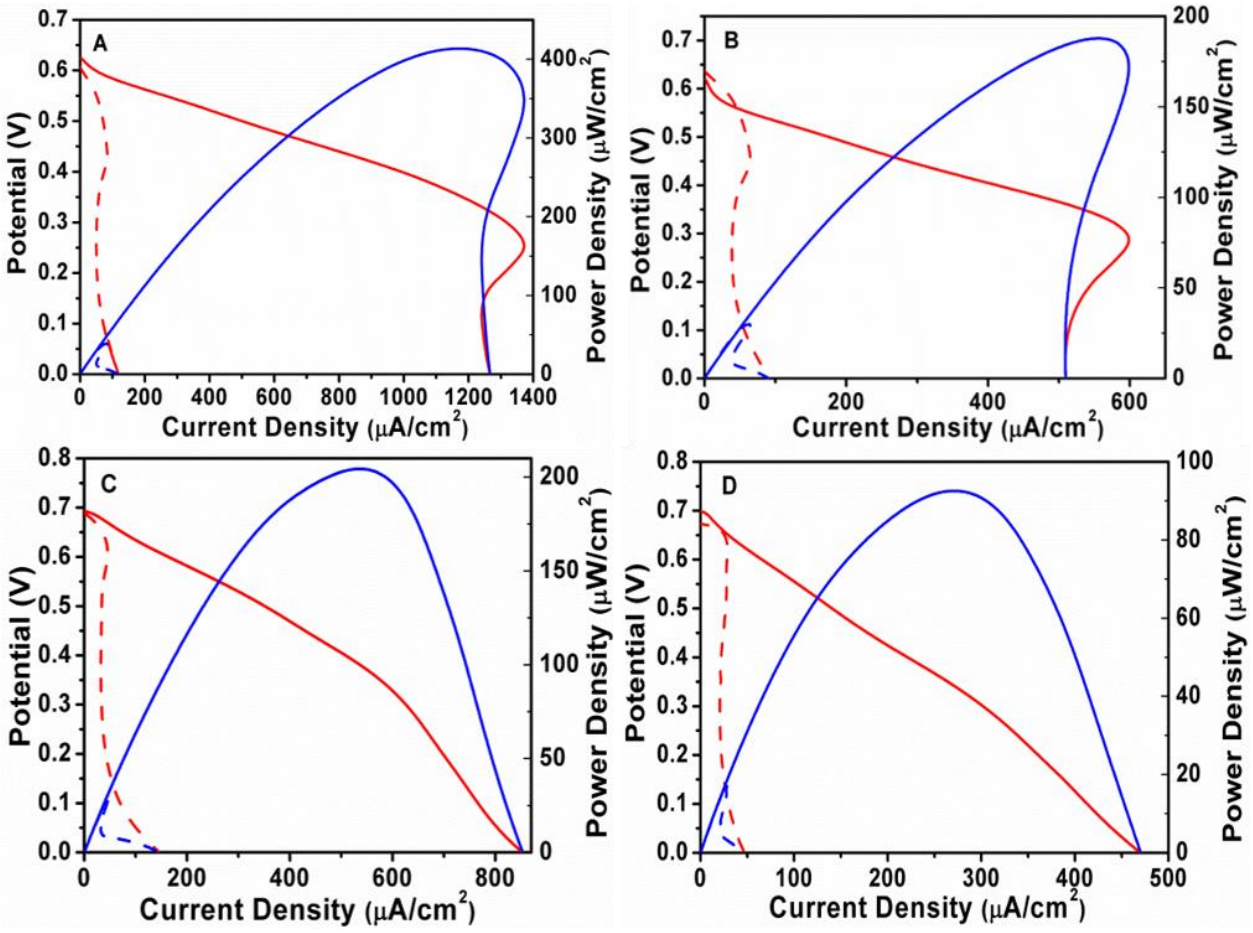

Figure 28. Representative polarization (red line) and power curve (blue line) sucrose/O_2 biofuel cell composed of LbL assembled bioanode (solid line) and control (dashed line). (A) Ni complex with GCE, (B) Ni complex with SPE, (C) MG with GCE and (D) MG with SPE. The power density was calculated from the current density and voltage.

The full LbL assembled sucrose bioanode demonstrates significant enhancement in current and power density compared with the control, demonstrating the efficiency of LbL assembled

sucrose enzyme cascade bioanode with both mediators in a biofuel cell. Upon comparison of GCE and SPE electrode, the biofuel cell with MG and $[Ni(phendion)(phen)_2]Cl_2$ modified GCE bioanode, produced power densities ($\mu W/cm^2$) that were 145.8% and 130.1% higher than that on SPE electrode, respectively. While comparing Ni complex and MG mediator, the biofuel cell with Ni complex modified GCE and SPE produced power densities ($\mu W/cm^2$) 93.7% and 107.0% higher than that with MG modified GCE and SPE bioanode, respectively. The maximum power density from MG and $[Ni(phendion)(phen)_2]Cl_2$ were 209 ± 3 $\mu W/cm^2$ and 405 ± 6 $\mu W/cm^2$ on GCE. It is noteworthy to observe that Handa et.al has obtained 2.9 mW/ cm^2 power density with sucrose cascade. However, it should be noted that our goal was to demonstrate LbL and show how the technique with use of GC and SPE conventional electrode (smaller surface area), less enzyme loading, sequential arrangement of enzymatic layers would result in enhanced power or current densities. Handa et.al uses carbon felt, multiple cascades, longer incubation times, and bilirubin cathode which led to obvious higher currents. We have implemented our system for longer incubation periods which actually led to 50% increase of current signal. Therefore, experimental condition and setup should be considered when directly comparing two different approaches for biofuel cell performance. Since this is first of its kind of cascade biofuel cell via LbL, we anticipate obtaining higher energy output with further addition of sophisticated carbon materials and biocathode in near future.

Nevertheless, the maximum power density obtained in our study showed great performance, succeeding most of other reported disaccharides biofuel cells in literature.

Table 2. The performance comparison of proposed biofuel cells with currently reported disaccharides and polysaccharides systems

Substrate concentration (mM)	OCP (mV)	Max. curr. Dens. ($\mu A/cm^2$)	Max. power dens. ($\mu W/cm^2$)	Ref.
Sucrose/O_2-MG/SPE	200	686 ± 21	412 ± 36	85 ± 6	This work
Sucrose/O_2-MG/GCE	200	692 ± 9	823 ± 32	209 ± 3	This work
Sucrose/O_2-Ni complex/SPE	200	619 ± 25	635 ± 73	176 ± 11	This work
Sucrose/O_2-Ni complex/GCE	200	604 ± 17	1400 ±46	405 ± 6	This work
Sucrose/O_2/carbon felt	50	/	12000	2900	[177]
Sucrose/O_2/Toray paper	100	/	344	42	[173]
Lactose/disk graphite	34	600	13	1.9	[175]
Trehalose/carbon cloth	32	/	100	/	[174]
Starch/GCE	0.5%	530	/	8.15	[176]

5.4 Conclusions

In this study, LbL assembly was utilized for construction of an enzyme cascade bioanode for use in a biofuel cell. The high current /power density obtained showed that LbL assembly is of great advantage in enzyme cascade bioanode fabrication and could be used in applications such as

small electronic devices, microfluidic devices etc. Further, LbL assembly showed its excellent adaptability in fabrication of controllable nanocomposite in various substrate surfaces. Therefore, LbL assembly was demonstrated to be a simple, reliable and efficient approach in development of multi-enzyme system for multifunctional applications. In future studies, investigation of the biocathode, other types of electrode surface, number of assembled enzyme layers, etc. can be studied to achieve further improvement of the performance of LbL assembled enzyme-cascade system.

6 Overall conclusion

Advanced multifunctional biointerface involving multi-biocatalysts, biopolymer and nanomaterials were established via LbL on various surfaces. A deeper understanding of the interactions between the components, surface properties of the modified electrode, as well as the interfacial electron transfer properties were achieved. LbL assembly showed great feasibility as a simple and efficient way to construct multifuctional biointerfaces with tailored nano-architecture. Such biointerfaces showed great potential in development of novel bioelectrocatalytic systems, such as discriminative biosensing, dissacharrides biofuel cell and potentially be used in applications such as small electronic devices, microfluidic devices etc. Concept of reversing the pH of the electrostatic interactions to desorb and adsorb new layers to regenerate the surfaces for developing reusable sensors were demonstrated.

7 Future work

In future study, to better control or manipulate the hybrid biointerface, the author suggest more investigation for thorough understanding of layer-layer interactions between biopolymer-CNT composites, for example, a quantitative model may be necessary on determination of dominate interactions between different CNT-biomolecule interface. Moreover, the diffusion properties of substrates, e.g. diffusion coefficient, upon LbL assembled biointerface of different density could be explored, which can be important in Flow-injection system or other bio-oriented applications, such as drug delivery. Further research is needed to improve the stability of the biointerfaces for long-term bioelectronics devices, such as application of synthetic biocatalysts and so on.

8 Summary

In this dissertation LbL assembly showed great feasibility as a simple and efficient way to construct multifuctional biocatalysts-nanomaterials biointerfaces for various bioelectrocatalytic systems. We have established our pioneer approach to employ LbL in fabrication of enzyme sensors for direct detection of organophosphorus pesticides, bi-enzyme LbL interfaces for discriminative detection of OP and non-OP pesticides, and cascade enzyme LbL interfaces for biofuel cell application. Moreover, we have demonstrated the concept of reversing the pH of the electrostatic interactions to desorb and adsorb new layers to regenerate the surfaces for developing reusable sensors.

LbL assembly is of great advantage in multi-enzyme-nanomaterial interfaces fabrication and could be used in applications such as small electronic devices, microfluidic devices etc. Nanomaterials, like CNTs were demonstrated that not only significantly facilitate electron transfer ability but also can serve as a favorable scaffolding structure for the immobilization of a variety of biomolecules, e.g. various enzymes and biopolymers. In future studies, the superior properties of LbL interfaces in biosensing, renewal and energy can be exploited in more bio-oriented applications such as, controlled drug delivery, biomedical healing patches, pads, etc.

9 Publications

1) **Yuanyuan Zhang**, Mary A. Arugula, Shannon T. Williams, Aleksandr L. Simonian. (2016). Layer-by-layer Assembly of Carbon Nanotubes Modified with Invertase/Glucose Dehydrogenase Cascade for Sucrose/O_2 Biofuel Cell. ***Journal of Electrochemical Society,*** 163(6), 449-454.
2) Mary A. Arugula, **Yuanyuan Zhang**, Aleksandr L. Simonian. (2016). Architectures of nano-biointerfaces: Relevance to future biosensing, environment and energy applications. ***International Journal of Parallel, Emergent and Distributed Systems.*** 1-14.
3) **Yuanyuan Zhang**, Mary A. Arugula, Shannon T. Williams, Aleksandr L. Simonian. (2015). Layer-by-layer assembled enzyme cascade for catalyzing oxidation of sucrose for biofuel cells. ***ECS Transactions,*** 66(36), 9-17.
4) **Yuanyuan Zhang**, Mary A. Arugula., Jeffrey S. Kirsch, Xiaoyun Yang, Eric Olsen, Aleksandr L. Simonian. (2015). Layer-by-layer Assembled Carbon Nanotube-Acetylcholinesterase/Biopolymer Renewable Interfaces: SPR and Electrochemical Characterization. ***Langmuir,*** 31 (4), 1462–1468.
5) **Yuanyuan Zhang**, Mary A. Arugula, Melinda Wales, James Wild, Aleksandr L. Simonian. (2015). A novel layer-by-layer assembled multi-enzyme/CNT biosensor for discriminative detection between organophosphorus and non-Organophosphrus Pesticides. ***Biosensors and Bioelectronics***, 67, 287–295.
6) **Yuanyuan Zhang**, Mary A. Arugula, Aleksandr L. Simonian (2014). Discriminative

Detection of Neurotoxins by a Layer-by-Layer Based Carbon Nanotube/bi-enzyme Biosensor. ***ECS Transactions***, 64(1), 133-141.

7) Xiaoyun Yang, Jeffrey S. Kirsch, **Yuanyuan Zhang**, Jeffrey Fergus, Aleksandr L. Simonian. (2014). Electrode Passivation by Phenolic Compounds: Modeling Analysis. ***Journal of the Electrochemical Society***, 161(8), E3036-E3041.

8) Xiaoyun Yang, Jeffrey S. Kirsch, **Yuanyuan Zhang**, Jeffrey Fergus, Aleksandr L. Simonian. (2013). Potential drop based model to analyze electrode passivation by fouling from phenolic compounds. ***ECS transactions***, 53(35), 1-14.

9) Mary A. Arugula, **Yuanyuan Zhang**, Aleksandr L. Simonian. (2013). Biosensors as 21st Century Technology for Detecting Genetically Modified Organisms in Food and Feed. ***Analytical chemistry***, 86(1), 119-129.

10 References

(1) Chen, D.; Wang, G.; Li, J. H. *J Phys Chem C* **2007**, *111*, 2351.

(2) Chang, B. S.; Zhang, M. X.; Qing, G. Y.; Sun, T. L. *Small* **2015**, *11*, 1097.

(3) Milton, R. D.; Wang, T.; Knoche, K. L.; Minteer, S. D. *Langmuir* **2016**, *32*, 2291.

(4) North, S. H.; Lock, E. H.; Taitt, C. R.; Walton, S. G. *Anal Bioanal Chem* **2010**, *397*, 925.

(5) Tiefenauer, L.; Ros, R. *Colloids and Surfaces B: Biointerfaces* **2002**, *23*, 95.

(6) Iler, R. K. *J Colloid Interf Sci* **1966**, *21*, 569.

(7) Kirkland, J. J. *Anal Chem* **1965**, *37*, 1458.

(8) Golander, C. G.; Arwin, H.; Eriksson, J. C.; Lundstrom, I.; Larsson, R. *Colloid Surface* **1982**, *5*, 1.

(9) Fromherz, P. Assembling of Proteins at Lipid Monolayers. In *Electron Microscopy at Molecular Dimensions*; Springer, Berlin, 1980, pp pp 338.

(10) Decher, G.; Hong, J. D. *Makromol Chem-M Symp* **1991**, *46*, 321.

(11) Lvov, Y.; Decher, G.; Mohwald, H. *Langmuir* **1993**, *9*, 481.

(12) Berndt, P.; Kurihara, K.; Kunitake, T. *Langmuir* **1992**, *8*, 2486.

(13) Lvov, Y.; Ariga, K.; Ichinose, I.; Kunitake, T. *Journal of the American Chemical Society* **1995**, *117*, 6117.

(14) Lvov, Y.; Ariga, K.; Kunitake, T. *Chem Lett* **1994**, 2323.

(15) Decher, G. *Science* **1997**, *277*, 1232.

(16) Ladam, G.; Schaad, P.; Voegel, J. C.; Schaaf, P.; Decher, G.; Cuisinier, F. *Langmuir* **2000**,

16, 1249.

(17) Caruso, F.; Furlong, D. N.; Ariga, K.; Ichinose, I.; Kunitake, T. *Langmuir* **1998**, *14*, 4559.

(18) Wang, L. Y.; Wang, Z. Q.; Zhang, X.; Shen, J. C.; Chi, L. F.; Fuchs, H. *Macromol Rapid Comm* **1997**, *18*, 509.

(19) Shimazaki, Y.; Mitsuishi, M.; Ito, S.; Yamamoto, M. *Langmuir* **1997**, *13*, 1385.

(20) Xiong, H. M.; Cheng, M. H.; Zhou, Z.; Zhang, X.; Shen, J. C. *Adv Mater* **1998**, *10*, 529.

(21) Anzai, J.; Kobayashi, Y.; Nakamura, N.; Nishimura, M.; Hoshi, T. *Langmuir* **1999**, *15*, 221.

(22) Wang, Y.; Angelatos, A. S.; Caruso, F. *Chem Mater* **2008**, *20*, 848.

(23) Spevacek, J.; Schneider, B. *Adv Colloid Interfac* **1987**, *27*, 81.

(24) Sun, J. Q.; Wu, T.; Sun, Y. P.; Wang, Z. Q.; Zhang, X.; Shen, J. C.; Cao, W. X. *Chem Commun* **1998**, 1853.

(25) Satake, A.; Miyajima, Y.; Kobuke, Y. *Chem Mater* **2005**, *17*, 716.

(26) Liu, P. *Eur Polym J* **2005**, *41*, 2693.

(27) O'Connell, M. J.; Boul, P.; Ericson, L. M.; Huffman, C.; Wang, Y. H.; Haroz, E.; Kuper, C.; Tour, J.; Ausman, K. D.; Smalley, R. E. *Chemical Physics Letters* **2001**, *342*, 265.

(28) Sakr, O. S.; Borchard, G. *Biomacromolecules* **2013**, *14*, 2117.

(29) Saurer, E. M.; Flessner, R. M.; Sullivan, S. P.; Prausnitz, M. R.; Lynn, D. M. *Biomacromolecules* **2010**, *11*, 3136.

(30) Shutava, T. G.; Lvov, Y. M. *J Nanosci Nanotechno* **2006**, *6*, 1655.

(31) Thierry, B.; Winnik, F. M.; Merhi, Y.; Silver, J.; Tabrizian, M. *Biomacromolecules* **2003**, *4*, 1564.

(32) Lvov, Y.; Haas, H.; Decher, G.; Mohwald, H.; Mikhailov, A.; Mtchedlishvily, B.; Morgunova, E.; Vainshtein, B. *Langmuir* **1994**, *10*, 4232.

(33) Primo, E. N.; Gutierrez, F. A.; Rubianes, M. D.; Rivas, G. A. *Electrochim Acta* **2015**, *182*, 391.

(34) Trigueiro, J. P. C.; Silva, G. G.; Pereira, F. V.; Lavall, R. L. *J Colloid Interf Sci* **2014**, *432*, 214.

(35) Pavinatto, A.; Mercante, L. A.; Leandro, C. S.; Mattoso, L. H.; Correa, D. S. *Journal of Electroanalytical Chemistry and Interfacial Electrochemistry* **2015**, *755*, 215.

(36) Cinti, S.; Arduini, F.; Moscone, D.; Palleschi, G.; Gonzalez-Macia, L.; Killard, A. J. *Sensors and Actuators B: Chemical* **2015**, *221*, 187.

(37) Yu, X. Y.; Wang, Y. Y.; Chen, X. M.; Wu, K. B.; Chen, D. C.; Ma, M.; Huang, Z. J.; Wu, W. Z.; Li, C. Y. *Anal Chem* **2015**, *87*, 4237.

(38) Zhang, X.; Wang, H. B.; Yang, C. M.; Du, D.; Lin, Y. H. *Biosens Bioelectron* **2013**, *41*, 669.

(39) Zang, S.; Liu, Y. J.; Lin, M. H.; Kang, J. L.; Sun, Y. M.; Lei, H. T. *Electrochim Acta* **2013**, *90*, 246.

(40) Karim, M. N.; Lee, J. E.; Lee, H. J. *Biosens Bioelectron* **2014**, *61*, 147.

(41) Jiang, C. Y.; Tsukruk, V. V. *Adv Mater* **2006**, *18*, 829.

(42) Ji, Q. M.; Honma, I.; Paek, S. M.; Akada, M.; Hill, J. P.; Vinu, A.; Ariga, K. *Angew Chem Int Edit* **2010**, *49*, 9737.

(43) Li, Z.; Lu, J.; Li, S. D.; Qin, S. H.; Qin, Y. M. *Adv Mater* **2012**, *24*, 6053.

(44) Moraes, M. L.; Lima, L. R.; Silva, R. R.; Cavicchioli, M.; Ribeiro, S. J. L. *Langmuir* **2013**,

29, 3829.

(45) Chung, K.; Rani, A.; Lee, J. E.; Kim, J. E.; Kim, Y.; Yang, H.; Kim, S. O.; Kim, D.; Kim, D. H. *Acs Applied Materials & Interfaces* **2015**, *7*, 144.

(46) Sigolaeva, L. V.; Pergushov, D. V.; Synatschke, C. V.; Wolf, A.; Dewald, I.; Kurochkin, I. N.; Fery, A.; Muller, A. H. E. *Soft Matter* **2013**, *9*, 2858.

(47) Barsan, M. M.; David, M.; Florescu, M.; Tugulea, L.; Brett, C. M. A. *Bioelectrochemistry* **2014**, *99*, 46.

(48) Mahadevan, A.; Gunawardena, D. A.; Karthikeyan, R.; Fernando, S. *Microchimica Acta* **2015**, *182*, 831.

(49) Wu, B.; Hou, S.; Miao, Z.; Zhang, C.; Ji, Y. *Nanomaterials* **2015**, *5*, 1544.

(50) Xiang, Y.; Zhang, Y. Y.; Jiang, B. Y.; Chai, Y. Q.; Yuan, R. *Sens. Actuator B-Chem.* **2011**, *155*, 317.

(51) Cai, X. J.; Gao, X.; Wang, L. S.; Wu, Q.; Lin, X. F. *Sens. Actuator B-Chem.* **2013**, *181*, 575.

(52) Begum, G.; Goodwin, W. B.; deGlee, B. M.; Sandhage, K. H.; Kroger, N. *J Mater Chem B* **2015**, *3*, 5232.

(53) Ochs, C. J.; Such, G. K.; Caruso, F. *Langmuir* **2011**, *27*, 1275.

(54) DeMuth, P. C.; Moon, J. J.; Suh, H.; Hammond, P. T.; Irvine, D. J. *Acs Nano* **2012**, *6*, 8041.

(55) Chen, Y. Y.; Zeng, G. H.; Pan, F.; Wang, J. B.; Chi, L. F. *Langmuir* **2013**, *29*, 2708.

(56) Huang, J.; Shu, Q.; Wang, L. Y.; Wu, H.; Wang, A. Y.; Mao, H. *Biomaterials* **2015**, *39*, 105.

(57) Pavlov, A. M.; Gabriel, S. A.; Sukhorukov, G. B.; Gould, D. J. *Nanoscale* **2015**, *7*, 9686.

(58) Xu, X.; Lü, S.; Gao, C.; Bai, X.; Feng, C.; Gao, N.; Liu, M. *Materials & Design* **2015**, *88*,

1127.

(59) Shukla, A.; Fang, J. C.; Puranam, S.; Jensen, F. R.; Hammond, P. T. *Adv Mater* **2012**, *24*, 492.

(60) Holmes, C. A.; Tabrizian, M. *Acs Applied Materials & Interfaces* **2013**, *5*, 524.

(61) Kozlovskaya, V.; Harbaugh, S.; Drachuk, I.; Shchepelina, O.; Kelley-Loughnane, N.; Stone, M.; Tsukruk, V. V. *Abstr Pap Am Chem S* **2011**, *241*.

(62) Gentile, P.; Frongia, M. E.; Cardellach, M.; Miller, C. A.; Stafford, G. P.; Leggett, G. J.; Hatton, P. V. *Acta Biomater* **2015**, *21*, 35.

(63) Broderick, A. H.; Manna, U.; Lynn, D. M. *Chem Mater* **2012**, *24*, 1786.

(64) Yang, Y. H.; Bolling, L.; Priolo, M. A.; Grunlan, J. C. *Adv Mater* **2013**, *25*, 503.

(65) Ahmed, I.; Farha, R.; Goldmann, M.; Ruhlmann, L. *Chem Commun* **2013**, *49*, 496.

(66) Li, H. L.; Pang, S. P.; Wu, S.; Feng, X. L.; Mullen, K.; Bubeck, C. *Journal of the American Chemical Society* **2011**, *133*, 9423.

(67) Ou, X. W.; Jiang, L.; Chen, P. L.; Zhu, M. S.; Hu, W. P.; Liu, M. H.; Zhu, J. F.; Ju, H. X. *Adv Funct Mater* **2013**, *23*, 2422.

(68) Li, Z. P.; Wang, J. Q.; Liu, X. H.; Liu, S.; Ou, J. F.; Yang, S. R. *J Mater Chem* **2011**, *21*, 3397.

(69) Lee, S. W.; Kim, J.; Chen, S.; Hammond, P. T.; Shao-Horn, Y. *Acs Nano* **2010**, *4*, 3889.

(70) Chen, P. Y.; Ladewski, R.; Miller, R.; Dang, X. N.; Qi, J. F.; Liau, F.; Belcher, A. M.; Hammond, P. T. *J Mater Chem A* **2013**, *1*, 2217.

(71) Hsu, C. L.; Lin, C. T.; Huang, J. H.; Chu, C. W.; Wei, K. H.; Li, L. J. *Acs Nano* **2012**, *6*,

5031.

(72) Zhang, W. Y.; Asiri, A. M.; Liu, D. L.; Du, D.; Lin, Y. H. *Trac-Trend Anal Chem* **2014**, *54*, 1.

(73) Yang, Y. Q.; Tu, H. Y.; Zhang, A. D.; Du, D.; Lin, Y. H. *J Mater Chem* **2012**, *22*, 4977.

(74) Du, D.; Liu, J.; Zhang, X. Y.; Cui, X. L.; Lin, Y. H. *J Mater Chem* **2011**, *21*, 8032.

(75) Liu, G. D.; Lin, Y. H. *Anal Chem* **2005**, *77*, 5894.

(76) Zhao, Y. T.; Zhang, W. Y.; Lin, Y. H.; Du, D. *Nanoscale* **2013**, *5*, 1121.

(77) Du, D.; Chen, S. Z.; Song, D. D.; Li, H. B.; Chen, X. *Biosens Bioelectron* **2008**, *24*, 475.

(78) Sun, X. Y.; Liu, B.; Xia, K. H. *Luminescence* **2011**, *26*, 616.

(79) Liang, R. Z.; Xu, S. M.; Yan, D. P.; Shi, W. Y.; Tian, R.; Yan, H.; Wei, M.; Evans, D. G.; Duan, X. *Adv Funct Mater* **2012**, *22*, 4940.

(80) Wu, B.; Hou, S.; Miao, Z.; Zhang, C.; Ji, Y. *Nanomaterials* **2015**, *5*, 1544.

(81) Acharya, S.; Das, B.; Thupakula, U.; Ariga, K.; Sarma, D. D.; Israelachvili, J.; Golan, Y. *Nano Lett.* **2013**, *13*, 409.

(82) Shrestha, L. K.; Yamauchi, Y.; Hill, J. P.; Miyazawa, K.; Ariga, K. *Journal of the American Chemical Society* **2013**, *135*, 586.

(83) Nepal, D.; Balasubramanian, S.; Simonian, A. L.; Davis, V. A. *Nano Lett* **2008**, *8*, 1896.

(84) Mantha, S.; Pedrosa, V. A.; Olsen, E. V.; Davis, V. A.; Simonian, A. L. *Langmuir* **2010**, *26*, 19114.

(85) Lee, S. W.; Kim, B. S.; Chen, S.; Shao-Horn, Y.; Hammond, P. T. *Journal of the American Chemical Society* **2009**, *131*, 671.

(86) Rogach, A. L.; Koktysh, D. S.; Harrison, M.; Kotov, N. A. *Chem Mater* **2000**, *12*, 1526.

(87) Wang, Y.; Wei, W. Z.; Liu, X. Y.; Zeng, X. D. *Mat Sci Eng C-Bio S* **2009**, *29*, 50.

(88) Decher, G.; Lehr, B.; Lowack, K.; Lvov, Y.; Schmitt, J. *Biosens Bioelectron* **1994**, *9*, 677.

(89) Huang, J. D.; Yang, Y.; Shi, H. B.; Song, Z.; Zhao, Z. X.; Anzai, J.; Osa, T.; Chen, Q. *Mat Sci Eng C-Bio S* **2006**, *26*, 113.

(90) Yan, X. B.; Chen, X. J.; Tay, B. K.; Khor, K. A. *Electrochem Commun* **2007**, *9*, 1269.

(91) Yu, A. M.; Caruso, F. *Anal Chem* **2003**, *75*, 3031.

(92) Gu, B. X.; Xu, C. X.; Zhu, G. P.; Liu, S. Q.; Chen, L. Y.; Wang, M. L.; Zhu, J. J. *J. Phys. Chem. B* **2009**, *113*, 6553.

(93) Du, D.; Ye, X. X.; Cai, J.; Liu, J. A.; Zhang, A. D. *Biosens Bioelectron* **2010**, *25*, 2503.

(94) Wang, J. *Electroanal* **2005**, *17*, 7.

(95) Balasubramanian, K.; Burghard, M. *Anal Bioanal Chem* **2006**, *385*, 452.

(96) Kirsch, J.; Siltanen, C.; Zhou, Q.; Revzin, A.; Simonian, A. *Chem Soc Rev* **2013**, *42*, 8733.

(97) Arugula, M. A.; Simonian, A. *Meas Sci Technol* **2014**, *25*.

(98) Liu, Y.; Wang, M. K.; Zhao, F.; Xu, Z. A.; Dong, S. J. *Biosens Bioelectron* **2005**, *21*, 984.

(99) Batra, B.; Pundir, C. S. *Biosens Bioelectron* **2013**, *47*, 496.

(100) Dounin, V.; Veloso, A. J.; Schulze, H.; Bachmann, T. T.; Kerman, K. *Anal Chim Acta* **2010**, *669*, 63.

(101) Sun, X.; Wang, X. Y. *Biosens Bioelectron* **2010**, *25*, 2611.

(102) Ivanov, A. N.; Younusov, R. R.; Evtugyn, G. A.; Arduini, F.; Moscone, D.; Palleschi, G. *Talanta* **2011**, *85*, 216.

(103) Petroianu, G. A.; Nurulain, S. M.; Nagelkerke, N.; Shafiullah, M.; Kassa, J.; Kuca, K. *Journal of Applied Toxicology* **2007**, *27*, 453.

(104) Musilek, K.; Holas, O.; Horova, A.; Pohanka, M.; Zdarova-Karasova, J.; Jun, D.; Kuca, K. *Pesticides in the Modern World-Effects of Pesticides Exposure* **2011**, 341.

(105) Shamim, N.; Hong, L.; Hidajat, K.; Uddin, M. S. *J Colloid Interf Sci* **2006**, *304*, 1.

(106) Surovtsev, V. I.; Borzenkov, V. M.; Detushev, K. V. *Biochemistry-Moscow+* **2009**, *74*, 162.

(107) Hertel, T.; Walkup, R. E.; Avouris, P. *Phys Rev B* **1998**, *58*, 13870.

(108) Mu, Q. X.; Liu, W.; Xing, Y. H.; Zhou, H. Y.; Li, Z. W.; Zhang, Y.; Ji, L. H.; Wang, F.; Si, Z. K.; Zhang, B.; Yan, B. *J Phys Chem C* **2008**, *112*, 3300.

(109) Tan, R. C.; Truong, T. N.; Mccammon, J. A.; Sussman, J. L. *Biochemistry* **1993**, *32*, 401.

(110) Boussif, O.; Lezoualch, F.; Zanta, M. A.; Mergny, M. D.; Scherman, D.; Demeneix, B.; Behr, J. P. *P Natl Acad Sci USA* **1995**, *92*, 7297.

(111) Gupta, R. C.; Melatovic, D. Toxicity of organophosphates and carbamates, in Mammalian Toxicology of Insecticides. Royal Society of Chemistry: Cambridge, UK., 2012, pp 104.

(112) Fukuto, T. R. *Environ Health Persp* **1990**, *87*, 245.

(113) Williams, F. M.; Charlton, C.; deBlaquiere, G. E.; Mutch, E.; Kelly, S. S.; Blain, P. G. *Hum Exp Toxicol* **1997**, *16*, 67.

(114) Kulys, J.; Dcosta, E. J. *Biosens Bioelectron* **1991**, *6*, 109.

(115) Mionetto, N.; Marty, J. L.; Karube, I. *Biosens Bioelectron* **1994**, *9*, 463.

(116) Palleschi, G.; Bernabei, M.; Cremisini, C.; Mascini, M. *Sens. Actuator B-Chem.* **1992**, *7*, 513.

(117) Wang, L. M.; Du, D.; Lu, D. L.; Lin, C. T.; Smith, J. N.; Timchalk, C.; Liu, F. Q.; Wang, J.; Lin, Y. H. *Anal Chim Acta* **2011**, *693*, 1.

(118) Sassolas, A.; Blum, L. J.; Leca-Bouvier, B. D. *Biotechnol Adv* **2012**, *30*, 489.

(119) Starodub, N. F.; Kanjuk, N. I.; Kukla, A. L.; Shirshov, Y. M. *Anal Chim Acta* **1999**, *385*, 461.

(120) Hou, S. H.; Ou, Z. M.; Chen, Q.; Wu, B. Y. *Biosens Bioelectron* **2012**, *33*, 44.

(121) Meng, X. W.; Wei, J. F.; Ren, X. L.; Ren, J.; Tang, F. Q. *Biosens Bioelectron* **2013**, *47*, 402.

(122) Zheng, Z. Z.; Li, X. Y.; Dai, Z. F.; Liu, S. Q.; Tang, Z. Y. *J Mater Chem* **2011**, *21*, 16955.

(123) Dave, K. I.; Miller, C. E.; Wild, J. R. *Chemico-Biological Interactions* **1993**, *87*, 55.

(124) Dumas, D. P.; Durst, H. D.; Landis, W. G.; Raushel, F. M.; Wild, J. R. *Archives of Biochemistry and Biophysics* **1990**, *277*, 155.

(125) Rainina, E. I.; Efremenco, E. N.; Varfolomeyev, S. D.; Simonian, A. L.; Wild, J. R. *Biosens Bioelectron* **1996**, *11*, 991.

(126) Russell, R. J.; Pishko, M. V.; Simonian, A. L.; Wild, J. R. *Anal Chem* **1999**, *71*, 4909.

(127) Simonian, A. L.; Good, T. A.; Wang, S. S.; Wild, J. R. *Anal Chim Acta* **2005**, *534*, 69.

(128) Wang, J.; Krause, R.; Block, K.; Musameh, M.; Mulchandani, A.; Schoning, M. J. *Biosens Bioelectron* **2003**, *18*, 255.

(129) Simonian, A. L.; Efremenko, E. N.; Wild, J. R. *Anal Chim Acta* **2001**, *444*, 179.

(130) Simonian, A. L.; Grimsley, J. K.; Flounders, A. W.; Schoeniger, J. S.; Cheng, T. C.; DeFrank, J. J.; Wild, J. R. *Anal Chim Acta* **2001**, *442*, 15.

(131) Simonian, A. L.; Rainina, E. I.; Wild, J. R. *Anal Lett* **1997**, *30*, 2453.

(132) Feng, W.; Ji, P. J. *Biotechnol Adv* **2011**, *29*, 889.

(133) Wang, Y.; Zhang, S.; Du, D.; Shao, Y. Y.; Li, Z. H.; Wang, J.; Engelhard, M. H.; Li, J. H.; Lin, Y. H. *J Mater Chem* **2011**, *21*, 5319.

(134) Zhang, J. L.; Zhang, F.; Yang, H. J.; Huang, X. L.; Liu, H.; Zhang, J. Y.; Guo, S. W. *Langmuir* **2010**, *26*, 6083.

(135) Upadhyay, S.; Rao, G. R.; Sharma, M. K.; Bhattacharya, B. K.; Rao, V. K.; Vijayaraghavan, R. *Biosens Bioelectron* **2009**, *25*, 832.

(136) Brady, D.; Jordaan, J. *Biotechnol Lett* **2009**, *31*, 1639.

(137) Lin, Y. H.; Lu, F.; Tu, Y.; Ren, Z. F. *Nano Lett.* **2004**, *4*, 191.

(138) Liu, Y.; Yu, D. S.; Zeng, C.; Miao, Z. C.; Dai, L. M. *Langmuir* **2010**, *26*, 6158.

(139) Huang, Y.; Wang, W.; Li, Z.; Qin, X. L.; Bu, L. J.; Tang, Z. Y.; Fu, Y. C.; Ma, M.; Xie, Q. J.; Yao, S. Z.; Hu, J. M. *Biosens Bioelectron* **2013**, *44*, 41.

(140) Wooten, M.; Karra, S.; Zhang, M. G.; Gorski, W. *Anal Chem* **2014**, *86*, 752.

(141) Ding, S. J.; Chang, B. W.; Wu, C. C.; Lai, M. F.; Chang, H. C. *Anal Chim Acta* **2005**, *554*, 43.

(142) Pedrosa, V. A.; Caetano, J.; Machado, S. A. S.; Bertotti, M. *Sensors-Basel* **2008**, *8*, 4600.

(143) Valdes-Ramirez, G.; Fournier, D.; Ramirez-Silva, M. T.; Marty, J. L. *Talanta* **2008**, *74*, 741.

(144) Pandey, P. C.; Upadhyay, S.; Pathak, H. C.; Pandey, C. M. D.; Tiwari, I. *Sens. Actuator B-Chem.* **2000**, *62*, 109.

(145) Cracknell, J. A.; Vincent, K. A.; Armstrong, F. A. *Chemical Reviews* **2008**, *108*, 2439.

(146) Luckarift, H. R.; Atanassov, P. B.; Johnson, G. R. *Enzymatic fuel cells: From fundamentals*

to applications; John Wiley & Sons2014.

(147) Luz, R. A.; Pereira, A. R.; de Souza, J. C.; Sales, F. C.; Crespilho, F. N. *ChemElectroChem* **2014**, *1*, 1751.

(148) Rengaraj, S.; Mani, V.; Kavanagh, P.; Rusling, J.; Leech, D. *Chem Commun* **2011**, *47*, 11861.

(149) Rusling, J. F.; Wasalathanthri, D. P.; Schenkman, J. B. *Soft Matter* **2014**, *10*, 8145.

(150) Deng, Z. J.; Morton, S. W.; Ben-Akiva, E.; Dreaden, E. C.; Shopsowitz, K. E.; Hammond, P. T. *Acs Nano* **2013**, *7*, 9571.

(151) Saetia, K.; Schnorr, J. M.; Mannarino, M. M.; Kim, S. Y.; Rutledge, G. C.; Swager, T. M.; Hammond, P. T. *Adv Funct Mater* **2014**, *24*, 492.

(152) Singh, M.; Holzinger, M.; Tabrizian, M.; Cosnier, S. *Carbon* **2015**, *81*, 731.

(153) Qureshi, S. S.; Zheng, Z. Q.; Sarwar, M. I.; Felix, O.; Decher, G. *Acs Nano* **2013**, *7*, 9336.

(154) Wang, D.; Shakeel, H.; Lovette, J.; Rice, G. W.; Heflin, J. R.; Agah, M. *Anal Chem* **2013**, *85*, 8135.

(155) Ariga, K.; Lvov, Y. M.; Kawakami, K.; Ji, Q. M.; Hill, J. P. *Adv Drug Deliver Rev* **2011**, *63*, 762.

(156) Arugula, M. A.; Zhang, Y. Y.; Simonian, A. L. *Anal Chem* **2014**, *86*, 119.

(157) Katz, E. *Bioelectronic Medicine* **2015**, *2*, 1.

(158) Lin, J. L.; Palomec, L.; Wheeldon, I. *Acs Catal* **2014**, *4*, 505.

(159) Moehlenbrock, M. J.; Minteer, S. D. *Chem Soc Rev* **2008**, *37*, 1188.

(160) Komathi, S.; Gopalan, A. I.; Lee, K. P. *Biosens Bioelectron* **2009**, *24*, 3131.

(161) Cui, R. J.; Huang, H. P.; Yin, Z. Z.; Gao, D.; Zhu, J. J. *Biosens Bioelectron* **2008**, *23*, 1666.

(162) Wu, B. Y.; Hou, S. H.; Yin, F.; Li, J.; Zhao, Z. X.; Huang, J. D.; Chen, Q. *Biosens Bioelectron* **2007**, *22*, 838.

(163) Zhang, Y. Y.; Arugula, M. A.; Wales, M.; Wild, J.; Simonian, A. L. *Biosens Bioelectron* **2015**, *67*, 287.

(164) Sun, J. J.; Zhao, H. Z.; Yang, Q. Z.; Song, J.; Xue, A. *Electrochim Acta* **2010**, *55*, 3041.

(165) Zhang, Y. Y.; Arugula, M. A.; Kirsch, J. S.; Yang, X. Y.; Olsen, E.; Simonian, A. L. *Langmuir* **2015**, *31*, 1462.

(166) Zhang, Y. Y.; Arugula, M. A.; Simonian, A. L. *ECS Transaction* **2014**, *64*, 133.

(167) Cosnier, S.; Le Goff, A.; Holzinger, M. *Electrochem Commun* **2014**, *38*, 19.

(168) Reuillard, B.; Le Goff, A.; Agnes, C.; Holzinger, M.; Zebda, A.; Gondran, C.; Elouarzaki, K.; Cosnier, S. *Physical Chemistry Chemical Physics* **2013**, *15*, 4892.

(169) Zebda, A.; Gondran, C.; Le Goff, A.; Holzinger, M.; Cinquin, P.; Cosnier, S. *Nat. Commun.* **2011**, *2*.

(170) Minteer, S. D.; Liaw, B. Y.; COoney, M. J. *Curr Opin Biotech* **2007**, *18*, 228.

(171) Davis, F.; Higson, S. P. *Biosensors and Bioelectronics* **2007**, *22*, 1224.

(172) Leech, D.; Kavanagh, P.; Schuhmann, W. *Electrochim Acta* **2012**, *84*, 223.

(173) Hickey, D. P.; Giroud, F.; Schmidtke, D. W.; Glatzhofer, D. T.; Minteer, S. D. *Acs Catal* **2013**, *3*, 2729.

(174) Pothukuchy, A.; Mano, N.; Georgiou, G.; Heller, A. *Biosens Bioelectron* **2006**, *22*, 678.

(175) Stoica, L.; Dimcheva, N.; Ackermann, Y.; Karnicka, K.; Guschin, D. A.; Kulesza, P. J.; Rogalski, J.; Haltrich, D.; Ludwig, R.; Gorton, L.; Schuhmann, W. *Fuel Cells* **2009**, *9*, 53.

(176) Lang, Q. L.; Yin, L.; Shi, J. G.; Li, L.; Xia, L.; Liu, A. H. *Biosens Bioelectron* **2014**, *51*, 158.

(177) Handa, Y.; Yamagiwa, K.; Ikeda, Y.; Yanagisawa, Y.; Watanabe, S.; Yabuuchi, N.; Komaba, S. *Chemphyschem* **2014**, *15*, 2145.

(178) Korani, A.; Salimi, A.; Hadadzadeh, H. *J Power Sources* **2015**, *282*, 586.

(179) Yang, X.; Yang, Q. D.; Xu, J.; Lee, C. S. *J Mater Chem* **2012**, *22*, 25492.

(180) Wang, Z. J.; Etienne, M.; Urbanova, V.; Kohring, G. W.; Walcarius, A. *Anal Bioanal Chem* **2013**, *405*, 3899.

(181) Devadas, B.; Mani, V.; Chen, S. M. *Int J Electrochem Sc* **2012**, *7*, 8064.

(182) Yan, Y. M.; Zheng, W.; Su, L.; Mao, L. Q. *Adv Mater* **2006**, *18*, 2639.